Structure function analysis of thioredoxin from *Wuchereria bancrofti*, a drug target for human lymphatic filariasis

Dissertation

zur Erlangung des Doktorgrades der Naturwissenschaften
an der Fakultät für Mathematik, Informatik und Naturwissenschaften
der Universität Hamburg

vorgelegt von

Nasser Yousef (M.Sc.)

aus Kairo, Ägypten

Hamburg 2014

Die vorliegende Arbeit wurde im Zeitraum von 2009 bis 2014 in der Arbeitsgruppe von Prof. Ch. Betzel am Institut für Biochemie und Molekularbiologie am Department Chemie der Universität Hamburg angefertigt.

Gutachter:

Herr Prof. **Christian Betzel**

Herr Prof. **Reinhard Bredehorst**

Tag der Disputation: 25.07.2014

To my wife and daughters

Table of Contents

List of figures

List of tables

List of abbreviations

LF	Human lymphatic filariasis
MF	Macrofilaria
mf	microfilaria
EN	Endemic normal
ADLA	Acute dermatolymphangioadenitis
NE	Nonendemic
AFL	Acute filarial lymphangitis
CP	Chronic pathology
TPE	Tropical pulmonary eosinophilia
ELISA	Enzyme- linked immunosorbent assay
CFA	Circulating filarial antigen
FDS	Filarial dance sign
DEC	Diethylcarbamazine
IVM	Ivermectin
ALB	Albendazol
MDA	Mass drug administration
GPELF	Global Programe to Eliminate Lyphatic Filariasis
NADPH	Nicotinamide adenine dinucleotide phosphate
RNS	Reactive nitrogen species
ASK1	Apoptosis signalling kinase 1
TrxR	Thioredoxin reductase
Trx	Thioredoxin
CLIC	Chloride intracellular channel
ICAT	Isotope coded affinity tag
TAP	Tandem affinity purification

PAPS	3-phosphoadenosine 5-phosphosulfate
FTR	Feredoxin-thioredoxin reductase
CNS	Central nervous system
I422	I Centered Tetragonal Space group
P42212	PrimitiveTetragonal Space group
CCD	Charge-coupled Device
CCP4i	Collaborative Computational Project Number 4
DESY	Deutsches Elektronen-Synchrotron
DLS	Dynamic Light Scattering
EMBL	European Molecular Biology Laboratory
RMS	Root mean square
FDA	Food and Drug Administration
F_c	Calculated Structure-factor
F_o	Measured Structure-factor
FPLC	Fast Protein Liquid Chromatography
HCl	Hydrochloric acid
HTS	High-Throughput Screening
MR	Molecular Replacement
MWCO	Molecular Weight Cut Off
NCBI	National Centre for Biotechnology Information
PAGE	Polyacrylamide Gel Electrophoresis
APS	Ammonium persulfate
CV	Column volume
PCS	Photon Correlation Spectroscopy
PCT	Pre-Crystallization Test
PDB	Protein Data Bank

PDB ID	Identification Code for Protein Data Bank
PEG	Polyethylene Glycol
R_{free}	*R*-factor, based on selection of reflections not considered for structure solution
R_{merge}	Reliability factor of all symmetry-equivalent reflexes
SDS	Sodium Dodecyl Sulphate
***Wb*Trx-1**	*Wuchereria bancrofti* thioredoxin
T	Temperature
Tris	Tris (hydroxymethyl) aminomethane
UK	United Kingdom
USA	United States of America
UV	Ultraviolet
Amp	Ampicillin
BSA	Bovin serum albumin
Cam	Chloramphincol
DTT	Dithiotheritol
EDTA	Ethylenediaminetetraacietic acid
IPTG	β-*d*-thiogalactopyranoside
OD	Optical density
ORF_S	Open reading frames
PCR	Polymerase chain reaction
ROS	Reactive oxygen species
RT	Room temperature
SDS	Saturation transfer difference
WT	*Wildtype*
Approx	Approximetly
***Aqua dest*/ dH_2O**	Distilled water

AUC	Analytical ultra centrifuge
BLAST	Basic Local Alignment Search Tool
bp	Base pair (s)
c	Concentration
cDNA	Complementray DNA
CIAP	Calf intestinal alkaline phosphatase
CM^R	Chloramphenicol resitance
D	Day (s)
DMSO	Dimethylsulfoxide
DNA	Deoxyribonucleic acid
dNTPs	2´-deoxynucleoside-5´-triphosphate
ds	Double strand (DNA/RNA)
E.coli	*Escherichia coli*
EtBr	Ethidium bromide
EtOH	Ethanol
f.c.	Final concentration
h	Hour
Hz	Hertz (unit)
I	Intensity
k	Kilo
L	Liter (unit)
LB	Luria Bertani
max	Maximum
MCS	Multiple cloning site
OD	Optical density (at wavelength of 600 nm)
ORF	Open reading frame
pfu	*Pyrococcus furious* (polymerase)

RMSD	Root-mean-square deviation
SEC	Size-exclusion chromatography
T	Temperature [K]
t	Time (s)
Taq	*Thermus aquaticus* (polymerase)
U	Unit (enzyme activity)
µ	Micro-(multyplied by 10^{-6})
UV	Ultraviolet
°	Degree
°C	Degree centigrade
Å	Angstrom
eV	Electron volt
g	Gram
k	Boltzmann's Constant
K	Kelvin
kDa	Kilo Dalton
M	Molar
mg	Milligram
min	Minute
ml	Milliliter
mm	Millimeter
mM	Milli-molar
nl	Nano-liter
nm	Nanometer
$\boldsymbol{R_H}$	Hydrodynamic Radius
rpm	Rounds per minute
$\mathbf{V_M}$	Matthews Coefficient

η	Viscosity
λ	Wavelength
µl	Micro-liter
µs	Micro-second
µM	Micro-molar
PX-12	1-Methyl-propyl-2-imidazol disulfide
TSA	7-[4-(dimethylamino) phenyl]-N-hydroxy-4, 6-dimethyl-7-oxohepta-2, 4- dienamide)
CDC	Center of Disease Control and Preventation
APL	Acut Promyelocytic Leukemia

Symbols for Amino Acids

A	**Ala**	Alanine
R	**Arg**	Arginine
N	**Asn**	Asparagine
D	**Asp**	Aspartate
C	**Cys**	Cysteine
E	**Glu**	Glutamate
Q	**Gln**	Glutamine
G	**Gly**	Glycine
H	**His**	Histidine
I	**Ile**	Isoleucine
L	**Leu**	Leucine
K	**Lys**	Lysine
M	**Met**	Methionine
F	**Phe**	Phenylalanine
P	**Pro**	Proline
S	**Ser**	Serine
T	**Thr**	Threonine
W	**Trp**	Tryptophan
Y	**Tyr**	Tyrosine
V	**Val**	Valine

1. Aim of this Work

Human lymphatic filariasis, also known as Elephantiasis, is the most common vector born disease in tropical countries caused by small round worms. The infection usually happened in the childhood and its symptoms occur later in life. The classic symptoms of the infected individuals are severe damage, painful swelling and disfiguration of the legs and organs. In 1998, the WHO started the Global Program to Eliminate Lymphatic Filariasis (GPELF), to complete the eradication of filariasis by 2020. Until now, no effective drug or vaccine has been developed to treat or prevent this disease.

The lymphatic parasites remain inside the lymphatic system and bath in the lymph, which contains immune cells and molecules. They survive for years in the presence of oxidative free radicals released from the host immune system. This is possible due to the ability of the parasite to produce and to secrete molecules, including thioredoxin to neutralize cytotoxics arising from reaction oxygen spices.

Thioredoxins are the major players in redox regulation, as they control the redox stat of other protein thiols. Some of the thioredoxin members have significant effects on the cell cycle. Thioredoxin was found to be involved in many reactions and it is essential for parasite survival and maturation.

The main aim of this thesis is the structure characterization of thioredoxin from *Wuchereria bancrofti*, which is an enzyme important for parasite survival. The three dimensional structure of *Wb*Trx-1 should be analyzed in order to obtain a detailed insight into active site architecture. Enzymatic activity will also analyze to have some information about the substrate binding enzyme. Also inhibition assay with specific thioredoxin inhibitor will take place in order to understand how the inhibitor looks like and in which part of the enzyme will bind.

It is known from previous reports that the *Wb*Trx-1 catalytic motife –WCPPC- is well conserved among living nematodas such as, Tryparedoxin (a thioredoxin-like protein) from *C. fasciculate, L. major and T. brucei.* Previous tryparedoxins were crystallized in an oxidized form, therefore a mutional study will be performed to avoid the disulphide formation in the active site and the three dimentional structure of the mutant will be analyzed with thioredoxin inhibitor.

Finally a docking study of *Wb*Trx-1 mutant with some small molecules will be performed to know the inhibition pockets introduced by the inhibitors.

The determination of the three dimensional structure of both thioredoxins *wild type* and the mutant with the docking study can lead to a better understanding of the chemical reactions and can help to provide a basis for drug design in order to break the transmission and reduce the lymphatic filariasis infection.

2. Summary – Zusammenfassung

2.1 Summary

Human lymphatic filariasis (LF) is a seriously parasitic disease that affects approximately 130 million people worldwide, particularly in Africa, Southern Asia, the western Pacific islands, the north eastern coast of Brazil and the Caribbean islands. In humans the etiological agents of lymphatic filariasis today are the nematode species *Wuchereria bancrofti*, which are responsible for 90% of the infections, additionally *Brugia malayi* and *Brugia timori*. The drugs nowadays used for the treatment of this disease only target the microfilaria circulating in the blood stream at the time of administration and they have no or only a moderate effect on the adult worms. The elimination of LF is however only possible by targeting the adult worms. Thus, there is still an urgent need to develop new drugs with the potential to target the adult worms in order to reduce the amount of filarial-infected individuals and to break the transmission. There are a number of reports indicating that filarial parasites have the ability to maintain in the mammalian host long time, also suggesting that they have evolved methods to resist immune response or the effect of harmful molecules. In addition to this, filarial parasites produce a number of antioxidants including thioredoxin to neutralize cytotoxic molecules that are released against the parasite during the response of the host immune system.

Thioredoxin (Trx-1) is an enzyme that plays a pivotal role during the growth of the parasite. The parasite's survival can be used for developing new potential drugs and potent therapeutic agents against the disease. This work describes the cloning, expression, purification and X-ray structure determination of the protein *Wb*Trx-1. It is expressed in *E.coli* (DE3) pLysS in a soluble form with an approximate molecular weight of 16 KDa. The protein was purified in two chromatography steps using sepharose and gel filtration columns. The protein was produced in mg quantities in *E. coli* and was used for all further investigations. An enzyme assay was established to check the activity of *Wb*Trx-1 by following the reduction of insulin, with the K_m being around 0.5 mM. The protein was characterized in solution by Dynamic Light Scattering (DLS). A single band was observed with a hydrodynamic radius (R_H) of 1.7 nm, corresponding to the molecular weight of the protein and demonstrating the existence of the monomeric form in solution. The protein was crystallized with the hanging drop vapour diffusion method using 100 mM Tris/HCl pH 5.6, 200 mM NaCl and 25% PEG 3350 as precipitant. The crystals diffracted to 1.95 Å resolution applying synchrotron radiation. They possess unit-cell parameters of a = b = 112.6 Å and c =

162.0 Å, corresponding to the space group I Centered Tetragonal (I422) with three molecules in the asymmetric unit. The structure was solved by molecular replacement using the coordinates of tryparedoxin from *Crithidia fasciculate* (PDB ID: 1QK8). The high resolution X-ray structure of thioredoxin from *Wuchereria bancrofti* (*Wb*Trx-1) was determined and refined to 1.95 Å resolution with a final R_{factor} of 17.9 % and an R_{free} of 22.8 %. The overall structure is homologous to those of thioredoxins from other organisms so far known, showing a typical thioredoxin fold with central parallel and anti parallel β- sheets, which is surrounded by α- helices.

The active site sequence consists of Trp-Cys-X-X-Cys, consistent to those regarding other thioredoxins. The electron density of the *Wb*Trx-1 structure shows that the active site Cys_{39} and Cys_{42} forms a disulfide bridge with a bond length of 2.2 Å. Due to the special formation of the disulfide bridge between the two cysteines in the active site (Cys_{39} and Cys_{42}), a mutational study was carried out. By this, the two cysteine residues in the active site were replaced by serines to avoid the formation of disulfides. Two different clones were applied (C39S and C42S). The expression and the purification of the variant *Wb*Trx-1-C42S shows the formation of dimers. The *Wb*Trx-1-C39S mutant was crystallized by the hanging drop vapour diffusion method using 100 mM Tris/HCl, pH 5.6, 200 mM $(NH_4)_2SO_4$ and 25% PEG 3000 as precipitant. The crystals diffracted to 2.49 Å resolution applying synchrotron radiation, showing unit-cell parameters of a = b = 193.1 Å and c = 111.6 Å, which correspond to the space group Primitive Tetragonal ($P4_22_12$) with twelve molecules in the asymmetric unit. A docking study was performed using the Hex 6.3 macromolecular docking program. Four inhibitors were used for the docking study with the *Wb*Trx-1-C39S mutant: TSA (7-[4-(dimethylamino) phenyl]-N-hydroxy-4, 6-dimethyl-7-oxohepta 2, 4- dienamide), 3-mercapto-4-methyle-4H-1, 2, 4-triazol, cisplatin (4-2-diamminedichloroplatinum) and arsenic trioxide (diarsenic trioxide). The docking results show new binding sites in *Wb*Trx-1-C39S close to the N-terminus with TSA and arsenic trioxide. However, triazol and cisplatin show new binding sites close to the C-terminus. Both binding sites are absent in the thioredoxin from the host counterpart. The low sequence identity and the high structural difference between *Wb*Trx-1 and *human* thioredoxin make the *Wb*Trx-1 a good candidate for drug design investigations to treat human lymphatic filariasis.

The high resolution structures of *Wb*Trx-1, *Wb*Trx-1-C39S and the docking studies provide novel and important insights, which promote later drug discovery investigations.

2.2 Zusammenfassungen

Die lymphatische Filariose (LF) ist eine durch Parasiten verursachte Krankheit, die sich auf rund 130 Millionen Menschen weltweit verbreitet und insbesondere in Afrika, in Südostasien, in den westlichen Pazifik Inseln, an der Nordostküste Brasiliens und in den Karibischen Inseln vertreten ist. Die ursächlichen Erreger der lymphatischen Filariose beim Menschen sind die Nematodenarten *Wuchereria bancrofti*, verantwortlich für 90% der Infektionen, zusätzlich die Arten *Brugia malayi* und *Brugia timori*. Die Medikamente, die heutztage für die Behandlung dieser Krankheit verwendet werden, wirken gegen die zirkulierenden Mikrofilaria im Blut ausschließlich zu dem Zeitpunkt der Verabreichung und haben keine oder nur eine mäßige Wirkung auf die erwachsenen Würmer. Eine wirksame Bekämpfung der LF ist nur möglich durch die Ausrichtung von Medikamenten gegen die adulten Würmer. Es besteht also dringender Bedarf zur Entwicklung neuer Medikamente, die gegen die erwachsenen Würmer gerichtet sind, um dadurch die große Menge an LF-infizierten Personen behandeln zu können und um die Übertragungsmechanismen zu unterbrechen. Es gibt eine Vielzahl von Berichten die beschreiben, dass unsegmentierte Fadenwürmer bzw. Parasiten die Fähigkeit haben, sich langfristig im menschlichen Wirt aufzuhalten. Dies deutet darauf hin, dass sie gegen eine Vielzahl von körperlichen Abwehrmechanismen resistent sind. Zusätzlich produzieren unsegmentierte Fadenwürmer bzw. ähnliche Parasiten eine Reihe von Antioxidantien, wie unter anderem das Enzym Thioredoxin-Peroxidase, um schädliche oder zytotoxische Moleküle während der Immunreaktion zu neutralisieren.

Thioredoxin (Trx-1) ist ein Enzym, dass eine wichtige Rolle beim Wachstum des Parasiten spielt. Das Überleben der Parasiten kann herangezogen werden um neue potente Zielmedikamente und hochwirksame Therapeutika gegen LF zu entwickeln. In dieser Arbeit wird das Klonieren, die Expression, die Aufreinigung und die Röntgenstrukturanalyse des Proteins *Wb*Trx-1 beschrieben. Das Protein wurde in *E. coli* (DE3) pLysS in einer löslichen Form mit ca. 16 KDa Molekulargewicht exprimiert. Die Proteinreinigung wurde in zwei Schritten mittels Sepharose- und Gelfiltrations-Chromatografie durchgeführt. Das Protein wurde in *E.coli* im Milligramm-Maßstab produziert und dann für alle weiteren Untersuchungen verwendet. Zur Kontrolle der enzymatischen Aktivität von *Wb*Trx-1 wurde ein Enzymassay zur Reduktion von Insulin entwickelt, der K_m-Wert betrug 0.5 mM. Das Protein wurde folgend durch Dynamische Lichtstreuung (DLS) untersucht. Es wurde eine einzige Bande beobachtet mit einem hydrodynamischen Radius (R_H) von 1.7 nm, was dem

Molekulargewicht des Proteins und dem Erscheinen als Momomer in Lösung entspricht. Das Protein wurde mittels der „hanging drop“ Dampfdiffusions-Methode kristallisiert, unter Verwendung von 100 mM Tris/HCl, pH 5,6, 200 mM NaCl und 25 % PEG 3350 als Fällungsmittel. Die Kristalle diffraktierten bis zu einer Auflösung von 1,95 Å unter der Verwendung von Synchrotronstrahlung. Die Zellkonstanten betrugen a = b = 112,6 Å und c = 162,0 Å, was der Raumgruppe I-zentriert Tetragonal (I422) mit drei Molekülen in der asymmetrischen Einheit entspricht. Die Struktur wurde durch molekularen Ersatz gelöst unter Verwendung der Koordinaten von Tryparedoxin aus *Crithidia fasciculate* (PDB ID: 1QK8). Die Röntgenstruktur des Enzyms Thioredoxin-Peroxidase aus *Wuchereria bancrofti* (*Wb*Trx-1) wurde mit einer Auflösung von 1,95 Å ermittelt und zu einem R_{factor} von 17,9 % und einem R_{free} von 22,8 % verfeinert. Die allumfassende Struktur ist homolog zu den bisher bekannten Thioredoxinen aus anderen Organismen und besitzt die typische Thioredoxin-Faltung mit zentralen parallel und antiparallel gefalteten β-Blättern, umgeben von α-Helices.

Die Sequenz im aktiven Zentrum besteht aus Trp-Cys-X-X-Cys, wie bei anderen Thioredoxinen bekannt. Die Elektronendichte der *Wb*Trx-1-Struktur zeigt, dass die aktiven Aminosäuren Cys_{39} und Cys_{42} eine Disulfidbrücke mit einer Bindungslänge von 2.2 Å bilden. Aufgrund der Disulfidbrückenbildung zwischen den beiden Cysteinen im aktiven Zentrum (Cys_{39} und Cys_{42}), wurde eine Mutationsstudie durchgeführt. Um die Bildung von Disulfidbrücken zu verhindern, wurden die Cysteine durch Serine ersetzt unter der Verwendung zweier verschiedener Klone. Der Expression und die Reinigung der Variante *Wb*Trx-1-C42S zeigte eine Bildung von Dimeren. Die *Wb*Trx-1-C39S Mutante wurde durch die „hanging drop“ Dampfdiffusionsmethode unter Verwendung von 100 mM Tris/HCl, pH 5,6, 200 mM $(NH4)_2SO_4$ und 25% PEG 3000 als Fällungsmittel kristallisiert. Die Kristalle zeigten eine Auflösung von 2,49 Å unter der Verwendung von Synchrotron-Strahlung. Sie besaßen Zellkonstanten a = b = 193,1 Å und c = 111,6 Å, dies entspricht der Raumgruppe Primitiv Tetragonal ($P4_22_12$) mit zwölf Molekülen in der asymmetrischen Einheit. Es folgte eine „Docking“-Studie mittels dem „Hex 6.3 Makromolekular Docking Programm“. Vier unterschiedliche Inhibitoren wurden für die Studie mit der *Wb*Trx-1-C39S Mutante verwendet: TSA (7- [4- (Dimethylamino) phenyl] -*N*-hydroxy-4, 6-dimethyl-7-oxo- 2, 4-heptadienamide), 3-Mercapto-4-Methyle-4H-1, 2, 4-Triazol, Cisplatin (4-2-Diammindichloridoplatin) und Arsentrioxid (Dsiarsenictrioxid). Die Docking-Ergebnisse mit TSA und Arsentrioxid zeigen neue Bindungsstellen in *Wb*Trx-1-C39S in der Nähe des N-Terminus. Triazol und Cisplatin hingegen zeigen neue Bindungsstellen in der Nähe des C-Terminus. Beide Bindungsstellen sind in dem Wirts-Enzym Thioredoxin-Peroxidase nicht

vorhanden. Die geringe Homologie und der hohe strukturelle Unterschied zwischen *Wb*Trx-1 und dem menschlichen Thioredoxin machen *Wb*Trx-1 einen guten Kandidaten für die Entwicklung von Arzneimitteln zur Untersuchung und Behandlung der lymphatischen Filariose.

Die hochaufgelöste Röntgenstrukturen von *Wb*Trx-1 und *Wb*Trx-1-C39S, wie auch die „Docking“-Studie liefern neuwertige und wichtige Einblicke, um die spätere Entwicklung von Therapeutika gegen die lymphatische Filariose zu fördern.

3. Introduction

3.1 Lymphatic filariasis

3.1.1 Biology and epidemiology

Lymphatic filariasis is one of the most common vector-borne diseases affecting 130 million people worldwide and it causes acute and chronic morbidity. It has spread across 81 tropical and subtropical countries including Africa, South East Asia, the Western Pacific of Islands, the north eastern coast of Brazil and the Caribbean Islands[1]. As estimated, 1.3 billion people are at risk of infection, where filariasis is endemic. In particular, more than 65% of the infected people live in South-East Asia, 30% in Africa and the rest in other tropical and subtropical areas (see Fig. 1).

Figure 1: Global distribution of Lymphatic Filariasis[2].

Filariasis is caused by eight different parasitic nematode worms: *Brugia malayi*, *Brugia timori*, *Mansonella ozzardi*, *Mansonella perstan*, *Mansonella streptocerca*, *Loa loa*, *Onchocera volvulus*, and *Wuchereria bancrofti*[3]. Of those, *W. bancrofti*, *B. malayi*, and *B. timori* are responsible for the infection in the lymphatic system of humans. *W. bancrofti* accounts for 90% of infections with lymphatic filariasis and occurs in most tropical and subtropical endemic regions. *B. malayi* originates from India in the west and spreads to South Korea in the north east and Indonesia in the south east, while *B. Timori* is located only in eastern Indonesia[4].

3.1.2 Transmission and infection

The lymphatic disease is transmitted by several kinds of mosquitoes, depending on the geographical location. They act as intermediate host and ensure the transmission of the disease between humans. *Wuchererie bancrofti* is transmitted by Culex quinquefasciatus, Anopheles and Aedes. Anophelesis, Coquilletidia and Mansonia are responsible for *Brugia malayi* transmission. *Brugia timori* is transmitted by Anopheles barbirostris (see Fig. 2)[5].

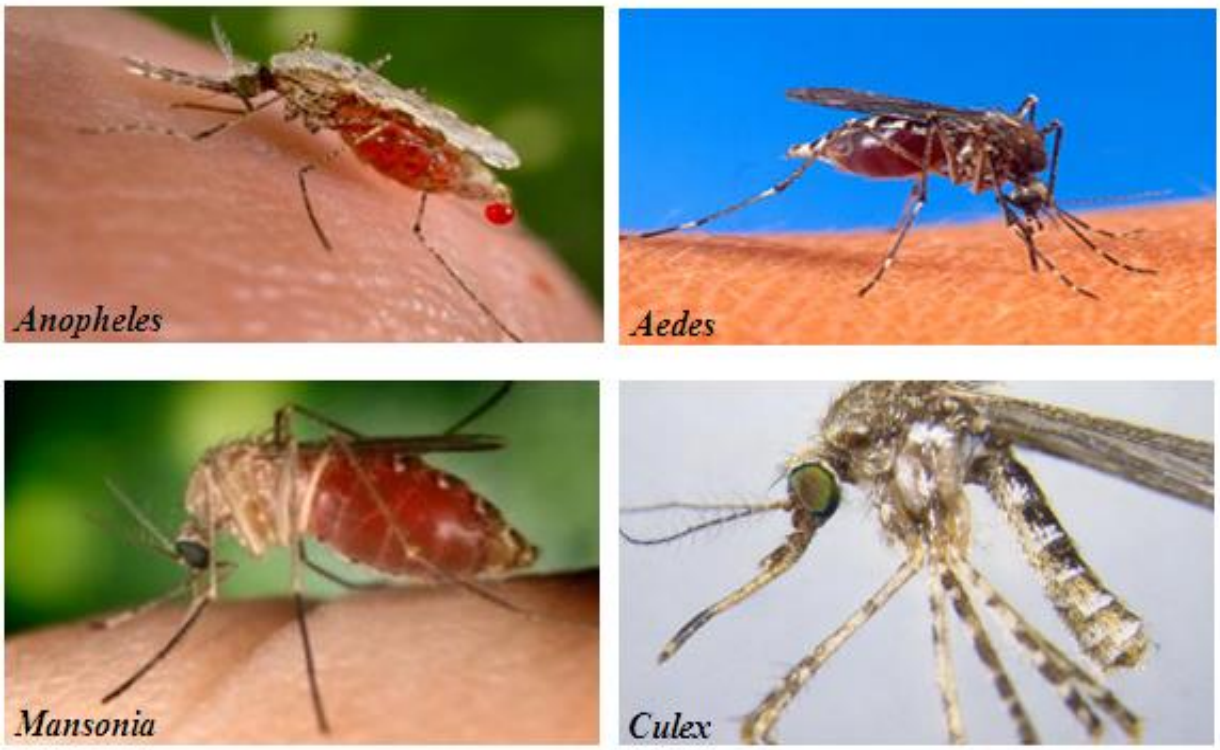

Figure 2: Different kinds of mosquitoes responsible for the lymphatic filariasis infection.

The life cycle of the parasite is identical to other vector-born diseases. When the female mosquitoes ingest microfilaria with blood from infected humans, the microfilaria develops into the infective filarial worm larvae (L3) in the thoracic muscles of the mosquitoes and then travels to the lymphatic through the bloodstream. The larvae enter the human body when the mosquitoes feed on blood[6].

In the lymphatic system, the larvae develop into adult sexual worms. Male worms are roughly 3–4 centimeters in length, whereas female worms are 8–10 centimetres in size. The female worms yield millions of microfilaria, which reach the bloodstream again after the 6 – 12 months incubation period (see Fig. 3). The male and female worms together form 'nests' in the human lymphatic system, which is an essential component of the body's immune system and is responsible for maintaining the delicate fluid balance between blood and body tissues.

Infected persons show one or more symptoms after the incubation period.The conditions can be divided into three stages: (1) Asymptomatic damage to the lymphatic system and kidneys (2) Acute attacks of filarial fever (3) Chronic conditions such as elephantiasis and hydrocele. The asymptomatic infection is identified by the observation of millions of microfilaria in the blood vessel or adult worms in the lymphatic system, without showing any symptoms. Kidney damage may cause blood and protein loss in the urine. Damage to the lymphatic system may enhance the risk of acute attacks such as acute dermatolymphangioadenitis (ADLA)[7].

Clinically asymptomatic microfilaremia is the most common manifestation of bancroftian filariasis. The asymptomatic form is associated with high levels of MF and circulating filarial antigen with the absence of an obvious asymptomatic pathology [8].

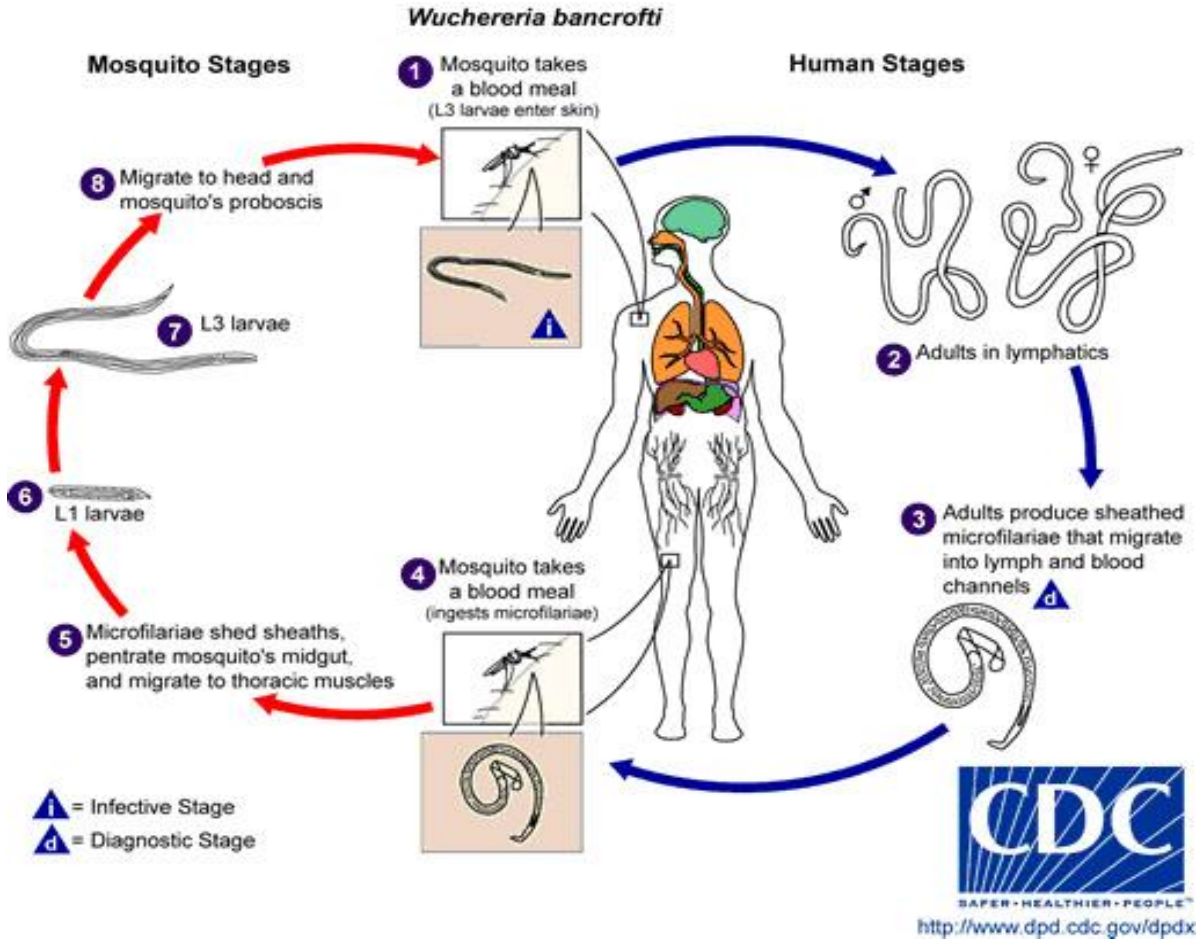

Figure 3: Life cycle of *W.bancrofti*. Adapted from http://www.dpd.cdc.gov/dpdx.

3.1.3 Identification methods for *W. bancrofti*

Various methods exist for the identification of *W. bancrofti* in the blood. Until now, the method for the diagnosis of filarial infection is through direct detection of the parasite in the blood. The microscopically examination is considered as the main standard method for filarial diagnosis. Nevertheless, other methods exist, like the detection of antibodies by immunodiagnostic tests, Circulating Filarial Antigen (World Health Organization) and DNA detection methods based on the Polymerase Chain Reaction[9, 10].

3.1.3.1 Morphological identification

The standard procedure used for the detection of microfilaria in the blood is microscopy. This is a simple technique for examining blood and other fluids for mf. Dry or wet smears are prepared on slides and are examined under the microscope. The sensitivity of microscopy can be improved using the Knott's concentration technique. This can be used to

examine the volumes of anticoagulated blood by mixing the blood with formalin, followed by centrifugation and further examination of the sediment using the dry or wet slide preparation methods[11].

The morphological identification is done by the examination of the sheath, the most striking characteristic identification marker of mfs of filarial parasites.The morphology of filarial species that are known to infect human are summarized in table 1.

Species	Size of Microfilaria	Morphology of microfilaria
Wuchereria bancrofti	210 – 320 mm by 8 – 10 mm	Sheathed. Tail pointed and clear
Brugia malayi	170 – 260 mm by 5 – 6 mm	Sheathed. Tail pointed with 2 nuclei
Loa loa	230 – 300 mm by 6 – 8 mm	Sheathed. Tail blunt with nuclei
Mansonella perstans	200 mm by 6 mm	Unsheathed. Tail blunt with nuclei
Mansonella ozzardi	250 mm by 6 – 7 mm	Unsheathed. Tail pointed and clear

Table 1. The morphology of the blood microfilaria that are known to infect human. Adapted from CDC.

3.1.3.2 Molecular identification

Initial methods for the molecular identification of filarial parasites were based on the development of specific radioactively labeled deoxyribonucleic acid (DNA) probes[12]. This method, however, required the use of radioactive materials and therefore was not very practical[13]. However, arise of the polymerase chain reaction (PCR) presented opportunities for improved diagnostic methods. The PCR is an enzyme-catalysed biochemical reaction in which small amounts of a specific DNA segment is amplified into large portions of linear double-stranded DNA, using two oligonucleotide primers and a DNA polymerase[14].

Using the PCR technique, a method for *W. bancrofti* identification was developed based on the SspI repeat, which is a specific sequence in *W. bancrofti*. This method yields a 188 bp fragment and can detect 0.1 pg of *W. bancrofti* genomic DNA, which represents approximately less than 1% of the DNA found in one microfilaria. This method was then tested on blood samples[15] and has also been improved for field testing on pools of mosquitoes [16].

3.1.3.3 Immunological identification methods

Immunoassays for antigen detection of circulating filarial antigens constitute a useful diagnostic approach, especially in very low mf levels. Enzyme link immunosorbent assay (ELISA) methods, based on the detection of circulating filarial antigens, have been developed for rapid testing of bancroftian filariasis[17]. Other methods for antigen detection, such as the Og4C3 and AD12-ICT have also been developed and tested[18]. The detection of 32 specific immunoglobulin G4 and monoclonal antibodies have also been exploited as diagnostic tools[19]. However, antibody detection is of limited value, due to the substantial antigenic cross reactivity between filaria and other helminths, and positive serologic tests do not distinguish between past and current infection.

3.1.4 Pathology of lymphatic filariasis

Lymphatic patients serve as the reservoir for continued transmission of the parasite. In contrast, individuals with severe pathology have few or no macrofilaria (MF), but display energetic specific immune responses[20]. In addition, the disease can be further divided according to the asymptomatic form into acute (early) and chronic phases. But of course it has been difficult to focus on acute or early infections as the time of infection cannot be easily ascertained[21]. Moreover, some individuals remain free of infections despite lifelong exposure to the parasites; these individuals are referred to as Nonendemic (NE).

There are two different acute manifestations of lymphatic filariasis in the early phase of infection: Acute filarial lymphangitis (AFL) and acute dermatolymphangioadenitis (ADLA). The former one is induced by the death of the filarial worms and may end in hydrocele formation (accumulation of lymph fluid in the tunica vaginalis) and occurs only in bancroftian filariasis, whereas ADLA is not induced by the worm but is associated with bacterial infections that may induce lymphedema (accumulation of lymph fluid in the legs, scrotum, breasts and arms)[22, 23]. In contrast to other parasitic infections the pathology in LF is mainly caused by the adult stage of the worm[24]. So far there is no immune reaction detected in the case of adult worms, as long as they are live in the host. Inflammation occurs when adult worms die. This is either due to being drug induced or spontaneously results in local necrosis around the parasite[25, 26]. Dead parasites are then either completely absorbed or partially calcified. Inside the affected tissues they create changes that induce expansion and thickening of the lymphatic vessel as well as fibrosis and lymphatic obstruction [21, 26, 27]. Histological staining shows granuloma formation, which is defined as infiltration of plasma

cells, eosinophils, neutrophils and macrophages, which have also been described in and around these infected vessels[21]. If these induced immune reactions are not limited, they can lead to different irreversible clinical manifestations such as lymphedema, which may progress to the most severe disease form called elephantiasis (non-reversible edema, with skin thickening and nodular or warty excrescences), urogenital disorders or to hydroceles (see Fig. 4)[28].

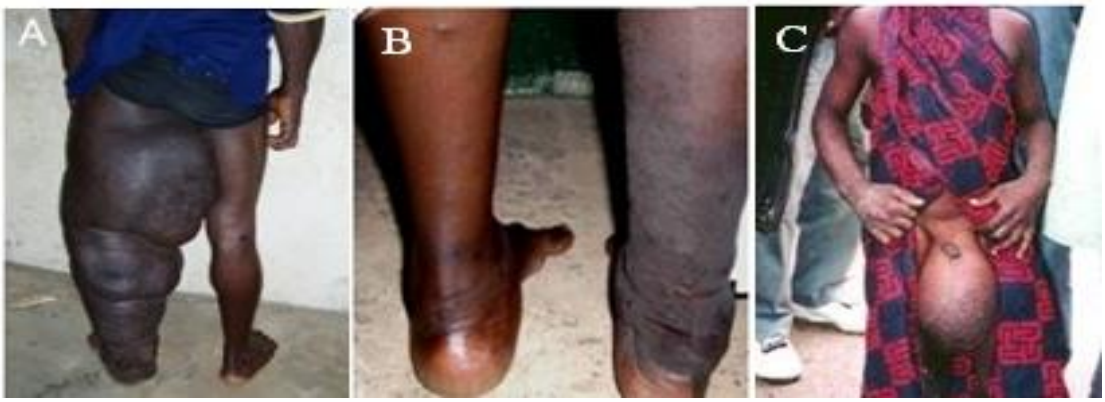

Figure 4: Examples of pathological outcomes of lymphatic filariasis. (A) Patient with elephantiasis, the severest form of lymphoedema. (B) Severe lymphedema in the right leg. (C) Example of hydrocele [29].

These individuals are often defined as chronic pathology (CP) patients. Actually, the apperance of lymphedema and hydrocele is not alternately exclusive and both are characterized by dilation of the lymphatic vessels and extravasation of fluid from the vessels into the surrounding tissues. The enlargement of the lymph vessels results in a less effective lymph flow, which is always orientated towards gravity in the legs. In contrast to hydrocele, individuals affected with lymphedema become more vulnerable to opportunistic microorganisms that may enter the lymphatics through smaller wounds; these little injuries would usually be unnoticed in people without lymphatic disease[25]. Moreover, the symptoms of lymphedema in legs have been characterized in seven stages and are summarized in table 2[1]. Most symptoms lie between stages 1, 2 and 3 but sometimes more extreme cases can be detected.

Besides these bacterial or fungal infections, other studies have provided evidence that pathology is a genetic trait, since its development is seen in clusters of families and several distinct polymorphisms have been identified. Furthermore, genetic traits have also been correlated with parasite burden and the susceptibility to infection[30, 31].

Lymphedema Stage	Symptoms
Stage 1	Swelling goes away overnight
Stage 2	Swelling does not go away overnight
Stage 3	Shallow skin folds
Stage 4	Knobs
Stage 5	Deep skins folds
Stage 6	Mossy lesions
Stage 7	Unable to care for self or perform daily activities

Table 2: Stages of lymphedema and its symptoms[1].

An extra rare pathological form present in less than 1% of all lymphatic filariasis (LF) infected people, is the so-called tropical pulmonary eosinophilia (TPE)[32]. Affected patients suffer from coughing, fevers and hepatosplenomegaly[33]. They are characterized by the absence of macrofilaria (MF) in the bloodstream because the worm strain is rapidly opsonized with anti-microfilarial antibodies and is finally cleared from the pulmonary vasculature. Trapped microfilaria (MF) degenerate and release antigenic components that stimulate local inflammatory processes with accumulation and activation of eosinophils in the lungs. Thus, asthmatic symptoms are induced as a result of pulmonary allergic responses mediated by specific IgE antibodies directed against the macrofilaria[34, 35].

3.1.5 Diagnosis and treatment of lymphatic filariasis

The diagnosis of lymphatic filaria traditionally relies on the determination of circulating macrofilaria in the bloodstream. In order to identify asymptomatic lymphatic filaria, nightly venous blood is checked for the presence of macrofilaria using membrane filters to enrich the worm offspring[36]. The detection of macrofilaria is essential for the diagnosis of the disease but this method is limited to infection patients. Therefore, other tests have been developed, such as a specific enzyme-linked immunosorbent assay (ELISA), or the

rapid card test to measure circulating filarial antigens (CFA), which are released from adult worms and can be detected in plasma samples of *W. bancrofti* infected people[17, 37, 38].

In contrast to the diagnosis of infections with *Brugia malayi* worms, it is possible to identify hidden or potential infections with *W. bancrofti* using these tests. Besides the determination of latent infection, the CFA even allows the identification of individuals with possible occurrence of low parasitemia. An extra diagnostic test for detecting an infection with *W. bancrofti* is the visualization of active nematodes via ultrasonography, since adult worms show a characteristic pattern of movements within the lymphatic vessels of the scrotum of male patients. This is termed filarial dance sign (FDS)[39, 40]. In patients infected with *B.malayi* ultrasonic imaging of adult filaria is of limited use, because these worm nests are not stable over time and cannot be localized in distinct parts of the body[41, 42]. Thus, worm nests will be detected only in a fraction of patients. However, with these tools it is now possible to differentiate between patent and latent-infected filariasis individuals and also confirm the prevalence of live nematodes. Although these methods are not viable for brugian infections, serology assays can be performed by analyzing brugia-specific immunoglobulins in ELISAs[43, 44].

There remains no vaccine against infections with the helminth. Thus, besides vector control, chemotherapy is the preferred method of choice to control or eliminate the disease [45]. Diethylcarbamazine (DEC), ivermectin (IVM) and albendazole (ALB) have been used in the last two decades for successful mass drug administration (MDA) against infections caused by filarial nematodes. These drugs are commonly used in order to interrupt the transmission with a consequent reduction in the burden of infection and to decrease morbidity[24]. The mode of action of DEC is not completely understood up to now, but it is known that this drug results in the sequestration of MF and their final destruction by the immune system. Murine and human *in-vitro* studies suggest that DEC blocks the cyclooxygenase pathway in parasites, which leads to the death of MF[24, 46]. Ivermectin is known to tolerate macrocyclic lactone which acts by hyperpolarization of parasitic glutamate-sensitive channels, thereby preventing neuronal transmission resulting in muscle paralysis[47, 48]. In contrast to DEC, local destruction of MF is not induced by IVM treatment. Recently, IVM was shown to decrease the amount of proteins released by the excretory/secretory vesicles of MF, thus preventing the secretion of immunomodulatory molecules by the worm, which usually reduces the host's immune response[45]. Finally, ALB is a broad-spectrum anthelmintic drug against flatworms, nematodes and cestodes. It inhibits the polymerization of worm β-tubulin and thereby the microtubule formation[49]. In

order to treat lymphatic filariasis, DEC or IVM each in combination with ALB are used by the Global Programme to Eliminate Lymphatic Filariasis (GPELF), depending on the geographical location. A single dose of DEC is effective in reducing acute and chronic cases of microfilaraemia for at least one year. This is the basis for MDA in areas without co-endemic, but with other parasite infections (onchocerciasis). Recently, it has been shown that diethylcarbamazine cannot be used in endemic regions, since its administration causes death of microfilaria (MF) and leads to irreversible local ocular damage. Therefore IVM is used in combination with ALB to treat lymphatic filaria in co-endemic countries[50]. Although DEC, IVM and ALB have been successfully used in the past to target the microfilaria, now these drugs show no or only moderate macrofilaricidal effects, but they do not completely target the adult worms, which would in turn eliminate the infection [51].

Repeated rounds of treatment have been used in order to break transmission, but to achieve success, the treatment needs to take place for many years, as long as the adult worms are alive, which can override 8 years in lymphatic filariasis. However long-term treatment has serious drawbacks, since there is some evidence of drug resistance[52]. Moreover, treatment with IVM or DEC causes microfilarial death, resulting in adverse reactions like fever, headache, dizziness, myalgia, arthralgia and lymph nodeenlargement, because *Wolbachia* (essential for worm survival) are released into the blood where they induce proinflammatory immune responses[53]. As mentioned before, there is a relationship between *Wolbachia* and the worm survival. This relationship has provided an alternative chemotherapeutic treatment since it is known that tetracyclines are effective against these Rickettsia-like bacteria[54, 55]. Furthermore, in contrast to the mainly microfilaricidal drugs mentioned above, therapy with tetracycline antibiotics directly targets the *Wolbachia* leading to an inhibition of the worm development[56]. Since doxycycline is contraindicated for children, pregnant or breast feeding women and in general is not practical for MDA's because of huge logistical challenges and the length of required treatment, there is still an urgent need for developing new and effective micro-and macrofilaricidal drugs in order to reduce the amount of filarial-infected individuals and to break the transmission process[57].

3.2 Thioredoxin

3.2.1 Biochemistry of thioredoxins

Thioredoxin (Trx) is an ubiquitous antioxidant enzyme that is found in all organisms from eukaryotics to mammalians. The thioredoxin (Trx) protein family constitute key players in maintaining cellular redox homeostasis and redox signaling[58]. Thioredoxin is the major ubiquitous disulfide reductase responsible for maintaining proteins in their reduced state, which is reduced by electrons from NADPH *via* thioredoxin reductase[59]. All thioredoxin proteins have the catalytic motif WCXXC located on a highly conserved fold. The cystein residues of this motif are the key players to reduce the disulfide bonds in the oxidized substrate[60]. The first Trx was discovered in 1964 in *Escherichia coli* and was described as an electron donor for ribonucleotide reductase, an enzyme required for DNA synthesis[61]. Thioredoxins (Trxs) play multivalent cellular roles. They act as reductases in redox control[59], protect proteins from oxidative aggregation and inactivation[62], help the cells cope with various environmental stresses (reactive oxygen species (ROS), peroxynitrite, arsenate[63, 64] and regulate programmed cell death *via* denitrosylation[65, 66]. Some Trxs also act as growth factors[67], modulate the inflammatory response[68], promote protein folding[69] and play important roles in the lifecycles of viruses and phages[60]. Moreover, disregulation of redox signaling and an increased formation of reactive oxygen species (ROS) and reactive nitrogen species (RNS) are correlated with numerous pathologies, including cancer, cardiovascular- and degenerative disorders[70]. One function of thioredoxin is to act as a structural component of another enzyme, by forming a complex. This is best characterized for the T7 DNA polymerase, where reduced thioredoxin-$(SH)_2$ binds with high affinity to the DNA polymerase, thereby forming a 1 : 1 complex that gives the enzyme high processivity [71]. Remarkably, only reduced thioredoxin-$(SH)_2$ binds, whereas oxidized thioredoxin-S_2 is unable to bind, despite their closely related 3D structures. A similar structure role is assumed for function in phage assembly[72]. Thereby, a situation which is highly reminiscent to that of the interaction with T_7 DNA polymerase is created. Similarly, in mammalian cells reduced thioredoxin-$(SH)_2$ and not oxidized thioredoxin-S_2, forms an inhibitory complex with apoptosis signalling Kinas 1 (ASK 1)[73]. This provides a means of redox regulation in apoptosis, with apoptosis being inhibited under conditions where reduced thioredoxin-$(SH)_2$ is the predominate intracellular thioredoxin species. Unique to plants is the link from light to reduction of disulfide bonds in enzyme regulation *via* multiple chloroplast thioredoxins and ferredoxin: thioredoxin systems[74]. In the extracellular environment, most proteins have a

number of stabilizing disulfide bonds. In contrast, inside the cell most residues contain several sulfhydryl groups that are reduced[75]. Thiordeoxin is the major protein disulfide reductase responsible for maintaining proteins in their reduced state and that proteins can be reduced by electrons from NADPH *via* thioredoxin reductase, as shown in Fig. 5.

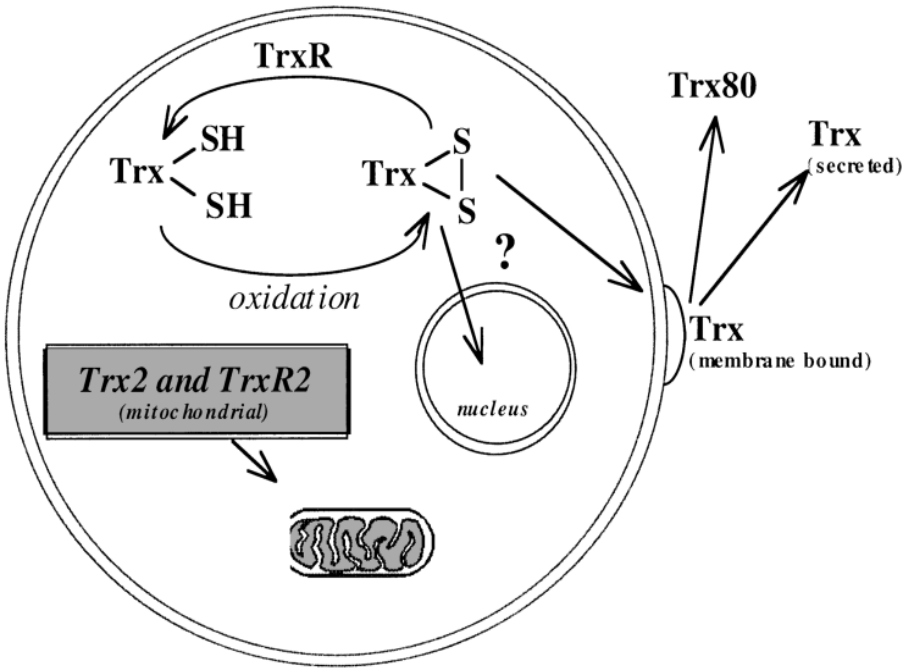

Figure 5. The compartmentalization of the thioredoxin system in a mammalian cell. The figure shows the localization of thioredoxin (Trx) and thioredoxin reductase (TrxR) in different cellular compartments, such as cytosol, nucleus, membrane associated, extracellulary (both Trx and Trx80) and with specific isomers in the mitochondria (Trx2 and TrxR2)[76].

At present more than 1900 references mention thioredoxin and its function and it is difficult to cover all of the research. However, several examples of physiological functions of thioredoxin are summarized in Table 3.

Table 3. Functions of thioredoxins in diverse organisms.

Organism	Functions of thioredoxin	Comments and references
All organisms	DNA synthesis, Protein disulfide reduction.	Thioredoxin is a hydrogen donor for ribonucleotide reductase Thioredoxin is a key player in keeping intracellular protein disulfides generally reduced.
Many organisms	Reduction of H_2O_2.	Many peroxiredoxins, catalyzing reduction of H_2O_2 and thereby preventing oxidative stress and apoptosis induction, require reduction by thioredoxin.
E. coli phages (T7, f1, M13)	Subunit of T7 DNA polymerase. Participates in filamentous phage assembly.	Increases processivity, specific for thioredoxin-$(SH)_2$ but not dependent on oxidoreductase activity.
	Participates in filamentous phage assembly.	Thioredoxin is the only host *E. coli* protein required for phage assembly and export.
Bacteria and yeas	Hydrogen donor for 3 0-phosphoadenylsulfate (PAPS) reductases.	Assimilation of sulfur by sulfate to sulfite reduction.
Plants	Regulation of chloroplast photosynthetic enzymes.	Photosynthesis regulation by light via ferredoxin.
Mammals	Redox regulation of transcription factors, e.g. NFkB, AP-1.	Different transcription factors are either activated or inhibited by Trx, which also may exert different activities in the nucleus compared to cytosol.
	Regulation of apoptosis.	Thioredoxin-$(SH)_2$ but not thioredoxin-S_2 makes a complex with ASK1, preventing downstream signaling for apoptosis.
	Immunomodulation.	Extracellular thioredoxin is both, a co-cytokine and chemokine and a truncated form stimulates eosinophiles.
	Pregnancy.	Intracellular and extracellular synthesis of thioredoxin from cytotrophoblasts assist implantation and establishment of pregnancy.
	Birth.	Protection from hyperoxia at birth by induction of thioredoxin.
	CNS.	Thioredoxin secreted from glial cells promotes neuronal survival at ischemia/reperfusion.

.All Trx proteins have the catalytic motif WCXXC located on a highly conserved fold. The cysteine residues of this motif are the key players used by Trxs to break disulfide bonds in oxidized substrate proteins. Upon completion of a catalytic cycle, these two cysteine residues are oxidized and form a disulfide. They are converted back to the reduced state by

thioredoxin reductase (TrxR) at the expense of the reduced form of nicotinamide adenine dinucleotide phosphate (NADPH) (see Fig. 6).

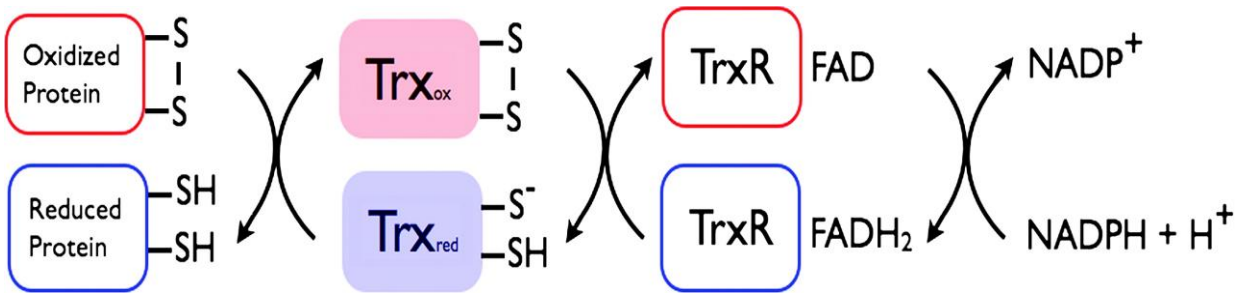

Figure 6: Electron flow from NADPH to oxidized substrate proteins. Schematic representation of the electron flow in which thioredoxin (Trx) reduces oxidized proteins with electrons coming from NADPH *via* the NADPH-dependent flavo-enzyme thioredoxin reductase (TrxR). Adapted from www.liebertonline.com/ars.

3.2.2 Structure of thioredoxins

The first structure of a Trx protein was described in 1975[77]. Nowadays, the crystal structures of many oxidized and reduced Trxs are known. The fold of Trxs consists of five β-strands surrounded by four α-helices. The β -sheets and α-helices can be divided in an N-terminal β_1 α_1 β_2 α_2 β_3 and a C-terminal β_4 β_5 α4 motif, connected by the α_3-helix (see Fig. 7)[77]. The β -strands of the N-terminal motif run parallel, and the strands of the C-terminal motif run anti-parallel. The α_2 and α_4 helices are located on one side of the central β-sheet, while the α_3-helix is located on the opposite side. The α_3-helix is orientated perpendicularly to helices α_2 and α_4. The catalytic CGPC motif is located on the surface of the protein in a short segment at the amino-end of the α_2-helix.

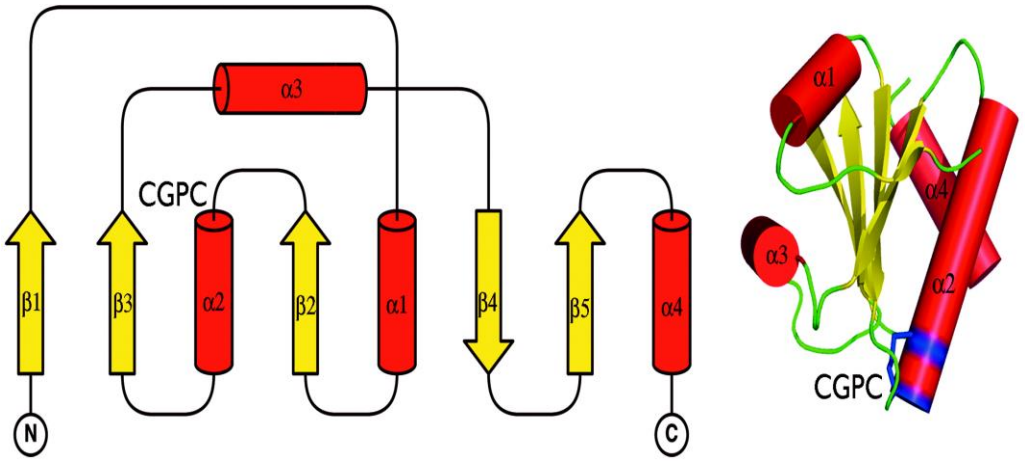

Figure 7: The secondary and three-dimensional structures of Trx (PDB code: 2O7K)[78].

The shortest version of this fold is known as the Trx fold with the lack of the β_1-strand and the α_1-helix[79]. The Trx fold comprises the complete structural fold of glutaredoxins (see Fig. 8)[80] and it is also observed in protein disulfide isomerases[81], disulfide oxidases[82], glutathione transferases[83], glutathione peroxidases[84], chloride intracellular channels (CLIC)[85] and the DsbG protein that controls the level of sulfenylation in the periplasme[86]. Thus, the Trx-fold has been used as a conserved protein fold to engineer proteins for particular tasks. Most of the proteins with a Trx-fold present a conserved CXXC catalytic motif[87, 88].

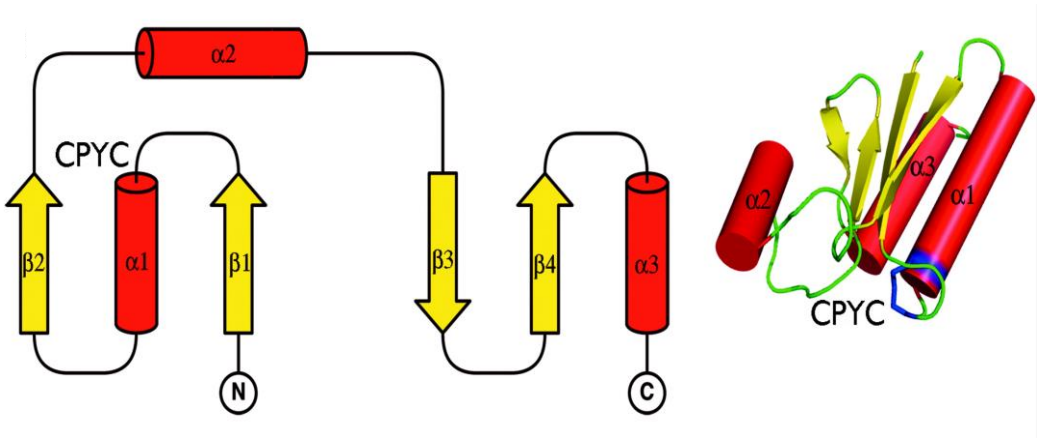

Figure 8: The secondary and three-dimensional structures of glutaredoxin (PDB code: 1EGO)[89].

3.2.3 Conserved residues in thioredoxins

Several residues that play important structural and catalytic roles are conserved among Trx proteins (see Fig. 9). Two of them, the cysteine residues are found in the catalytic site and are essential for the activity of Trxs. The other conserved residues are not strictly required for activity, but dictate the thermodynamic and redox properties of the protein.

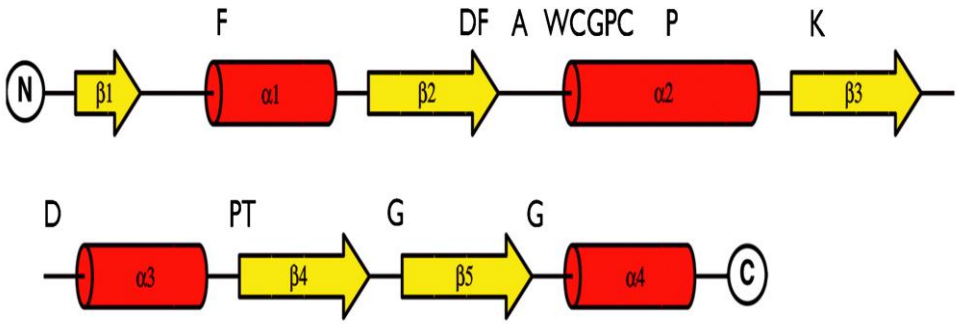

Figure 9: Conserved residues in Trxs. The conserved sequence amino acids of the Trx proteins family are shown in one letter code on top of the secondary structure[90].

Trxs are also characterized by the presence of three conserved prolines; with the first one located between the catalytic cysteine residues of the CGPC motif. This proline is the key residue that determines the reducing power of Trxs; replacing it by a serine or a threonine has a dramatic effect on the redox and stability properties of the protein[91, 92]. The second conserved proline is located five residues after the catalytic motif. This proline residue introduces a kink in the α_2-helix, which separates the CGPC motif, located at the amino end of the α_2-helix, from the rest of the helix. Mutating this residue destabilizes the Trx structure but has no effect on the redox properties of the protein[93, 94]. The third proline is positioned on the opposite side of the CGPC active site motif. This proline is always found in cis-conformation and it is important for maintaining both, the conformation of the active site and the redox potential of the protein. Replacing it by an alanine has an effect on the efficiency of catalysis[95].

A conserved threonine is located next to this cis-proline. This residue is involved in structuring the region opposite to the CGPC active site motif. The side chain oxygen (Oγ1) of this threonine forms hydrogen bonds with the main chain oxygens of the cis-proline and of the former residue[87].

Several aromatic residues are conserved in Trxs. First, there are two phenylalanine residues located in the N-terminal α1-helix and at the end of the β_2-strand, respectively. These residues are both part of the same internal hydrophobic cluster in which several

isoleucine and valine residues of the central β-sheet are also involved[87]. This cluster is structurally important so that the N-terminal phenylalanine positions the α1-helix correctly.

Three glycine residues are conserved among Trxs. The first one, which is in the CGPC motif, maintains the conformation of the active site and influences the redox potential. The other two flank the β_5-strand and determine its length. They are structurally important as they are found at equivalent positions for this type of turn in other structures[96, 97].

There is also a conserved tryptophan, located directly before the CGPC sequence motif. This residue is important for the thermodynamic stability of Trx[98]. The conserved alanine, which is located in the turn before the tryptophan, is in van der Waals contact with this residue. It is important to have a small residue at this position, like an alanine, because a larger residue would shift the position of the indole side chain. Both the tryptophan and the alanine form a structural cluster in which there is also a conserved aspartate located in the turn between β_3 and α_3.

Noticeably, a mutant of Trx in which this tryptophan is replaced by an alanine has the tendency to form a domainswapped dimer that is devoid of any of the biochemical activities known for Trx-fold proteins. This domainswapped dimer is kinetically stable for a long time and might be an example of how multimeric proteins evolved from their monomeric ancestors by domain swapping[99, 100].

Finally, Trxs contain two conserved charged residues, an aspartate and a lysine located in the β_2-strand and the β_3-strand, respectively[101]. They are part of a charged region and are present between the β-sheet and the kinked α_2-helix. This region is shielded from the environment by the disulfide that is present in the oxidized state of the protein. For a long time this aspartate has been considered to be the key residue responsible for activating the C-terminal cysteine of the CGPC motif as a nucleophile[102]. Results reported recently give the suggestion that it is not the case[103]. The results showed that the C-terminal thiol can be activated even in the absence of the aspartate and that the distance between the oxygens ($O_{\sigma 1}$ and $O_{\sigma 2}$) of the aspartate and the C-terminal thiol (S_γ) increases up to 10 Å in the mixed disulfide complex, preventing them from interacting. They proposed that the C-terminal thiol is activated by hydrogen bonds to backbone amides[103]. All conserved residues are shown in Fig. 10.

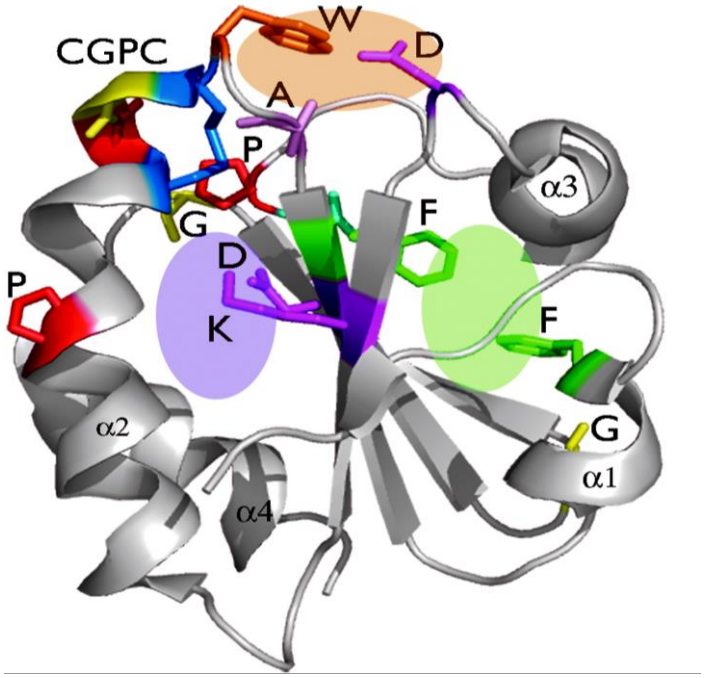

Figure 10: Conserved residues in Trxs. The conserved regions are located in the center and around the active site of Trx. The conserved residues are shown in stick presentation. Tryptophan (orange), charged residues (magenta), cysteines (blue), glycines (yellow), phenylalanines (green), and prolines (red). The hydrophobic region (green), the charged region (magenta), and the exposed structural cluster (orange) are indicated with a semitransparent oval shape.

3.2.4 Reaction mechanism of thioredoxins

The reaction catalyzed by Trx can be regarded as a transfer of the disulfide bond from the substrate protein to Trx. In other words, the electrons coming from Trx are shuttled to the substrate protein. Thus, in spite of the reducing environment of the compartment in which they are usually located, Trx forms a disulfide bond after a single catalytic cycle. The disulfide bond is not a structural disulfide, but functions as a redox switch. It is surface exposed and is only accessible from one side of the protein[104]. Oxidized Trx is more stable than reduced Trx. The difference in stability between the oxidized and reduced states of Trx provides the necessary driving force for the reaction and predicts the way in which the reaction is thermodynamically favourable.

The reaction starts with a nucleophilic attack of the N-terminal thiol of the CGPC motif on the disulfide of the target protein, releasing a free thiol and forming an intermolecular disulfide between Trx and the target protein. This first step of the mechanism depends on the low pKa value of the N-terminal cysteine within the CGPC motif, which is significantly lower than the pKa of free cysteine residues in solution[105]. Under physiological conditions, a large fraction of the sulfur of the N-terminal cysteine is therefore

present as a thiolate and enables this residue to attack disulfides in proteins as a nucleophile. The low pKa value results from the stabilization of the negative charge of the thiolate anion *via* the formation of hydrogen bonds between the sulfur of the cysteine and its neighbouring residues[106]. In contrast, the sulfur of the C-terminal cysteine has a high pKa and is present as a thiol. This contributes to stabilizing the N-terminal thiolate, thus increasing the reaction rate[107]. Once the intramolecular disulfide has been formed between Trx and its substrate, the C-terminal thiol has to be activated as a thiolate to allow the dissociation of the complex.

The dissociation mechanism of a Trx intermolecular disulfide complex has been discovered controversy for years. It now appears that the C-terminal cysteine is stabilized as a thiolate by hydrogen bonds between this residue and the backbone amides of the active site tryptophan and of the N-terminal cysteine. As a consequence, the pKa of the C-terminal cysteine is in the intermolecular disulfide complex[103]. The last step of the catalytic cycle also needs to be completed with the correct selectivity based on quantum chemical calculations[108]. The mechanism behind the favoured reaction during complex dissociation is the C-terminal cysteine of Trx, which attacks the intermolecular disulfide complex on the N-sterminal cysteine of Trx and not on the cysteine from the substrate protein. This results in a reduced substrate protein and oxidized Trx. Trx is then reduced by TrxR at the expense of NADPH, enabling the protein to start another reaction cycle[109]. The reaction mechanism of the disulfide reduction by thioredoxin is shown in Fig. 11.

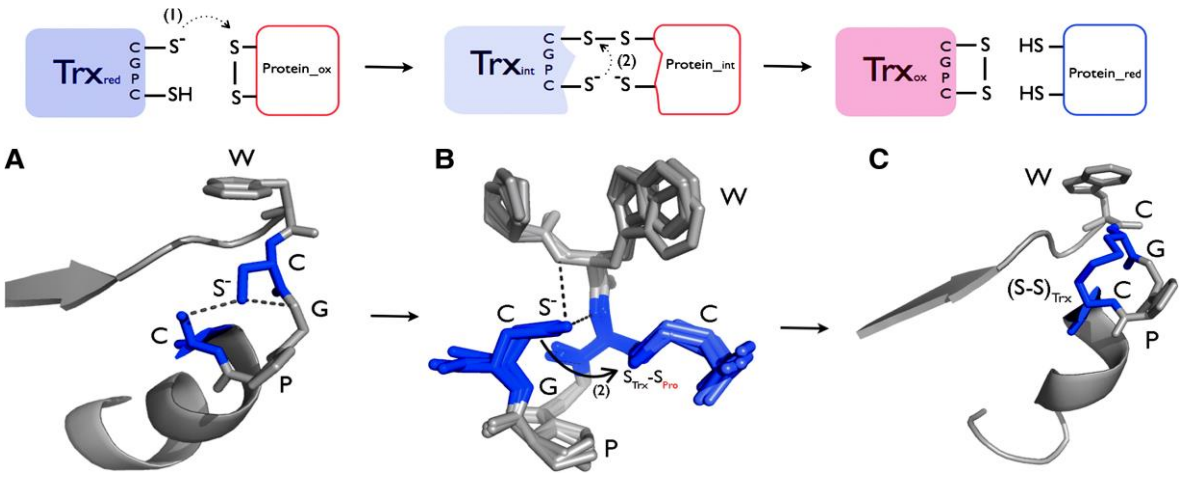

Figure 11: Reaction mechanism of disulfide reduction by thioredoxin.

3.2.5 Thermodynamic stability of Trx

The reduced form of Trx is less stable than the oxidized Trx form. The difference in the stability between the two forms provides the driving force for the reaction and predicts the reaction as thermodynamically favourable (see Fig. 12).

There are some factors that affect the rate of the thiol-disulfide exchange, the pKa of the nucleophillic cysteine[110], the electrostatic environment near the amino acid[107, 111], the geometry to form a linear transition state[112], the molecular strain[113] and the entropy [114], furthermore, the pH of the surrounding solvent[115] and the pKa of the leaving thiol groups of the oxidized substrate [110].

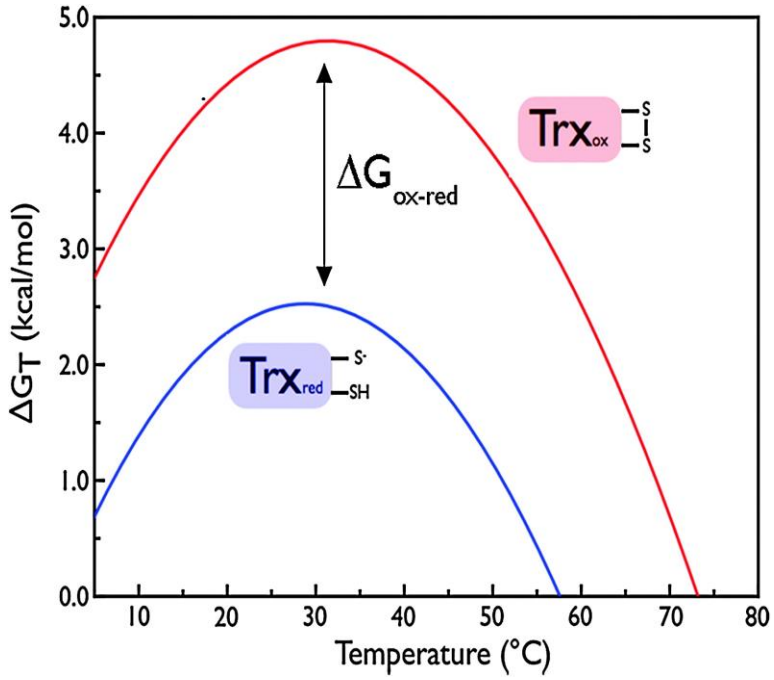

Figure 12. Thermodynamic stability of Trx. The stability of oxidized Trx (red curve) is higher in comparison with reduced Trx (blue curve).

3.2.6 Trapping of Trx substrate

Thioredoxins play a centre role in living cells and they are almost at the intersection between different processes. Several techniques have been developed in order to identify the interaction proteins with Trx. Three of the most commonly used techniques to trap Trx substrate are explained below (see Fig. 13).

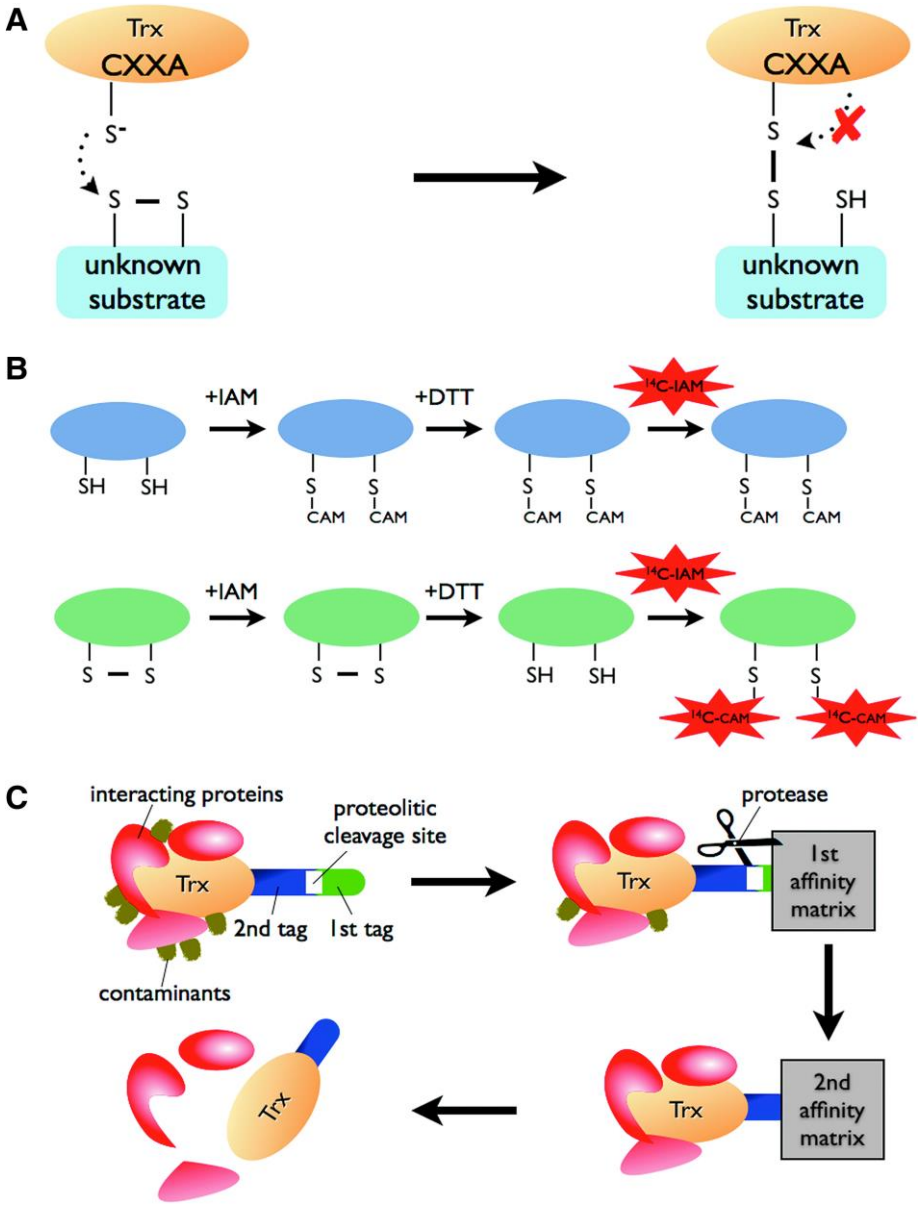

Figure 13: Trapping thioredoxin substrates. (A) Mutation of the second cystein in the CXXC active motif allows the trapping of Trx substrate and formation of stable complex. (B) The accessible thiols groups are methylated with iodoacetamide (IAM) to keep the protein reduced. The disulphide bonds are then reduced by DTT and the newly accessible thiols are then labelled with radioactive ^{14}C-IAM. (C) The TAP-tag at the C-terminus of Trx allows purification of the complex involving Trx and protein-protein interaction using two affinity columns. A protease cleavage site is present between the tags, allowing the removal of the most C-terminus located tag before starting the second affinity purification.

The first technique is the mutation of the second Cys in the active site motif CXXC to an alanin[116]. It is well known that the second Cys in the active site is responsible for the dissociation of the mixed disulfide complex. Mutation of this Cys prevents the dissociation and allows the formation of a stable complex between Trx and its substrate. The mutant protein can be expressed and the complex can be purified using affinity chromatography[86]. Alternatively, the mutant can be mobilized on a resin and used to capture target proteins in cellular extracts[117-119].

The second technique depends on the differential labelling of reduced and oxidized cysteines. Various molecules and protocols can be used; the principle is similar within these techniques and comprises the modification of the reduced cysteine residues with small molecules, such as iodoacetamide. The oxidized cysteines are thereafter reduced and modified with other molecules, such as 4-vinylpyridine[120] or *N*-ethylmaleimide[121, 122]. The proteins are then analyzed by mass spectroscopy and the difference in mass is used to define whether the cysteines were either reduced or involved in disulfide bonds in the cell. Alternatively, the cysteine residues can be modified by two different isotopes of the same molecule, light (^{12}C) and heavy (^{13}C or ^{14}C) and by iodoacitamide-based Isotope Coded Affinity Tag reagents (ICAT)[123, 124].

The third technique makes use of identifying Trx substrates by purifying proteins bound to Trx applying Tandem Affinity Purification (TAP), followed by ms/ms mass spectrometrical analysis[125]. The TAP-tag was attached to the C-terminus of Trx (Ec-Trx1) and the Trx substrate complexes were then purified with two different affinity columns to preserve the protein-protein interaction. More than 80 *E. coli* proteins co-purifying with Ec_Trx1 have been identified this way, involving Ec_Trx1 in at least 26 several cellular processes.

3.2.7 Diversity within an ubiquitous family

3.2.7.1 Bacterial thioredoxin

Thioredoxin 1 (Ec_Trx1) and thioredoxin 2 (Ec_Trx2) are two reductases present in the cytoplasm of *E. coli*. Ec_Trx1 contains 108 amino acids. This has become the model of the Trx superfamily. In addition to ribonucleotide reductase, Ec_Trx1 catalyzes the reduction of other cytoplasmic proteins, such as methionine sulfoxide reductases and 3-phosphoadenosine 5-phosphosulfate (PAPS) reductases[62]. Moreover, Ec_Trx1 is required for the growth of several bacteriophages including T7, M13, and f1[126]. Ec_Trx1 also binds to the DNA polymerase encoded by the viral genome and increases its processivity by remodelling the protein to favour its interaction with DNA as well as other replication proteins[127]. In 1974, a deletion mutant strain that completely lacked Ec_Trx1 has been isolated[128]. This indicated that other cytoplasmic proteins were able to reduce ribonucleotide reductase. The search for alternative hydrogen donors led to the discovery of several glutaredoxins and of a second thioredoxin, Ec_Trx2[129].

Ec_Trx2 shares 28% sequence identity with Ec_Trx1. It is able to reduce ribonucleotide reductase, DsbD, and PAPS reductase. Ec_Trx2 has two characteristics that differentiate it from Ec_Trx1 and suggest that this protein may have a specific cellular function. First, the expression of Ec_Trx2 is controlled by OxyR, a transcription factor that controls a response to oxidative stress[130]. Second, Ec_Trx2 possesses presents an additional N-terminal domain of 32 amino acids that contains two CXXC motifs (see Fig. 14). It was found that these additional cysteine residues bind Zn^{2+} with an extremely high affinity ($10^{18}M^{-1}$)[131]. These zinc-binding CXXC motifs are conserved in all Ec_Trx2 homologues that have been identified so far, making Ec_Trx2 the prototype of a new zinc binding Trx family.

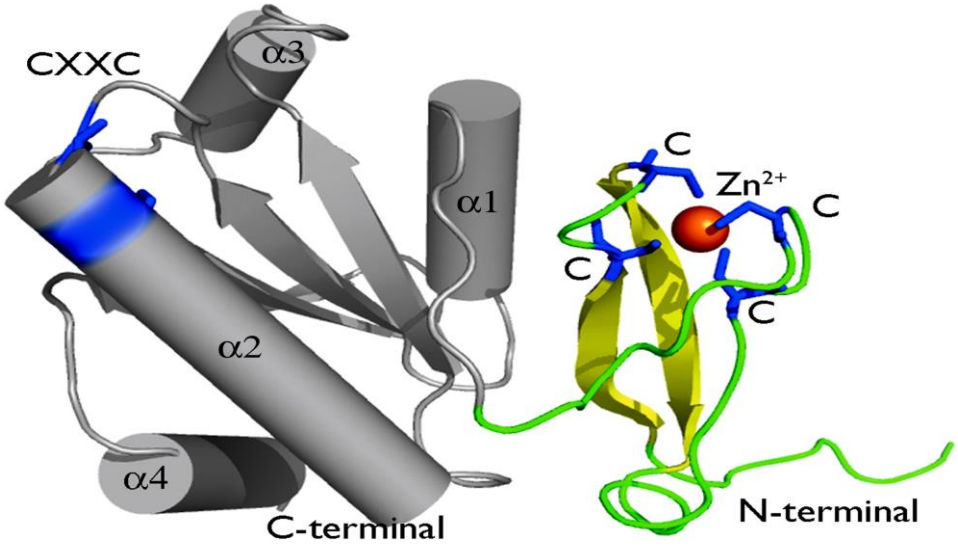

Figure 14: Trx2 from *Rhodobacter capsulatus* (PDB code: 2PPT).

3.2.7.2 Yeast and mammalian thioredoxins

In the yeast *Saccharomyces cerevisiae*, there are two cytosolic (Sc_Trx1, Sc_Trx2) and one mitochondrial (Sc_Trx3) Trxs[132]. Yeast mutants lacking both cytosolic Trxs are viable. They have a longer S phase in their cell cycle and are auxotrophic for sulfur amino acids[133]. Mutants lacking Sc_Trx3 are hypersensitive to hydroperoxide. Thus, Sc_Trx3 seems to function as an antioxidant against ROS generated in mitochondria[134].

Mammalian cells possess two Trx isoforms, ma_Trx1, which is present in the cytosol, and ma_Trx2, which contains a 60 residue N-terminal sequence and is present in the mitochondria. Although ma_Trx1 has no nuclear localization sequence, it has also been detected in the nucleus of certain normal and tumor cells[135]. In addition to the catalytic cysteines present in the CGPC motif, ma_Trx1 contains 3 extra cysteine residues. Two of these cysteines (C_{62} and C_{69}) flank the α_3-helix that links both motifs of the Trx-fold and the third extra cysteine (C_{73}) is located in a turn close to the active site CGPC motif[136]. These extra cysteines are involved in regulating the function of Trx *via* post-translational modifications, such as glutathionylation and S-nitrosylation[137]. Furthermore, under oxidizing conditions, a disulfide can be formed between C_{69} and C_{72}. The formation of this disulfide is predicted to have a profound effect on the structure of Trx and decreases the rate by which the active site is regenerated by TrxR [138].

3.2.7.3 Plant thioredoxins

Plants have the greatest group of Trxs found in all organisms. For example, at least 20 Trx genes have been detected in the genome of *Arabidospis thalianaand*. It is likely that the variety found in *A. thalianais* is representative for higher plants, such as poplar, pinus and tomato[139]. On the basis of their sequence, plant Trxs can be divided into six major groups: Trx f, h, m, o, x, and y.Whereas the Trxs m, x, and y are related to prokaryotic Trxs, the Trxs f, h, and o are specific to eukaryotic organisms. Plant Trxs are found in the cytoplasm, mitochondria and chloroplasts. Mitochondrial and cytoplasmic Trxs can be reduced by TrxR reductase, whereas Trxs present in chloroplasts are recycled by a ferredoxin-thioredoxin reductase (FTR)[139]. Although plants Trxs possess the classical structural features of Trxs, some of them have specific characteristics. For example, Poplar Trx h has an additional cysteine residue playing a role in an atypical catalytic mechanism. Furthermore, some Trxs h have an unusual CXXS active site motif and are recycled by glutathione, whereas others have a canonical CGPC motif and are reduced by glutaredoxins [140].

Recently, the crystal structures of thioredoxins from various parasites like *Plasmodium falciparum, Trypanosoma brucei* and *Schistosoma mansoni* have also been determined to 1.8, 1.4 and 1.6 Å resolution, respectively [141-143].

4. Materials and Methods

4.1 Materials

4.1.1. Plasmid

pRSET B plasmid (Invitrogen) is a pUC-derived expression vector designed for high level protein expression and purification. Expression of the gene of interest in controlled by the strong phage T7 promoter and provides an ampicillin resistance gene. In addition, DNA inserts are located downstream and in frame with a sequence that encoded an N-terminal fusion peptide. This sequence includes an ATG translations initiation codon, a 6-fold polyhistidine tag that functions as a metal binding domain in the translate protein, a transcript stabilizing sequence from gene 10 of phage T7, the Xpress ^{TM} epitope, and the enterokinase cleavage recognition sequence, as show in Fig. 15.

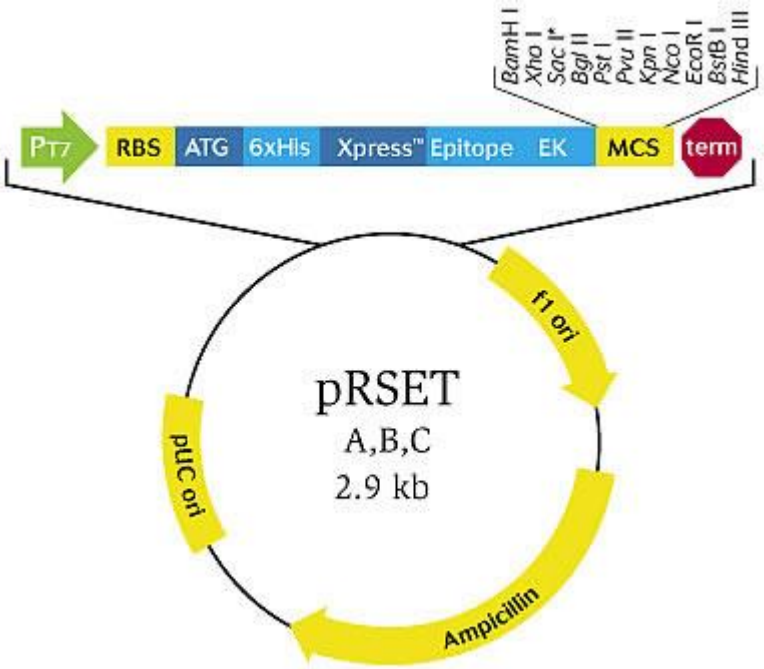

Figure 15: Vector map of pRSET B

4.1.2. Laboratory equipments

Beamline	X13 consortium beamline, HASYLAB/DESY, Hamburg, GERMANY Synchrotron source: bending magnet Focal spot: 2 mm x 0.4 mm Detector MARCCD 165 mm
Centrifuges	Centrifuge 5804R (Eppendorf, Germany) Centrifuge 5415R (Eppendorf, Germany) Centrifuge 5424R (Eppendorf, Germany) Centrifuge 5415C (Eppendorf, Germany) Megafuge, 1.0 R (Heraeus)
PCR machine	Mastercycler personal (Eppendorf)
Spectrophotometer	GeneQuant 1300 (GE Healthcare, UK)
Water baths and Incubators	Kelvitron (Thermo scientific, USA) GLF 3033 (GLF, Germany)
Thermoblock	Thermostat 3401 (Eppendorf, Germany)
Crystallization robot	Honeybee 961 (Genomic Solutions, USA)
DLS instrumentation	SpectroSIZE 300 (Nabitec, Germany)
Crystal plate incubator	RUMED 3001 (Rubarth, Germany)
Microbalance	Sartorius TE3102S (Sartorius, Germany) Sartorius LP224S-0CE (Sartorius, Germany)
pH Meter	Five Easy FE20 (Diversified Scientific Inc., USA) pH 211 (Hanna Instruments, USA)
FPLC machine	ÄKTA Purifier P-901 (GE Healthcare, UK)
Photospectrometry	Nanoprop 2000c (ThermoScientific, Peqlab, Germany)
Pippetting robots	Lissy (Zinsser, Germany)
SDS-PAGE	EV734 Power Supply (Consort, Belgium) Hoefer Mighty Small II SE 250 Electrophoresis chamber (Hoefer, USA)

Agarose gels	Horizon 11.14 (Biometra, Germany) PowerPac Basic (Bio Rad, USA)
Tube Rotators	Roller mixer SRT6D (Stuart, UK) Rotor SB3 (Stuart, UK)
Micropipettes	Micropipettes Research (Eppendorf, Germany)
Thermomixer	Thermomixer comfort (Eppendorf, Germany)
UV- light source	CrystalLIGHT 100 (Nabeitec, Germany)
Microwave	MR-6450 (Hitachi, Japan)
Scanner	Canon 9950S (Canon, USA)

4.1.3. Chemicals, reagents and kits

Sigma-Aldrich Chemie	β-Mercaptoethanol Bromphenol blue Di Methyl Sulfoxide (DEMSO)

3.1.4. Molecular weight markers

Protein markers	Bench Mark prestained protein ladder (Invitrogen, Karlsruhe, Germany) Magic Mark Western standard (Invitrogen, Karlsruhe, Germany)
DNA marker	1kb DNA ladder, (Invitrogen, Karlsruhe, Germany)

4.1.5. Buffers and solutions

For all buffer preparations double distilled water was used.

Phosphate buffer	0.5 M K_2HPO_4 with 0.5 M KH_2PO_4, pH 7
PBS	20 mM phosphate buffer pH 7.2 with 120 mM NaCl
TBS	20 mM Tris / HCl pH 8,0 and 5 mM EDTA
DNA loading buffer	30% Glycerol

	0.25% Bromophenol Blue 0.25% Xylene Cyanol
Electrophoresis buffer (1x)	100 ml/ 10x TG-buffer 10 ml/ 10% SDS
5x protein loading buffer	250 mM Tris-HCl, pH 6.8 500 mM DTT 0% SDS 0.5% Bromophenol blue 50% Glycerol
10x TBE buffer	1.8 M Tris-base 1.8 M Boric acid 20 mM EDTA
Ethidium bromide	10 mg/ml in dH_2O

4.1.6 Bacteria culture media

LB	1.0 % Bacto-Trypton, 0.5 % Bacto-Yeast-Extract, 1.0 % NaCl in dH_2O, Autoclaved For LB-agar: 1.5 % agar in LB-medium
Selective antibiotic	50 mg/ml ampicillin in 50 ml water; stock solution 25 mg/ml chloramphenicol in 50% ethanol (abs.); stock Solution
IPTG	1 M in dH_2O, Autoclaved; stock solution
Protein purification	
Lysis buffer	10 mM Tris-HCl pH 8.0 and 5 mM EDTA
Wash buffer	20 mM Tris-HCl pH 8.0, 5 mM EDTA and 10 mM NaCl
Elution buffer	20 mM Tris-HCl pH 8.0, 5 mM EDTA and 100 mM NaCl
Gel Filtration buffer	20 mM Tris-HCl pH 8.0 and 5mM EDTA and 100mM NaCl
Competent cells	100 mM $CaCl_2$, autoclaved 10 % glycerol

SDS-PAGE	
1 x running buffer	129 g glycin, 25 mM tris, 0.1 % SDS in dH_2O
6 x sample buffer	2 % SDS (w/v), 50 mM tris, pH 6.8, 10 % glycin (w/v), 0.02 % bromophenol blue (w/v), 0.05 % β-mercaptoethanol (v/v)
APS	10 % in dH_2O
Stacking gel buffer	0.5 M Tris/HCl, pH 6.9
Separating gel buffer	1.5 M Tris/HCl, pH 8.9
SDS buffer	10 % (w/v) in dH_2O
Staining solution	45 % Methanol (v/v), 10 % glacial acetic acid (v/v), 0.1 % Coomassie blue in dH_2O
Destaining solution	45 % methanol (v/v), 10 % glacial acetic acid (v/v), in dH_2O
Q-Sepharose regeneration	
Wash buffers	1 M NaCl, 2 column volume 100 mM NaOH, 2 column volume 70 % ethanol, 2 column volume Binding buffer
Equilibrium buffer	10 mM Tris-HCl pH 8.0 and 5mM EDTA

4.2 Methods

4.2.1 Molecular biology methods

4.2.1.1 Polymerase chain reaction (PCR)

PCR were used for DNA fragment amplification using *Taq*-polymerase containing PCR supermix (Invitrogen, USA). The reaction was carried out using a mastercycler personal (Eppendorf, Germany) and the mix was applied according to the standard's protocol.

For the reaction, primers (Invitrogen, Germany) were diluted to a final concentration of 30 pM and 1 µl of each forward and reverse, 1 µl (approximately 100 ng) template and 47 µl PCR supermix were mixed in a PCR tube. The first step in the amplification reaction was denaturation for 5 min at 95 °C followed by 30 cycles of denaturtion for 45 s at 95 °C, annealing for 1 min at 65 °C (based on the oligonucleotide annealing temperature, determined by the supplier) and followed by elongation for 2 min at 72 °C (this step could be modified based on the number of basepairs to be amplified, as *Taq*-polymerase is able to amplify 1,000 basepairs per minute). When the reaction was carried out overnight, samples were stored at 4 °C within the PCR machine. The success of the PCR product was applied to 1 % agarose gel.

4.2.1.2 Cloning of *Wb*Trx-1 in pRSET B vector without His-tag

The open reading frame of *Wb*Trx-1 was amplified by polymerase chain reaction (PCR) from pRSET B vector that encode for the cDNA of *Wb*Trx-1 gene. The following primers were used to clone the gene of interest between NdeI and XhoI as restriction sites.

Forward primer:

5´ GGGAATTCCATATGATGGCTGATTTACTTGCT 3´

Reverse primer:

5´ AACTCGAGTGAGCGGCAGCATTA 3´

To perform PCR, a 50 µl reaction mixture was set up in 0.5 ml tube containing DNA template (20-50 ng), 1 µl dNTPs mix (12.5 mM), 1 µl forward and reverse primers (100 nM), 10x DNA polymerase buffer (10% of total volume), *Taq* DNA polymerase (5-10), and the required volume of ddH_2O. The PCR amplification was performed on a mastercycler personal (Eppendorf, Hamburg, Germany) using the following cycling condition:

Initial denaturation	96 °C	2 min.	
Denaturation	96 °C	30 sec	
Annealing	54 °C	1 min.	→ 30 cycles
Elongation	72 °C	1 min	
Final elongation	72 °C	5 min	

4.2.1.3 Purification of DNA

The amplified DNA was purified using the peqGOLD DNA extraction kit (peqLab, Erlangen, Germany), according to the manufactures protocol.

4.2.1.4 Restriction digestion of DNA fragments

The amplified DNA fragments as well as the pRSET B vector were digested using 2 units of both NdeI and XhoI restriction endonucleases per µg DNA and the recommended buffer in a final volume of 50 µl. The reaction was performed at 37 °C

4.2.1.5 Dephosphorylation of plasmid DNA

After digestion, the pRSET B vector was dephosphorylated by addition of 1µl calf intestinal alkaline phosphates (CIAP) followed by incubation at 37 °C for 1h, while the digested DNA fragments were stored in ice. The digestion products were purified using the nucleospin extract II kit (Macherey-Nagel, Duren, Germany), following the PCR product purification protocol of the supplier.

4.2.1.6 Ligation

Plasmid vector and DNA fragments were ligated using a molecular ratio of 1:5 by T4 ligase (2 units) and 10x ligation buffer in a total volume of 40 µl. The reaction mixture was incubated overnight at 18 °C. Afterwards the ligation mixtures were directly incubated at 60 °C for 30 min to kill the ligase enzyme and the reaction mixture was transformed into TOP 10 or DH5α *E.coli* cells. The cells were plated out onto an agar plates containing 100 µg/ml ampicillin and incubated overnight at 37 °C.

4.2.2 Mutagenesis

4.2.2.1 Site directed mutagenesis

The mutagenesis was carried out to replace the two active site amino acid cysteines by amino acid serine one by one in two different colons Cys39ser and Cys42ser. The random mutagenesis libraries by Megaprimer PCR for the whole plasmid (MEGAWHOP) were used. MEGAWHOP protocol is especially ideal for creating random mutagenesis.

The following primers were designed for each mutation to change the cysteine coding base pairs into serine coding base pairs.

Forward primer:

Cys39ser: **GCACATTGGAGCCCACCGTGA**

Cys42ser: **TGCCCACCGAGCCGACAATTT**

Reverse primer:

GCTAGTTATTGCTCAGCGGTG

The reaction mixture was used as follows:

10x reaction buffer	5µl
Plasmid DNA	50 ng
Primer (sense)	125 ng
Primer (anti-sense)	125 ng
dNTPs (12.5 mM)	1 µl
Adjust to 49 µl with dd H_2O	
Pfu DNA polymerase	1 µl

The primer *Wb*Trx-1-Cys39Ser*f*, *Wb*Trx-1-Cys39Ser*r*, *Wb*Trx-1-Cys42Ser*f* and *Wb*Trx-1-Cys42Ser*r* were used to point mutation as well as to amplify the whole plasmid including the mutated genes using the following cycling:

Initial denaturation	95 °C	30 sec.	
Denaturation	95 °C	30 sec	
Annealing	55 °C	1 min.	→ 25 cycles
Elongation	68 °C	2 min	

4.2.2.2 Site directed mutagenesis of overlap extension

Mutation of the entire active site cysteines residues Cys_{39} and Cys_{42} into serine residues has been performed by PCR-based method of overlap extension for the whole plasmid pREST B-*Wb*Trx-1- NdeI and pREST B-*Wb*Trx-1- XhoI served as a template and Megaprimer PCR forward and reverse was used as to induce site specific mutation using the following PCR cycling reaction:

Initial denaturation	95 °C	2 min.	
Denaturation	95 °C	30 sec	
Annealing	65 °C	30 sec.	→ 30 cycles
Elongation	72 °C	30 sec.	

The PCR product was digested with 1 µl *DpnI* restriction endouuclase for 1h at 37 °C. *DpnI* only removes methylated parental DNA. The PCR product was transformed into *E.coli* DH5α cells and incubated overnight at 37 °C. The resulting colonies that carry the mutated plasmid mutation were confirmed by DNA sequencing.

4.2.2.3 Removal of template-DNA from a PCR reaction

After PCR, the template-deoxyriboneucleic acid (DNA) has to be removed from the mixture. This reaction is carried out by *DpnI* restriction endonuclease (NEB, USA). It specifically cuts methylated and hemi-methylated DNA with the motif GA-(CH_3)-TC.
For digestion 1 µl (20 U) of *DpnI* was added to 45-50 µl of the PCR reaction and incubated for 1-2 h at 37 °C. After that, the DNA was purified using the PCR purification kit (Invitrogen, USA).

4.2.2.4 DNA purification

The purification of PCR products from salts and restrictions enzymes, the PureLink PCR purification kit was used according to the manufacture's specifications. Instead of elution buffer, 50 µl dH_2O autoclaved was used to elute DNA.

4.2.2.5 Agrose gelelectrophoresis

Agarose electrophoresis is a technique to separate DNA fragments based on their size. Negatively charged DNA is attached by the anode and moves through an agarose gel depending on agarose concentration, size and conformation of the fragment and applied power. Typically 1 g of agarose was heated in 100 ml 1x TBE buffer. The solution was

cooled to 50 °C and 5 µl ethidium bromide solution (Sigma, USA) were added to visualise DNA fragment with UV-light.

Samples were mixed with 5x loading buffer containing glycerol to increase the density of the solution. To run the gel, 100 V were applied to the agarose gel apparatus. The result was documented with a photo applaying UV-light.

4.2.3 Preparation of chemically competent cells with $CaCl_2$

A single *E.coli* colony or 200 µl from glycerol stock were used to inoculate 100 ml Luria Bertani (LB)-medium and incubate overnight at 37 °C. The over night culture was diluted to 1:50 in LB-medium (10 ml of overnight culture was added to 500 ml LB-medium) and grow at 37 °C to an optical density at 600 nm of 0.6-0.8.

Reaching the required OD_{600}, the solution was cooled immediately on ice for 10 min and centrifuged at 4 °C and 4,000 rpm for 10 min.

The supernatant was discarded and the cells were resuspended in a sterile solution containing 0.1 M $CaCl_2$ and incubated for 15 min on ice.

This suspension was again centrifuged at 4 °C and 4,000 rpm for 10 min and the supernatant was discarded. The cells were resuspended in 5 ml cold 0.1 M $CaCl_2$ / 10 % glycerol containing buffer. Aliquots of 200 µl were shock frozen in liquid nitrogen and stored at -80 °C.

4.2.4 Isolation and purification of plasmids

A single *E.coli* colony was used to inoculate 3 ml LB-medium containing selective antibiotic and incubate at 37 °C overnight. Plasmids were isolated with the peqGOLD plasmid Miniprep Kit (peqlab, Germany) according to the manufacture's protocol.

4.2.5 DNA-Sequencing

To investigate the success of cloning or mutation insertion plasmid DNA was sequenced by SeqLab with extended hotshot sequencing. Samples were prepared by mixing 6 µl of DNA with 1 µl of sequencing forward or reverse primer.

4.2.6 Transformation of plasmid into *E.coli* cells

An aliquot of chemically competent cells was thawed on ice and incubate with 100 ng of the plasmid DNA for 10 min on ice. A water bath (GFL, Germany) was preheated to 42 °C

and cell-DNA mixture was incubated for 1 min at 42 °C. Subsequently the sample was cooled on ice for 1 min and 1 ml sterile LB-medium was added. The suspension was then incubated for 30 min at 37 °C. After that, it was centrifuged at room temperature (RT) for 30 s and the supernatant was decanted. Cells were resuspended with residual LB-medium and plated in a sterile environment (Plates containing 1.5 % agar-agar and respective antibiotic for selection). After incubation overnight at 37 °C, colonies were picked and further analysed. For subsequent DNA isolation, competent *E.coli* XL10-Gold, Top10 or DH5α cells, for expression DE3 (pLysS) cells were used for transformation.

4.2.7 Preparation of glycerol stocks

For glycerol stock preparation, respective plasmids were transformed into *E.coli* DE3 (pLysS) expression cells and plated on LB-Amp agar. An overnight culture was inoculated with a single colony and incubated at 37 °C. 600 µl of overnight culture were mixed with 400 µl of sterile glycerol and stored at -80 °C.

4.2.8 Cell disruption for protein purification

Bacterial pellets were thawed at RT. After that, a spatula tip of lysozyme powder was added and suspension incubated at RT for 10 min. The cells were mixed with the protease inhibitor phenylmethylsulphoxide (PMSF) (Sigma, USA) to a final concentration of 100 µM and transferred to a glass beaker. Sonification was carried out with a Branson sonifier 250 (Emerson Electric Co, USA) for 10 min at 40 kHz output frequency. The lysate was centrifuged at 50,000 g and at 4 °C for 50 min. The cell pellet was discarded and the supernatant was used for purification.

4.2.9 Regeneration of Q-sepharose column

Remove ionically bound proteins by washing the column at 1 to 1.5 ml/min in a reversed flow direction with 2 column volumes (CVs) of a 1 M NaCl solution, contact time 10 to 15 minutes. Remove precipitated proteins, hydrophobically bound proteins and lipoproteins by washing the column in a reversed flow direction with 2 column volumes (CVs) of 1 M NaOH solution at a flow rate of 1.2 to 1.4 ml/min. Remove strongly hydrophobically bound proteins, lipoproteins and lipids by washing the column in a reversed flow direction with 2 column volumes (CVs) of 70% ethanol or 30% isopropanol at a flow rate of 1.2 to 1.4 ml/min. Apply increasing concentration gradients to avoid air bubble

formation, when using high concentrations of organic solvents. The column after cleaning, equilibrate with approximately 2 column volumes (CVs) of lysis buffer before use.

4.2.10 Expression of *Wb*Trx-1 wild type and *Wb*Trx-1-C39S variant

The open reading frame for *Wuchereria bancrofti* Trx-1 (Accession number AAN34968.1) and the active site mutant *Wb*Trx-1-C39S was initially amplified from genomic DNA; using PCR standered protocols and cloned into pRSET B expression vector (Invetrogen) via NdeI and XhoI restrictions sites. The resulting pRSET B-*Wb*Trx-1 plasmid was transformed into *E.coli* BL21 (DE3 plysS) (Novagen, USA). The cells were growing at 37 °C in LB medium, which was supplemented with 100µ ml^{-1}ampicillin and 34µ ml^{-1} chloramphenicol. The culture was growing until OD_{600} = 0.7 and IPTG (isopropyl-β-thiogalactoside) was added to the final concentration of 1 mM. The culture was growing for additional 3 hours and then the cells were harvested by centrifugation, resuspended in buffer (A) containing 10 mM Tris-HCl pH 8.0 and 5 mM EDTA and disrupted by sonication. The recombinant protein was obtained from the cytoplasmic fraction after ultracentrifugation at 39000g for 15 min.

4.2.11 Purification of *Wb*Trx-1 wild type and *Wb*Trx-1-C39S variant

4.2.11.1 Ion exchange chromatography

The Cytoplasmic fraction containing the recombinant *Wb*Trx-1 (*Wb*Trx-1-C39S) was applied to Q-sepharose high performance 75 ml column (Amersham Biosciences) equilibrated with buffer (A) (20 mM Tris-HCl pH 8.0 and 5 mM EDTA) and incubated for 2h. The column was washed first with buffer (A) containing 20 mM NaCl. The *Wb*Trx-1 recombinant protein was eluted with buffer (A) containing 100 mM NaCl.

4.2.11.2 Fast Protein Liquid Chromatography (FPLC)

The elution fraction from Q-sepharose column was further purified by size exclusion chromatography using Hiload 26/60 superdex 200 ml column equilibrated with buffer (A) (20 mM Tris-HCl pH 8.0, 5mM EDTA and 100 mM NaCl), and the pure protein was eluted with a linear gradient from 0 to 100% of the same buffer. All purification steps were performed at 4 °C and the pure protein was analyzed with SDS-PAGE and comassi blue[144].

4.2.12 Protein quantification with Nanodrop 2000c

The protein concentration was determined with a Nanodrop 2000c (Thermo Scientific, peqLab, Germany). 2 µl of protein buffer were pipetted to the sensor, the lever arm was brought down and measurement was blanked. For concentration determination, the procedure was repeated with 2 µl of protein solution. Measurements were carried out in duplicates.

Values for molar extinction coefficient (ε) and molecular weight were entered and the protein concentration was displayed by the software, calculated on the basis of Lambert-Beer –law.

$$A_{280} = \varepsilon * b * c$$

A_{280} = absorption at 280 nm

ε = molar extinction coefficient [M^{-1} cm^{-1}]

b = path length [cm]

c = protein concentration [mg/ml]

4.2.13 Enzymatic Assay for thioredoxin (*Wb*Trx-1)

To assay the thioredoxin aactivity, the thiol-disulfide oxidoreductase activity was measured using insulin (Sigma I5500) as an electron acceptor[145]. The reaction mixture (1 ml) containing 0.13 mM bovine insulin in 100 mM sodium phosphate buffer pH 7.0 was mixed with 6 µM of enzyme solution and incubates at room temperature. The reaction was started by adding 5µl of 100 mM dithiothreitol (DTT) and the increase of absorbency at 650 nm was monitored.

4.2.14 Inhibition of thioredoxin (*Wb*Trx-1)

The affinity of competitive inhibitor is described by the IC_{50} value. This value determines which inhibitor concentration is necessary to inhibit 50% of the enzyme activity. The IC_{50} value was determined in this work for the anti thioredoxin inhibitor 1-methylpropyl 2-imidazolyl disulfide (PX-12) by a linear regression. The enzyme inhibitor was pre-incubated with *Wb*Trx-1 and the substrate for 20 minutes at RT and then the reaction was started by addition of 100 mM DTT. The enzyme activity values were obtained from the mean of three idependent measurements. The analysis of the determination of IC_{50} was performed by using the programme Excel.

4.2.15 SDS-polyacrylamide gel electrophoresis (PAGE) [144]

In this work, discontinuous SDS-polyacrylamide gels were used consisting of a stacking gel and a separating gel. In this method, proteins accumulate in the stacking gel with larger pores and lower pH dependent manner under these conditions only on the charge of their mobility, however, the molecular size is affected. After admission to the separating gel with the higher pH the net charge of proteins increases and the mobility will be dependent on the molecular weight. By boiling with SDS, the proteins filled with negative charges and lose their original conformation and they will be arranged according to their molecular weights. The proteins migrate according to the applied voltage with a mass proportional to their Velocity through the pores of the separating gel to the anode. The pore size of the gel is determined by the concentration of acrylamide and bisacrylamide. The SDS-gels were 104 mm X 98 mm X 1 mm. Before applying, the samples were 1:1 diluted in reducing sample buffer and heated 4 min at 95 °C. l0 µl of the protein molecular weight marker (dilution 1:20 in reducing sample buffer) were applied.

4.2.16 Crystallization experiments

For the crystallization experiments the vapour diffusion method was applied. In a closed system containing a solution of the so-called precipitants, a drop with a highly concentrated protein solution is placed. The precipitants are containing substances, which are suitable for protein precipitation (salts, organic solvents, polyethylene glycol) are defined by buffer additives pH values adjusted. In the vapour diffusion effect, a slow concentration of the protein takes place under optimal conditions till the formation of protein crystals occurs [146, 147]. 1 ml precipitant [148]solutions (1.8 mM ammonium sulphate and 100 mM tris buffer at pH 8.0) was added to the wells, equal parts of protein and precipitants solution (2 µl) were pipetted to siliconized cover glass. The cover glas was sealed on the wells with silicone grease.

4.2.16.1 Crystallization of *Wb*Trx-1 and *Wb*Trx-1-C39S

After completion of the first step of protein purification the protein was immediately subjected to different stages of the crystallization protocols.

4.2.16.2 Dynamic Light Scattering (DLS)

Dynamic light scattering (DLS) system Spectroscatter 201 (Molecular Dimensions, UK) is an instrument which can be used to determine the size distribution profile of small particles in suspension or polymers in solution. Analysis of the autocorrelation function in terms of particle size distribution is done by the program CONTIN[149]. A truly monodisperse sample would give rise to a single exponential decay to which fitting of a calculated particle size distribution is relatively straightforward. Dynamic light scattering (also known as Photon Correlation Spectroscopy (PCS) is the general designation for a method to determine the size of small particles in the submicron range. These particles are found in Brownian motion in suspension or emulsion. The diffusion coefficient **D** for this is inversely proportional to the radius (hydrodynamic radius) $\mathbf{r}_h$ of the particles.

$$D = \frac{k \times T}{3 \times \pi \times \eta \times r_k}$$

(k = Boltzmann's constant) Temperature **T** and viscosity **η** of the solutions are important parameters, which must be accurately known. Since particles in solutions have Brownian motion, the back scattered light will have a frequency shift (Doppler-Shift). The resulting intensity variation is recorded by a highly sensitive detector.

4.2.16.3 Pre-Crystallization Test

The PCT Pre-Crystallization Test was used to determine the optimal protein concentration to start crystallization screening. Highly concentrated samples resulted in amorphous precipitate, while diluted samples had produced transparent drops. Amorphous precipitate and clear drop production was avoided by changing the protein concentration accordingly.

The four reagents of the PCT kit, used to evaluate protein concentration for crystallization screening, are:

1) Reagent A1: 0.1 M Tris hydrochloride pH 8.5, 2.0 M ammonium sulphate

2) Reagent B1: 0.1 M Tris hydrochloride pH 8.5, 1.0 M ammonium sulphate

3) Reagent A2: 0.1 M Tris hydrochloride pH 8.5, 0.2 M magnesium chloride hexahydrate, 30% w/v polyethylene glycol 4,000

4) Reagent B2: 0.1 M Tris hydrochloride pH 8.5, 0.2 M magnesium chloride hexahydrate, 15% w/v polyethylene glycol 4,000

4.2.16.4 Robotic Screening

In structural genomics/proteomics, major advances in protein crystallization have been made using robotics Fig. 16, which has automated the crystallization experiments and reduced the amount of protein required by an order of magnitude, improving the reproducibility of the experiments and allowing a large number of set ups[150].

Figure 16: Zinsser Pipetting Robot (Digilab Genomic Solution, Germany).

4.2.16.5 Optimization of *Wb*Trx-1 Crystals

The hanging drop vapour diffusion method has been applied to improve initially obtained crystals using Linbro Plates. A 2 µl protein solution was mixed with 2 µl reservoir solution and equilibrated against 1.0 ml reservoir solution. X-ray diffracting crystals, possessing approx. dimensions of 350×350×300 μm^3 were obtained by incubating plates at 20 °C for two weeks. Optimal size crystals were produced using 25% PEG 3350, 200 mM NaCl and 100 mM Tris/HCl pH 5.6.

4.2.16.6 Optimization of *Wb*Trx-1-C39S Crystals

The PCT™ Pre-Crystallization Test (Hampton Research, USA) was used to optimize the protein concentration prior to screening experiments. The initial crystallizations conditions were further optimized applying the hanging-drop vapour-diffusion method using 25% PEG 3000, 200 mM $(NH4)_2SO_4$ and 100 smM Tris/HCl pH 5.6. Drops of 2µl of the protein solution and 2µl of the reservoir solution were equilibrated against 1 ml of reservoir solution. Crystals of approximately 300×300×350 μm^3 were obtained after 3 weeks.

4.2.16.7 Data Collection

Native X-ray diffraction data from single crystals were collected by exposing them at the synchrotron Consortium-Beamline X13, DESY, Hamburg. A crystal was mounted on a nylon loop and flash-cooled in cold nitrogen-gas stream at 100 K. All intensity data were indexed, integrated and scaled with the HKL-2000 package[151]. Phase information was generated using the Molecular Replacement (MR) strategy. Therefore, the program Molrep[152] from the CCP4i suite[153] was used.

4.2.16.8 Matthews Coefficient (V_M)

One of the most important crystal parameters is the fraction of the unit cell (or asymmetric unit) that is considered as solvent. The most often used way to calculate the *solvent content* is via the Matthews parameter[154]. The Matthews coefficient provides this number. The Matthews coefficient (V_M) is calculated as:

$$\frac{\text{volume of unit cell}}{\text{the molecular weight of macromolecule} \times Z \times X}$$

Z is the number of asymmetric units in the unit cell (i.e. the number of symmetry operators in a space group). The unknown variable, X, is the number of molecules in the asymmetric unit.

4.2.16.9 Cryogenic Techniques

After successful data collection, a small Dewar was filled with liquid nitrogen to keep the internal environment in freezing temperature, while the crystal was still on the goniometer. The head of the cryo-tongs was placed into the nitrogen along with cryo-vial and forceps until they stopped boiling Fig. 17.

Figure 17: Cryogenic technique accessories.

For cryo-protecting and to keep the crystals, the tong was clamped around the crystal and quickly returned with the crystal to the liquid nitrogen in the Dewar. With another pair of forceps clamped the base of the cryo-pin, and the crystal was released from the cryo-tongs. The crystal was transferred to the cryo-vial. During the whole procedure of crystal preservation, the crystal was kept strictly under the liquid nitrogen surface, as little change in temperature can damage the crystal order and ultimately the data quality. The cryo-pin was screwed onto the cryo-vial using the magnetic wand and was transferred into the liquid nitrogen filled Dewar.

4.2.16.10 Macromolecular Crystallography Beamline X13

Beamline X13 was a bending magnet macromolecular crystallography beamline located in the former HASYLAB Hall 5. It was a monochromatic fixed wavelength beamline operating at a wavelength of 0.8123 Å (15.3 keV). The beamline was equipped with a MARCCD detector (165 mm). The station was optimized for rapid data collection and high resolution studies.

4.2.17 Model Building and Refinement

After solving the phase problem, the three dimensional model of the protein was build using the programe Coot[155] and refined by using the programe Refmac5[156].

4.2.17.1 Coot: Crystallographic Object-Oriented Toolkit

Coot is designed for macromolecular model building, model completion and validation, particularly suitable for protein modelling using X-ray data. Coot displays maps and models and allows model manipulations such as idealization, real space refinement, manual

rotation/translation, rigid-body fitting, ligand search, solvation, mutations, rotamers, sand demonstration of Ramachandran plots, skeletonization, display of non-crystallographic symmetry and much more.

4.2.17.2 Refmac5

Refmac5 is a refinement program for macromolecular structures. The Refmac5 program can carry out rigid body, restrained or unrestrained refinement against X-ray data. Refmac5 will refine an atomic model by adjusting the model parameters (coordinates, B-factors, etc.) in order to obtain the model which best explains the experimental data (i.e. maximizes the likelihood). Progress is monitored by the R-factor and Free R-factor[157], as well as by the likelihood scores themselves[156].

4.3 Docking of *Wb*Trx-1-C39S with small molecules

The three dimensional structure model of *Wb*Trx-1-C39S was used for docking with several inhibitors to characterize the pocket of the ligand binding site, using the Hex 6.3 macromolecular docking program with default parameters of the docking module. Hex 6.3 employs spherical polar Fourier correlation to accelerate the search for candidate low-energy conformations, which removes the time-consuming requirement for explicitly generating different orientations of the mobile molecule[158].

5. Results and Discussion

5.1 Cloning of *Wb*Trx-1

To clone the *Wb*Trx-1 gene, the corresponding DNA sequence was amplified by PCR from plasmid harbouring the respective cDNA of the *Wb*Trx-1 protein. The forward and reverse primers containing NdeI and XhoI restriction sites, respectively, have been used to amplify both fragments. The expected size of the amplified DNA was verified by agarose gel electrophoresis as shown in Fig. 18 A.

The amplified fragments were digested for 3h at 37 °C (see Fig. 18 B) and cloned in a frame without His-tag *via* the NdeI and XhoI restriction sites into the prokaryotic expression vector pRSET B (Invitrogen). The resulting pRSET B-*Wb*Trx-1 contained the *Wb*Trx-1 gene under the control of the T7 promoter. The correct sequence of the cloned gene was confirmed by the dideoxy-mediated chain termination sequencing method.

The cloned DNA-sequence coding for *Wb*Trx-1 was expressed in *E.coli* BL21 (DE3) plysS and the best results in terms of expression quantity were obtained after expression induced by 0.4 mM IPTG for 4 h at 37 °C.

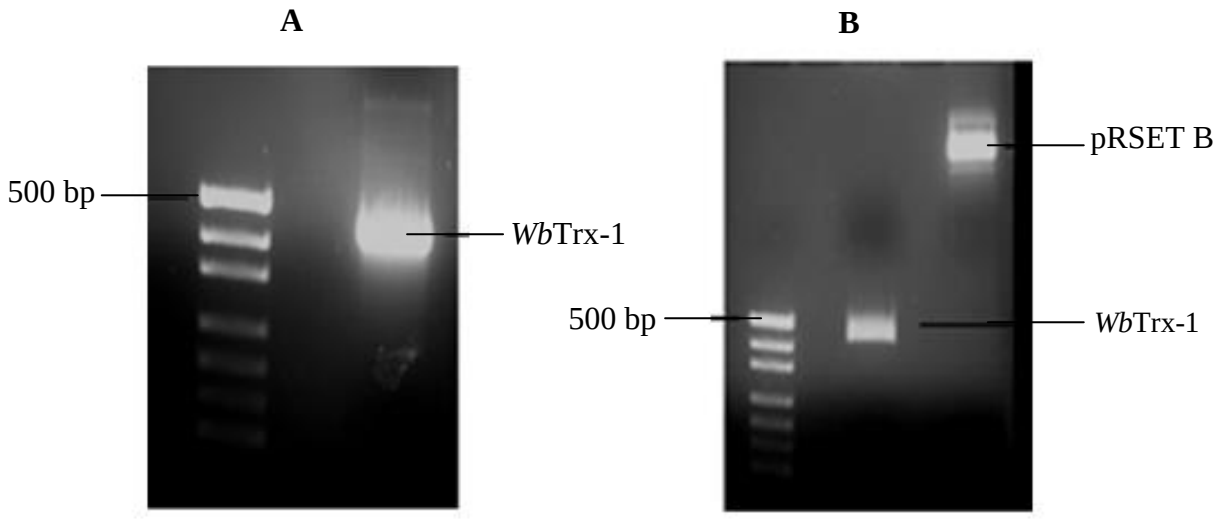

Figure 18: (A) Gel electrophoretic analysis of the PCR amplification of the *Wb*Trx-1 gen with NdeI and XhoI restriction sites using a 2% agarose gel. (B) Digestion of both *Wb*Trx-1 and pRSET B vector with NdeI and XhoI restriction sites for 3h at 37° C using a 2% agarose gel.

5.2 Expression of *Wb*Trx-1

*Wb*Trx-1 was successfully overexpressed in a soluble form using BL21 (DE3) plysS cells and showed a clear band approximately at 16 KDa, as shown in Fig. 19 A.

5.3 Purification of *Wb*Trx-1

After expression, the cells were disrupted by sonication followed by ultracentrifugation at 39,000 g for 15 min at 4 °C. The pellets were discarded and the supernatant containing the recombinant protein was further purified by two purification steps as described before.

5.3.1 Ion exchange chromatography

The recombinant protein was obtained from the cytoplasmic fraction after ultracentrifugation and the supernatant was applied to a regenerated Q-sepharose high performance 75 ml column (Amersham Biosciences) and equilibrated with buffer A (20 mM Tris-HCl pH 8.0 and 5 mM EDTA), as shown in Fig. 19.

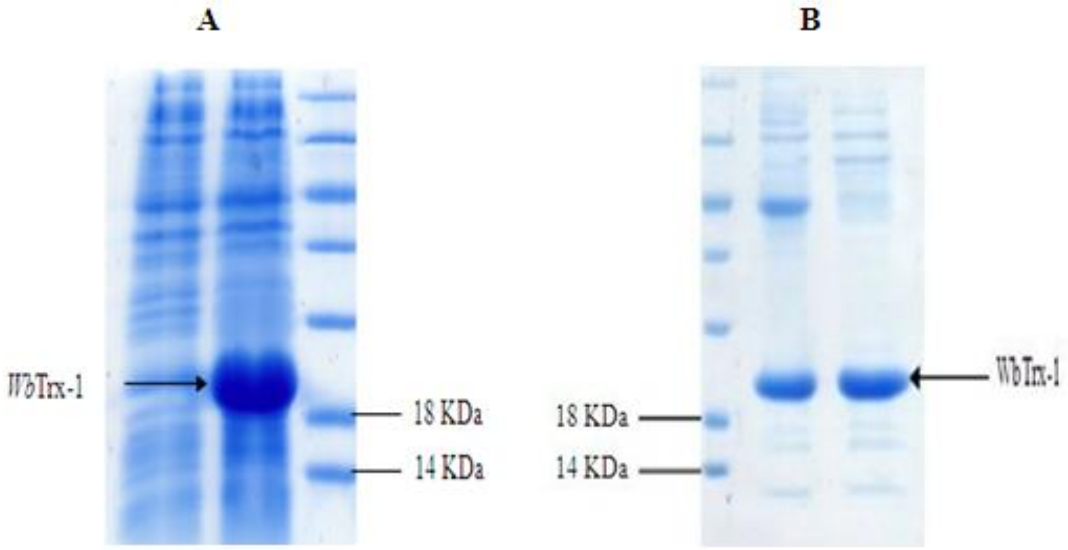

Figure 19: (A) Expression of *Wb*Trx-1 using *E.coli* (BL21) plysS for 4h at 37 °C using 0.4 mM IPTG as inducer. (B) First step of *Wb*Trx-1 purification by ion exchange chromatography.

5.3.2 Size exclusion chromatography

The eluted protein was further purified by gel filtration using a Hiload 26/60 Superdex 200 column (Amersham Biosciences) and was equilibrated with buffer (A) containing 100 mM NaCl. All the fractions were analyzed by 15% SDS-PAGE and Coomassie blue staining[144]. They show more than 95 % purity, as shown in Fig. 20.

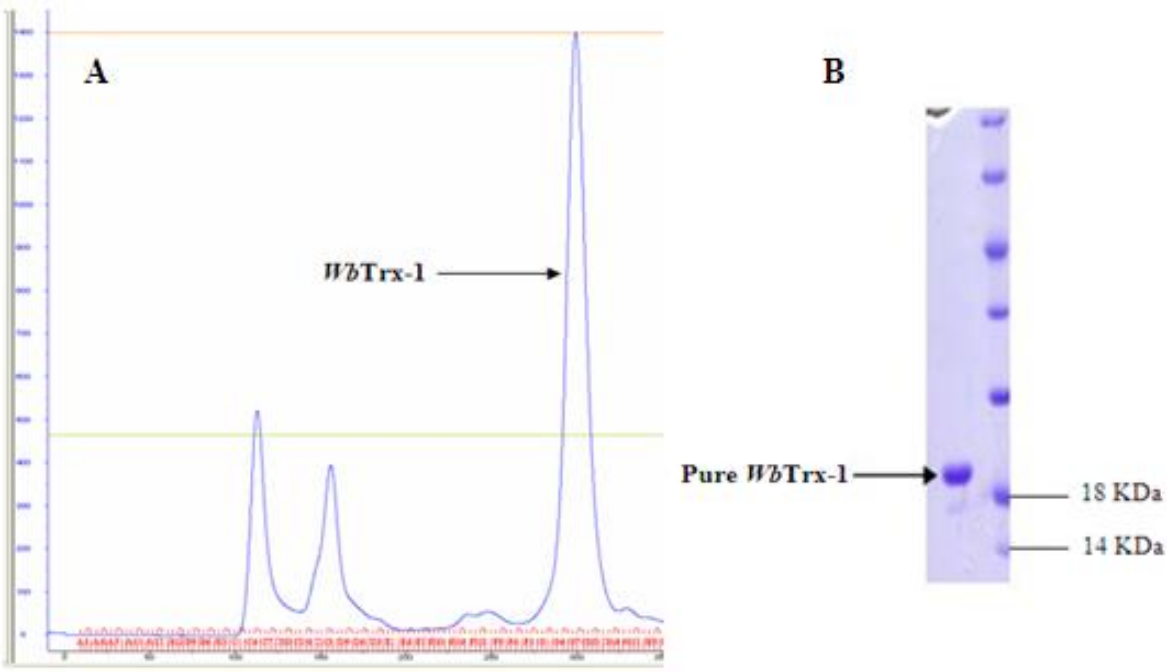

Figure 20: Purification of *Wb*Trx-1. (A) Eluted fractions from the gel filtration. (B) SDS-PAGE of purified *Wb*Trx-1.

5.3.3 Enzymatic assay of *Wb*Trx-1

When the two interacting disulfides of insulin are split by reduction, the free B chain aggregates and precipitates from a neutral solution at low concentration [159]. In this reaction, *Wb*Trx-1 can reduce insulin and the turbidity can be measured at 650 nm wavelength against time, as shown in Fig. 21.

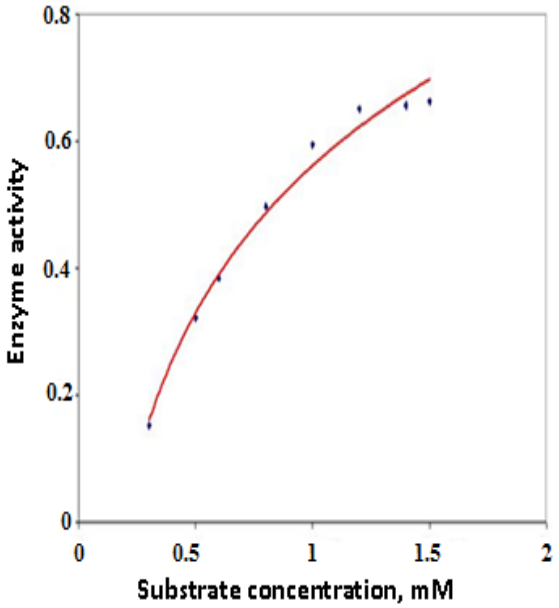

Figure 21: Thioredoxin catalyzed reduction of insulin by dithiohreitol.The reaction mixture contained a final concentration volume of 0.1M phosphate buffer pH 7, 2 mM EDTA, 0.13 mM bovine insulin and 0.33 mM DTT. The *Wb*Trx-1 6 mM concentration was presented. The DDT without *WbT*rx-1 served as control. The absorbance at 650 nm is plotted against the time.

Michaelis-Menten kinetics is a model in which the reaction rate v is related to the substrate concentration [S]. The formula is given by:

$$v = \frac{V_{max}\,[S]}{K_M + [S]}$$

Vmax= maximum rate attainable

K_M= Michaelis-Menten constant

[S] at half maximum rate

5.4 Crystallization of *Wb*Trx-1

The first step of the 3-dimensional structure determination of a protein is to obtain high quality protein crystals. It is commonly known that this is the bottleneck in many projects. Protein crystal growth is not predictable and numerous experimental trials are necessary to find the proper conditions. To obtain regular X-ray-suitable crystals many optimization steps are required.

Besides the purity of the protein, there are several factors which have to be optimized to facilitate the crystal growth, such as protein concentration, precipitant, pH, temperature, etc. Crystallization depends on the protein solution conditions and the molecular structure may be affected along with a subsequent change in the particle size. Thus monitoring the size of a protein molecule is one way to analyze and optimize stability in the protein solution under its native conditions. Proteins can aggregate to heterogeneous complexes thus preventing crystallization. To analyze a possible aggregation, a fast and accurate analytical technique was used, called Dynamic Light Scattering (DLS). This technique was applied to determine the size distribution profile of the protein particles in solution. DLS was shown to be ideal for protein characterization and to check the monodispersive nature of the protein solution.

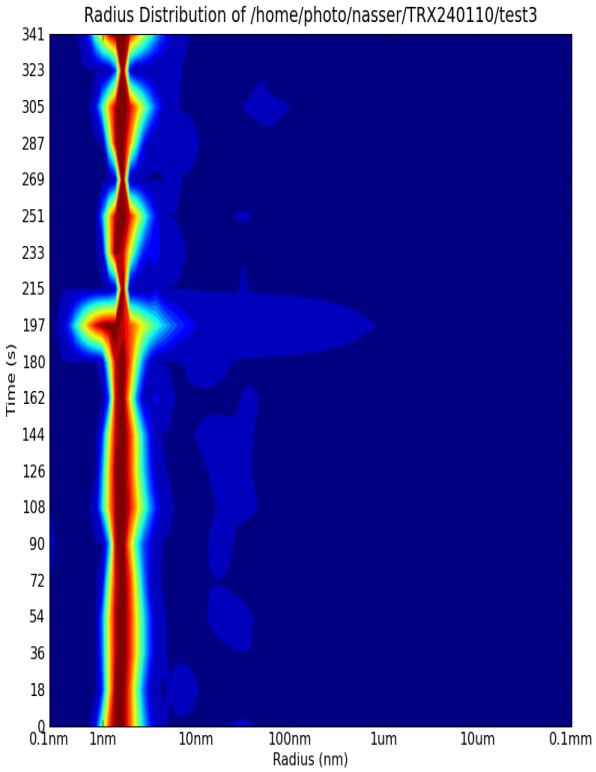

Figure 22: DLS measurement showing a monodispersive protein in solution.

When applied to the *Wb*Trx-1 preparation, a strong single signal was obtained, indicating that the protein existed in a homogeneous non-aggregated form (see Fig. 22). The purified samples of *Wb*Trx-1 indicated a molecular mass of 16 kDa on SDS-PAGE and the results of dynamic light-scattering (DLS) showed that the hydrodynamic radius (R_H) of *Wb*Trx-1 at a protein concentration of 10 mg/ml was 1.7 nm. This assumes a globular shape of the protein and so the molecular mass corresponding to this hydrodynamic radius can be estimated to be around 16 kDa. This indicates that all *Wb*Trx-1 molecules existed in monomeric forms in solution.

Having demonstrated the homogeneity of the protein solution, the next important step was to determine the precipitant that will be used for crystallization. It is known from statistical studies that ammonium sulphate is a precipitant, which was used for crystallization for more than 60 % of the proteins crystallized so far. The crystal growth was optimized using the hanging drop method and by varying the concentration of ammonium sulphate (the precipitant) from 1.2 – 2 M and also varying the pH from 5-9. Another important factor which affects crystallization is the protein concentration. Samples which are too concentrated result in amorphous precipitation, while samples which are too diluted will result in clear drops. To address this point, several protein concentrations ranging from 7-15 mg/ml have been checked with the previously mentioned ammonium sulphate concentrations range. This test showed that the protein concentration of 10 mg/ml was the appropriate concentration to start crystallization. Regular uniform crystals were obtained, as shown in Fig. 23, using the following optimized crystallization condition: 100 mM Tris/HCl pH 5.6, 200 mM NaCl and 25% PEG 3350 as precipitant.

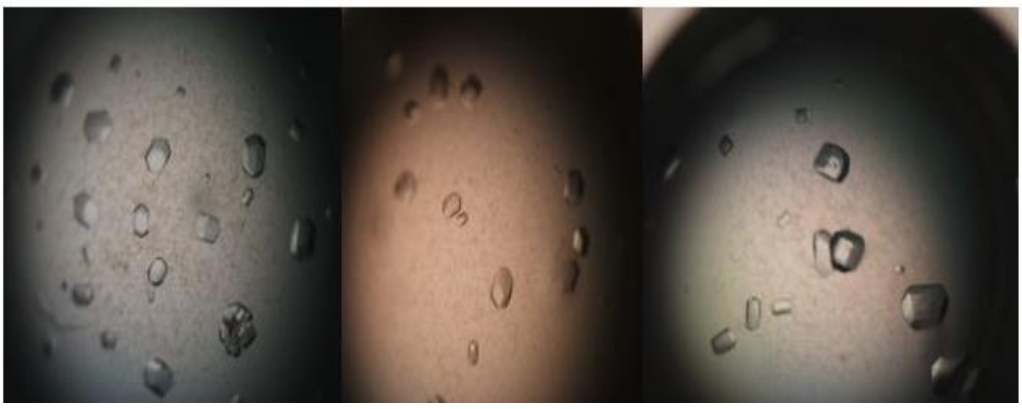

Figure 23: *Wb*Trx-1 Crystals.

2 µl *Wb*Trx-1 were mixed with 2 µl precipitant solution (100mM Tris/HCl pH 5.6, 200mM NaCl and 25% PEG 3350) and incubated at 20 °C temperature. After two weeks, good shaped crystals with dimensions of approximately 350×350×300 µm^3 were obtained.

5.4.1 Data Collection

The next key step in the structure determination process is the collection of X-ray diffraction data. Native diffraction data were collected at the Consortium-Beam Line X13, DESY, Hamburg. The detector type used was a Mar CCD 165 mm and the wavelength was 0.8123 Å. Data collection was performed at 100 K and ice production was prevented by soaking the crystals in the same mother liquor containing additional 15% glycerol just before mounting. Sufficient data with a maximum resolution of 1.95 Å were collected. The data were processed using the HKL-2000 program package[160]. The space group was identified to be I422 with unit cell dimensions of a = b = 112.6 Å and c = 162.0 Å. The matthews coefficient[154] (V_M = 2.6 $Å^3 / Da$) suggested three molecules in the asymmetric unit with a solvent content of 54 %, as shown in Fig. 24.

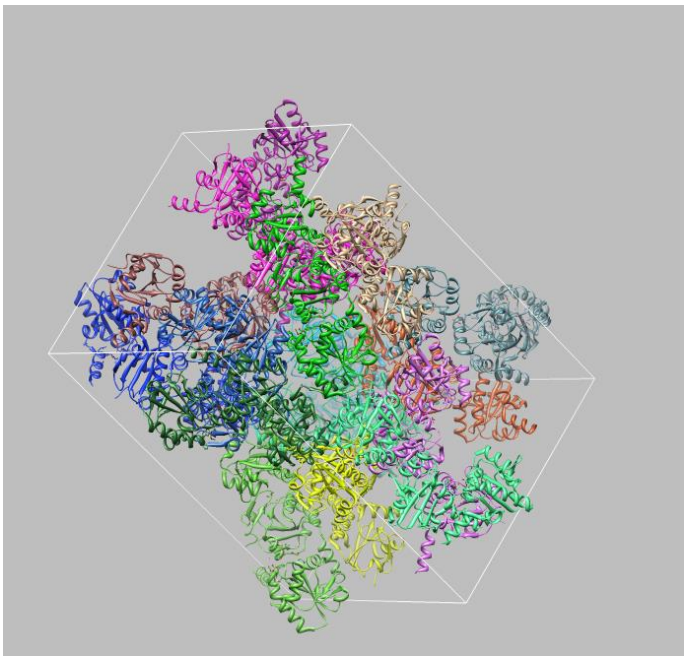

Figure 24: Position of the molecules in the unit cell.

5.4.2 Structure Solution

The last part of the structure determination process is the construction of a 3D model. To calculate the electron density, phase information was obtained by Molecular Replacement (MR) using the program Molrep[152] from the CCP4i suite. A search model was constructed using the homologous structure of tryparedoxin-I from *Crithidia fasciculata* (PDB ID: 1QK8), as the reported primary amino acid sequence of *Wb*Trx-1 showed 38.3 % sequence identity (Fig. 25). Different strategies were applied to this model, using the original model as it is and also using the residual replacement with polyalanines. Fortunately, statistical values were satisfactory and phase information was obtained successfully.

```
WbTrx-1     ---MADLLANID-LKKADGTVKKGSDALANKKVVALYFSAHWCPPCRQFTPILKEFYEEV 56
1Qk8        MSGLDKYLPGIEKLRRGDGEVEVKS---LAGKLVFFYFSASWCPPCRGFTPQLIEFYDKF 57
               : . *..*: *::.** *:  *      *:* :**** ****** *** * ***::.

WbTrx-1     DDDQ-FEIVFVSLDHSEEDLNNYVKESHGDWYHVPFGSSE-IEKLKNKYEVAGIPMLIVI 114
1Qk8        HESKNFEVVFCTWDEEEDGFAGYFAKMP--WLAVPFAQSEAVQKLSKHFNVESIPTLIGV 115
            .:.: **:** : *..*:.: .*. :    *  ***..** ::**.::::* .** ** :

WbTrx-1     KSD-GNVITKNGRADVSGKAPPQTLSSWLAAA 145
1Qk8        DADSGDVVTTRARATLV-KDPEGEQFPWKDAP 146
            .:* *:*:*...** :  * *     .*  *.
```

Figure 25: Sequence alignment between *Wb*Trx-1 and tryparedoxin from *Crithidia fasciculata* (PDB ID: 1QK8). The figure was prepared using the ClustalW2. The active site residues are marked with a black box and the conserved residues with a star.

5.4.3 Model Building and Refinement

Substantial phase information was generated mainly with good statistical values. Model building and refinement was performed using the programs Coot and Refmac5. The crystallized 16 kDa catalytic domain of *Wb*Trx-1 contains 144 of 145 amino acids with the absence of the first amino acid methionine and including 349 water molecules. The model was refined at a resolution of 1.95 Å with $R_{crystal}$ of 17.9% and R_{free} of 22.8%. All amino acids are in the preferred and allowed regions and there are no Ramachandran plot outliers[161]. The data collection and refinement parameters are shown in Table 4.

Table 4: Data collection and refinement statistics.

Parameters	***Wb*Trx-1**
Space group	I422
a = b (Å)	112.6
c (Å)	162.0
V_M ($Å^3$/ Da)	2.6
Solvent content (%)	53.8
Completeness of data (%)	99.0 (83.4)
No. of total reflections	348075
No. of used reflections	35184
Average I/sigma intensity	29.8 (9.9)
Resolution (Å)	28.4-1.95
Redundancy	9.9 (9.1)
R_{merge} (%)	6.2 (18.8)
$R_{crystal}$ (%)	17.9 (22.5)
R_{free} (%)	22.8 (25.5)
Protein atoms	3389
Solvent atoms	349
Average B-factor ($Å^2$)	
Main-chain atoms	18.8
Side chain atoms	21.5
Root mean square deviation	
Bonds (Å)	0.0243
Bond angles (^{o})	1.956
Residues in regions of the Ramachandran plot (%)	
Most favored	94.6 %
Allowed	5.4 %
Disallowed	0.0

Values in parentheses are for the highest resolution shell.
R_{merge}: $\sum_{hkl} \sum_{i|} I_i(hkl) - \rangle I(hkl) \langle| / \sum_{hkl} \sum_i I_i(hkl)$, where$\rangle$ I (hkl) $\langle$is the mean intensity of the observations I_i (hkl) of reflection hkl.

5.4.5 Description of the Molecule

The full length amino acid sequence of *Wb*Trx-1 was applied to the ExPASy Proteomics Server[162]. Some of the primary sequence statistics are summarized in Table 5.

Chain ID	Chain A
Formula	$C_{728}H_{1124}N_{186}O_{220}S_4$
No. of amino acids	145
Molecular weight (Da)	16130.2
Theoretical pI	5.16
Total No. of atoms	2262
No. of negatively residues	22
No. of positively residues	16
No. of cysteines	2

Table 5: Statistical values of the primary amino acid sequence of *Wb*Trx-1.

A total of 145 amino acids have been detected in the structure except the first amino acid, which corresponds to the protein molecular weight of 16 kDa. The protein has one disulphide bond between the only two cysteines in the active site, as will be discuss later.

The three-dimensional structure of the *Wb*Trx-1 shows the scaffold characteristic of thioredoxins as so far known and published. The *Wb*Trx-1 structure consists of central strand parallel and antiparallel β-sheets surrounded by α-helices[59]. Helix 5 is broken into two halves, α_5A and α_5B, due to the presence of Pro_{132} and Pro_{133}. Determination of the structure confirms the presence of one disulfide bond between Cys_{39} and Cys_{42} in the active site, as shown in Fig. 26.

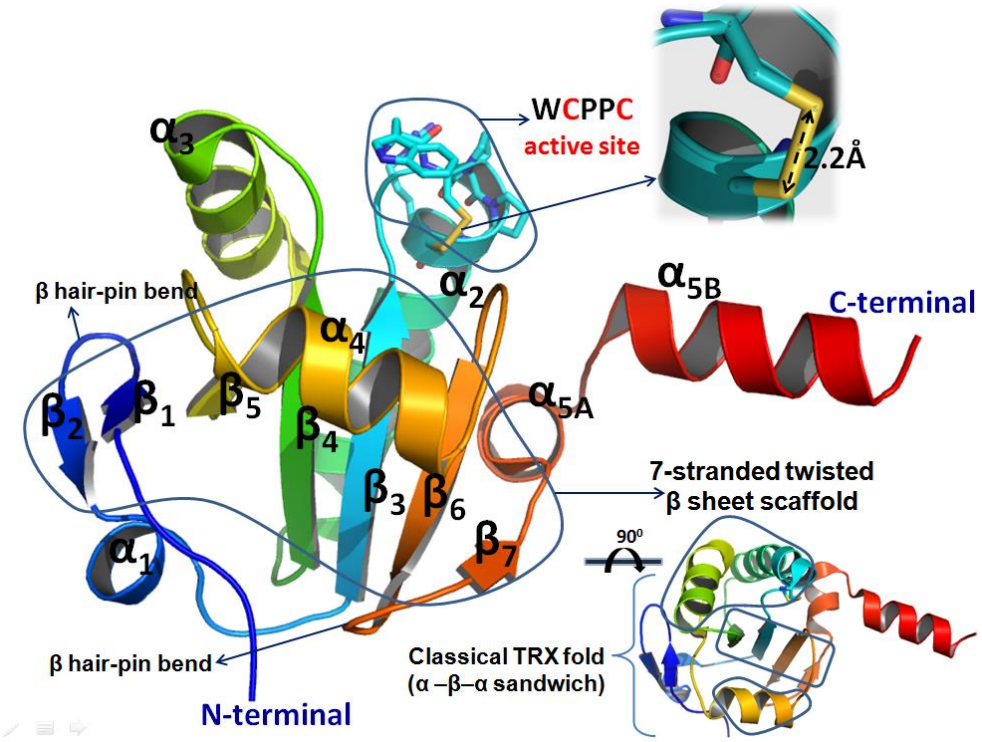

Figure 26. The three dimensional structure of *Wb*Trx-1. The central β-sheets are surrounded by α-helixes. The redox active site is located in the N-terminus between the main body of the molecule and helix α_5b.

The overall structure of *Wb*Trx-1 resembles more to tryparedoxins than mammalian thioredoxins or glutaredoxins[163], which is in line with sequence and structural alignments. Nevertheless, it incorporates the classical thioredoxin fold with a four stranded β sheet flanked by three α helices with two on one side and one on the other[164]. The central β sheet carries a motif of β_3-α_2-β_4-α_3-β_5-α_4-β_6 with alternating parallel ($\beta_3\beta_4\beta_5$) and anti-parallel ($\beta_5\beta_6$) beta strands. A similar pattern of shared β-α-β is found in tryparedoxins (PDB Codes 3S9F and 1QK8). Additionally, the structure has two β hair pin bends, one at the N-terminal ($\beta_1\beta_2$) and the other at the C-terminal ($\beta_6\beta_7$).

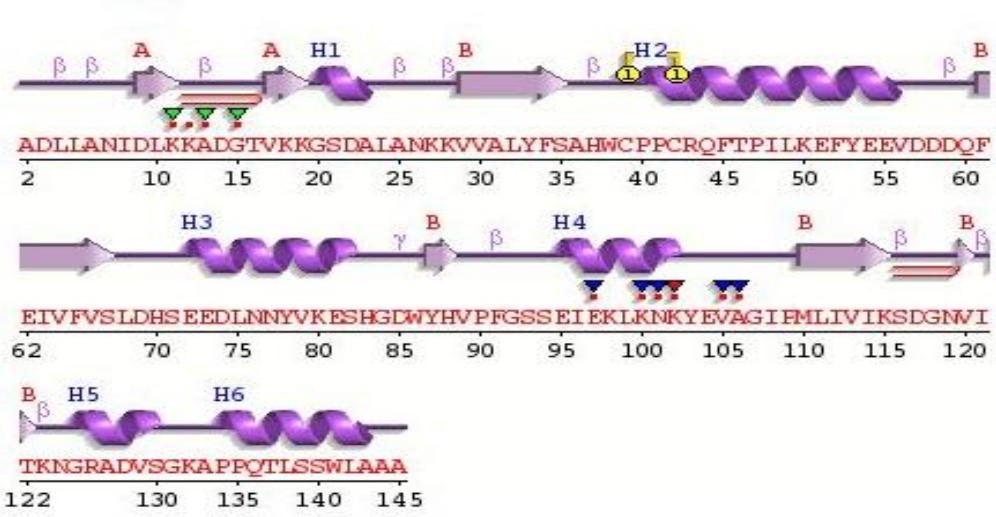

Figure 27: Secondary structure of *Wb*Trx-1.

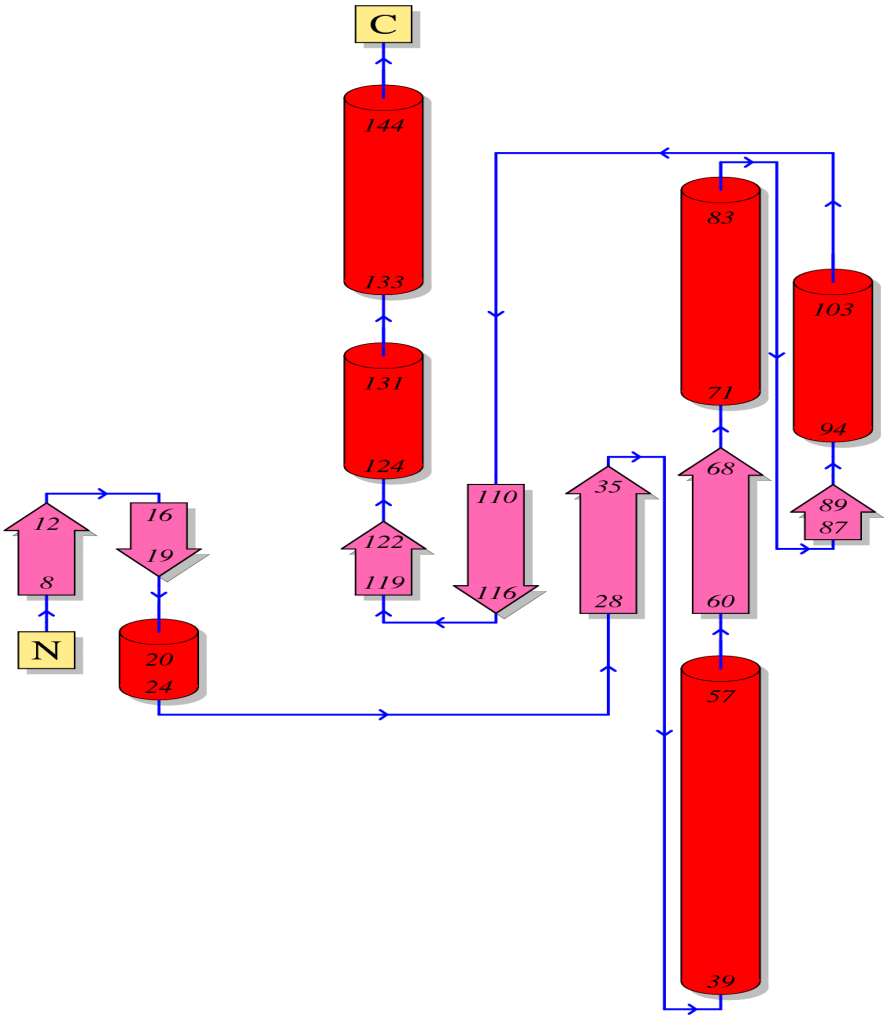

Figure 28: A topology diagram of the *Wb*Trx-1 structure.

The secondary and topology of a protein structure is a highly simplified description of its fold, including only the sequence of secondary structure elements and their relative spatial positions and approximate orientations (see Figures 27 and 28). This topology cartoons are useful for understanding particular folds and to undertake comparisons between similar thirodoxin folds. From this topology diagram, it is observed that the *Wb*Trx-1 has the α/β fold catalytic conserved structure, which was observed in all known thirodoxins so far[59].

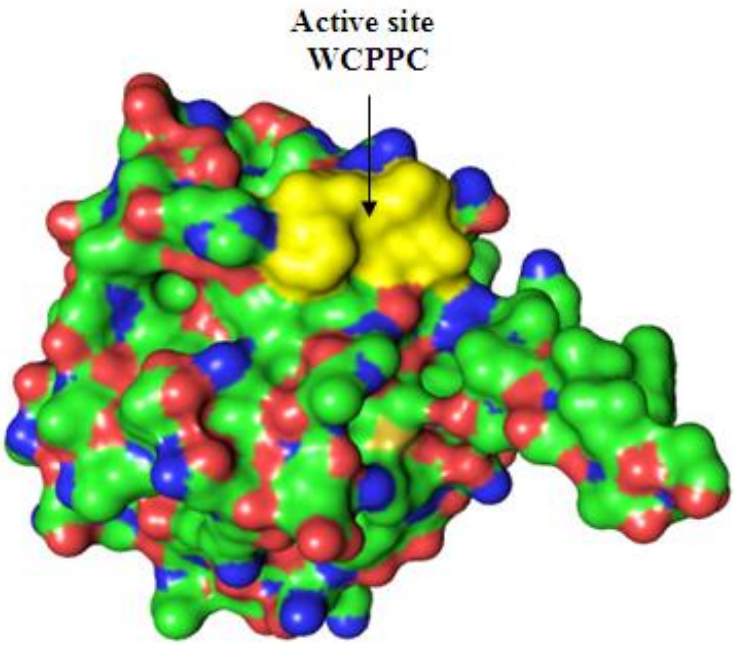

Figure 29: Electrostatic potential surface of *Wb*Trx-1. The surface is coloured according to its electrostatic potential, with the positively charged electrostatic potential coloured blue and the negatively charged electrostatic potential coloured red. The location of the active site residues is indicated with yellow.

The chemical properties of the groups comprising the protein surfaces are important, as these groups determine the distinct interactions of the protein with water. It was suggested that large polar surfaces of proteins contribute to an increased stability. *Wb*Trx-1 exhibits some structural features, like the area of Asp and Glu residues being high exposed at the surface. It has a high content of Glu and Asp residues and a low content of Arg and Lys residues at the surface. This may support the ability of the enzyme to withstand alkaline conditions (see Fig. 29).

5.4.6 Interactions between *Wb*Trx-1 chains

*Wb*Trx-1 was crystallized with three molecules in the asymmetric unit, chains A, B and C. Chain A in connected to Chain B and chain C respectively to form the protein trimmer. The *Wb*Trx-1 trimmer associated with some points of symmetry showed hydrogen bonds and non-covalent interactions across the interface of the respective chains. These interactions between the amino acid side-chains stabilized the ultimate quaternary structure of the protein. Since the three chains were identical and almost the same number and similar amino acid side chains from both sides developed the same number of hydrogen bonded environment giving real contribution to the trimer development. Chain A is connected to chain B *via* hydrogen bond between Glu_{104} from Chain A and Lys_{123} from chain B with a bond length of 3.0 Å. Similarly Lys_{80} from chain A is connected to Glu_{51} from chain C and forming hydrogen bond with a bond length of 2.8 Å, as shown in Fig. 30.

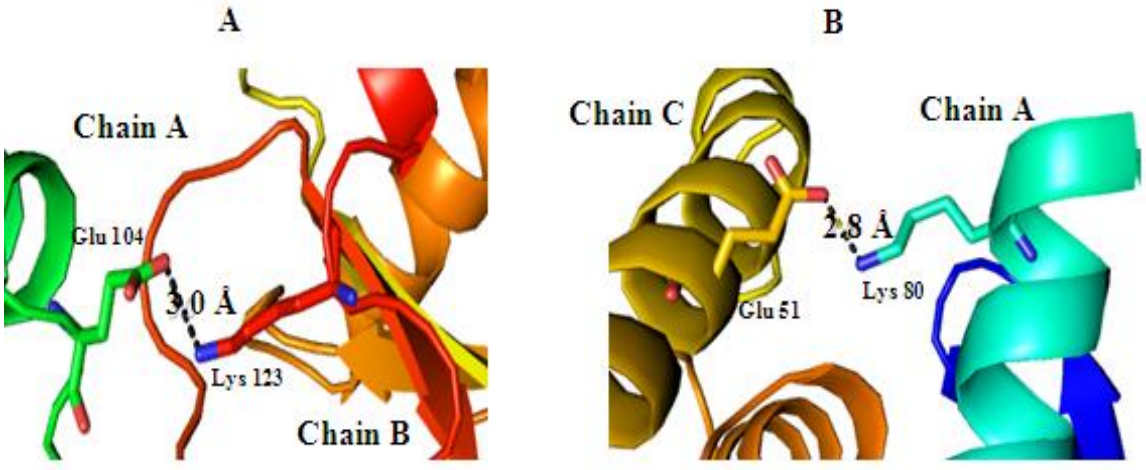

Figure 30: The hydrogen bond interactions between amino acid side-chains A, B and C. (A) Hydrogen bond between Glu_{104} from chain A and Lys_{123} from chain B. (B) Hydrogen bond between Lys_{80} from chain A and Glu_{51} from chain C. The structure is orientated to see the interactions.

The total number of hydrogen bond and non-covalent interactions between chain A and chain B are summarized in Table 6.

	Residue name	Atom name	Chain		Residue name	Atom name	Chain	Distance
1	LYS_{100}	C	A	←→	ALA_{106}	CB	B	3.89
2	LYS_{100}	O	A	←→	ALA_{106}	CB	B	3.49
3	ASN_{101}	CA	A	←→	ALA_{106}	CB	B	3.78
4	ASN_{101}	CG	A	←→	GLY_{107}	N	B	3.86
5	ASN_{101}	OD1	A	←→	ALA_{106}	CA	B	3.88
6	ASN_{101}	OD1	A	←→	ALA_{106}	C	B	3.34
7	ASN_{101}	OD1	A	←→	ALA_{106}	O	B	3.66
8	ASN_{101}	OD1	A	←→	ALA_{106}	CB	B	3.32
9	ASN_{101}	OD1	A	←→	GLY_{107}	N	B	3.29
10	ASN_{101}	OD1	A	←→	GLY_{107}	CA	B	3.72
11	GLU_{104}	O	A	←→	GLU_{104}	CB	B	3.85
12	GLU_{104}	CD	A	←→	LYS_{123}	NZ	B	3.47
13	GLU_{104}	OE1	A	←→	LYS_{123}	NZ	B	3.74
14	GLU_{104}	OE2	A	←→	LYS_{123}	CE	B	3.79
15	GLU_{104}	OE2	A	←→	LYS_{123}	NZ	B	3.98
16	VAL_{105}	O	A	←→	ALA_{106}	CB	B	3.77
17	ALA_{106}	CA	A	←→	ASN_{101}	OD1	B	3.78
18	ALA_{106}	C	A	←→	ASN_{101}	OD1	B	3.27
19	ALA_{106}	O	A	←→	ASN_{101}	OD1	B	3.53
20	ALA_{106}	CB	A	←→	LYS_{100}	O	B	3.40
21	ALA_{106}	CB	A	←→	ASN_{101}	CA	B	3.86
22	ALA_{106}	CB	A	←→	ASN_{101}	OD1	B	3.29
23	ALA_{106}	CB	A	←→	VAL_{105}	O	B	3.71
24	GLY_{107}	N	A	←→	ASN_{101}	CG	B	3.74
25	GLY_{107}	N	A	←→	ASN_{101}	OD1	B	3.33
26	GLY_{107}	CA	A	←→	ASN_{101}	CG	B	3.88
27	GLY_{107}	CA	A	←→	ASN_{101}	OD1	B	3.86
28	ASN_{119}	OD1	A	←→	LEU_{142}	O	B	3.63
29	ASN_{119}	ND2	A	←→	ALA_{143}	CA	B	3.66
30	LYS_{123}	NZ	A	←→	GLU_{104}	OE2	B	3.70

Table 6: Interactions across the interface of chain A and B.

One hydrogen bond and 30 non-bond contacts have been observed between the side chains of respective amino acids or between the side chain and the main backbone. In particular, the interactions between chain A and chain C showed one hydrogen bond and 8 non-bond contacts, (see Table 7).

	Residue name	**Atom name**	**Chain**		**Residue name**	**Atom name**	**Chain**	**Distance**
1	GLY_{15}	CA	A	←→	GLU_{81}	O	C	3.65
2	GLY_{15}	O	A	←→	GLU_{81}	CG	C	3.53
3	THR_{15}	CG2	A	←→	GLU_{81}	OE1	C	3.78
4	Lys_{80}	CD	A	←→	GLU_{51}	OE2	C	3.49
5	Lys_{80}	CE	A	←→	GLU_{51}	OE2	C	3.45
6	Lys_{80}	NZ	A	←→	GLU_{51}	CG	C	3.50
7	Lys_{80}	NZ	A	←→	GLU_{51}	CD	C	3.58
8	Lys_{80}	NZ	A	←→	GLU_{51}	OE2	C	3.76

Table 7: Interactions across the interface of chain A and C.

5.4.7 Comparison of the overall structure with related enzymes

*Wb*Trx-1 showed some distinct features, while these differences could play important roles in determining the specificities of the particular thioredoxin. It is now necessary to compare *Wb*Trx-1 with some other thioredoxins with respect to folding and conformation. Searching the protein data bank for related thioredoxins, which have the highest sequence homology with *Wb*Trx-1, revealed several examples. Next, the comparison of *Wb*Trx-1 with tryparedoxin-1 from *Crithidia fasciculata* (PDB ID: 1QK8), *E.coli* thioredoxin (PDB ID: 2TRX) and human oxidized thioredoxin (PDB ID: 1ERU) will be shown.

As mentioned before, the amino acid alignment sequence between *Wb*Trx-1 and tryparedoxin from *Crithidia fasciculate* has been used to solve the *Wb*Trx-1 structure by molecular replacement. The proteins possess an identity of 38.3%.

A comparison between *Wb*Trx-1 in green with the tryparedoxin fom *Crithidia fasciculata* (PDB ID: 1QK8) in orange is shown in Fig. 31. 144 residues from *Wb*Trx-1 are aligned against 143 residues from 1QK8. 93 Cα atoms have been aligned with a RMS deviation for all atoms of 1.05 Å. Some deletions and insertions have been observed.

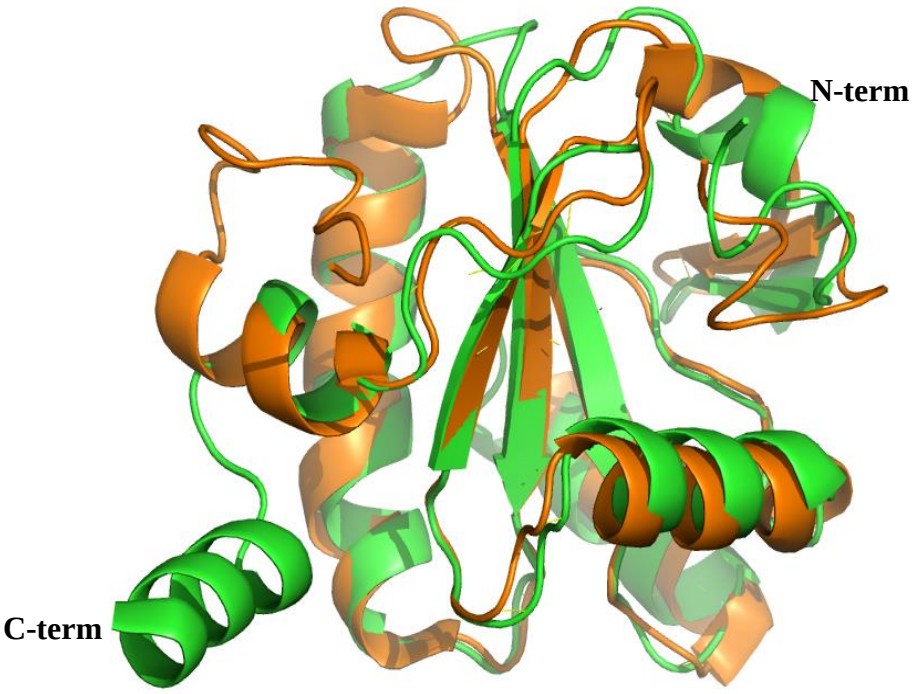

Figure 31: Cartoon plot of the superposition of *Wb*Tr-x-1 (green) with the tryparedoxin fom *Crithidia fasciculata* (orange).

The sequence alignment between *Wb*Trx-1 and *E.coli* thioredoxin is shown in Fig. 32, the identity is 21.9% between the two proteins.

```
WbTrx-1     MADLLANIDLKKADGTVKKGSDALANKKVVALYFSAHWCPPCRQFTPILKEFYEEVDDDQ 60
2TRX        -SDKIIHLTDDSFD------TDVLKADGAILVDFWAEWCGPCKMIAPILDEIADEYQG-K 52
             :* : ::  .. *      :*.*  . .: : * *.** **: ::***.*: :* :. :

WbTrx-1     FEIVFVSLDHSEEDLNNYVKESHGDWYHVPFGSSEIEKLKNKYEVAGIPMLIVIKSDGNV 120
2TRX        LTVAKLNIDQNPGTAP------------------------KYGIRGIPTLLLFKNGEVA 87
            : :. :.:*:.                              ** : *** *:::*..  .

WbTrx-1     ITKNGRADVSGKAPPQTLSSWLAAA 145
2TRX        ATKVG--ALSKGQLKEFLDANLA-- 108
             ** *   :*     : *.: **
```

Figure 32: Sequence alignment between *Wb*Trx-1 and thioredoxin from *E.coli* (PDB ID: 2TRX). The figure was prepared using the ClustalW2. The active site residues are marked with a black box and the conserved residues with a star.

*Wb*Trx-1 is then compared with another thioredoxin from *E.coli* (PDB ID: 2TRX). 144 residues from *Wb*Tr-x1(green) were aligned against 108 residues from *E.coli* thioredoxin (turquoise). 57 Cα atoms have been aligned with a RMS deviation of 1.40 Å. This higher RMS value is consistent with Fig. 33, which showed some deletions and insertions in loop and helical regions.

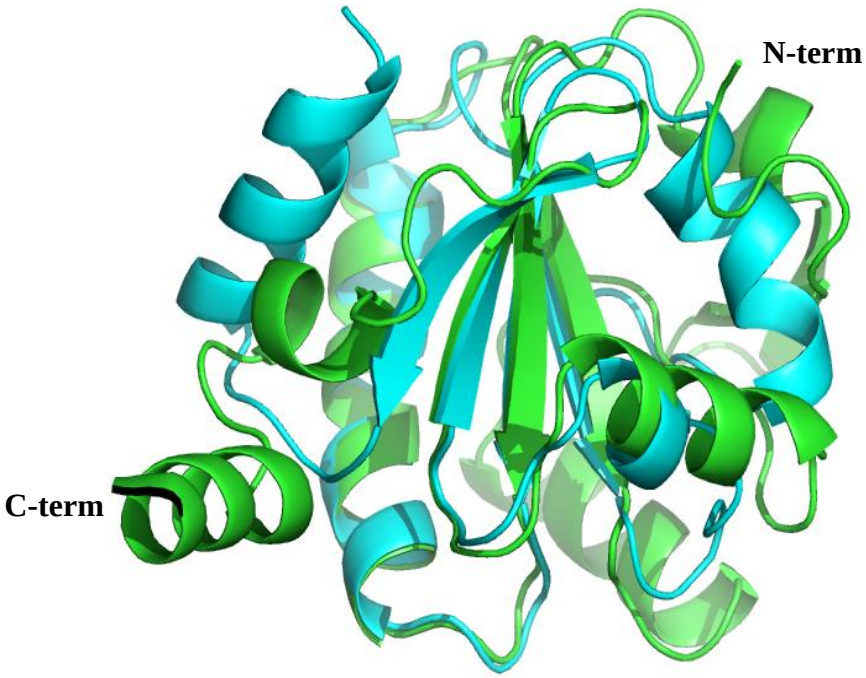

Figure 33: Cartoon plot of the superposition of *Wb*Trx-1 (green) with *E.coli* thioredoxin (turquoise).

The sequence alignment between *Wb*Trx-1 and *human* thioredoxin is shown in Fig. 34, and the identity is 18.1% between the two proteins.

```
WbTrx-1     MADLLANIDLKKADGTVKKGSDALANKKVVALYFSAHWCPPCRQFTPILKEFYEEVDDDQ 60
1ERU        ---MVKQIESKTA---FQEALDAAG-DKLVVVDFSATWCGPCKMIKPFFHSLSEKYSN-- 51
               :: :*: *.*   .::. ** . .*:*.: *** ** **: :.*::::.: *: .:

WbTrx-1     FEIVFVSLDHSEEDLNNYVKESHGDWYHVPFGSSEIEKLKNKYEVAGIPMLIVIKSDGNV 120
1ERU        --VIFLEVDVDD----------------------CQDVASECEVKCMPTFQFFKKGQKV 86
              ::*:.:* .:                         :.: .: **  :* : .:*.. :*

WbTrx-1     ITKNGRADVSGKAPPQTLSSWLAAA 145
1ERU        GEFSGANKEKLEATINELV------ 105
               .*  . . :*. : *
```

Figure 34: Sequence alignment between *Wb*Trx-1 and human thioredoxin (PDB ID: 1ERU). The figure was prepared using the ClustalW2. The active site residues are marked with a black box and the conserved residues with a star.

*Wb*Trx-1 is finally compared with oxidized thioredoxin from human (PDB ID: 1ERU). 144 residues from *Wb*Tr-x1(green) were aligned against 105 residues from human thioredoxin (rose). 53 Cα atoms have been aligned with a RMS deviation of 5.29 Å. This high RMS value is in consistent with Fig. 35, which showed more deletions and more insertions of loops and helices.

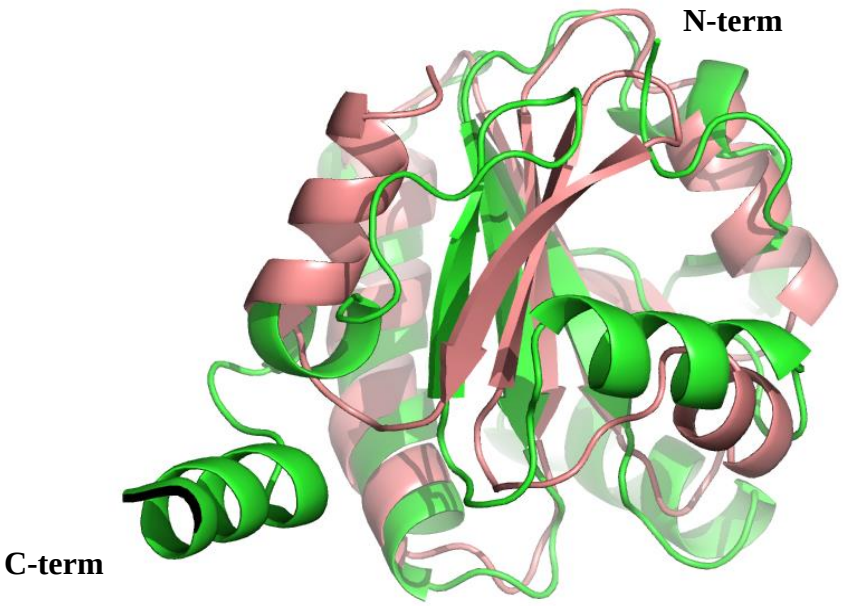

Figure 35: Cartoon plot of the superposition of *Wb*Trx-1 (green) with human thioredoxin (rose).

The high resolution of all four structures allows a reasonable comparison to be made with respect to the quality of the models. Pairwise least square superposition of the four structures showed that 36–64 % of the Cα-atoms are in common positions and gave a root mean square deviation of 1.05–5.29 Å (see Table 8). The structural resemblance with regard to root mean square deviation, fraction of common Cα-atoms and the amino acid sequence identity is in the following order: *Wb*Trx-1–1QK8 > *Wb*Trx-1–2TRX > *Wb*Trx-1–1ERU.

	***Wb*Trx-1 – 1QK8**	***Wb*Trx-1 – 2TRX**	***Wb*Trx-1 – 1ERU**
Number of residues	**144 – 143**	**144 – 108**	**144 - 105**
Alignment residues	**93 (64 %)**	**57 (39 %)**	**53 (36 %)**
Root mean square deviation (Å)	**1.05**	**1.40**	**5.29**

Table 8. Pairwise superposition of Cα-atoms of *Wb*Trx-1, 1QK8, 2TRX, and 1ERU.

5.4.8 Active site

The active site sequence is Trp-Cys-X-X-Cys, as known for all thioredoxins. The redox active cysteine pair is in an oxidized disulfide form, like *Wb*Trx-1, or in the reduced thiol form similar to reduced human thioredoxin, but the conformational changes between the two forms are usually small[148]. The electron density of the *Wb*Trx-1 structure shows that the active site amino acids Cys_{39} and Cys_{42} form a disulfide bridge with a bond length of 2.2 Å, as shown in Fig. 36. This is comparable to the reduced human thioredoxin, in which the distance between the two active site cysteines Cys_{32} and Cys_{35} is 3.9 Å. Cys_{39} of *Wb*Trx-1 is exposed at the surface, whereas Cys_{42} is in a more buried location.

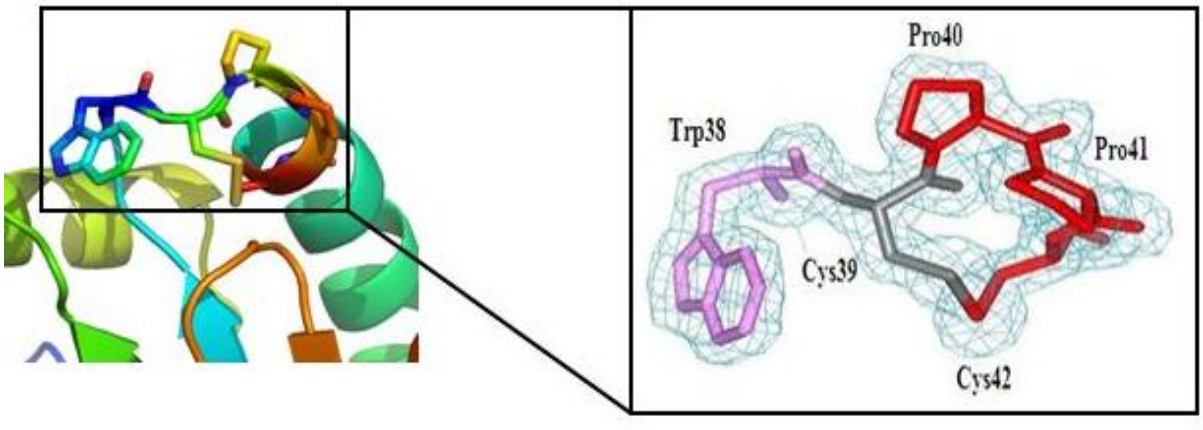

Figure 36. Zoom of the active site. $2F_0$-F_c map, contoured at 1σ, of the redox active WCPPC motif of *Wb*Trx-1. The active site is in the oxidized form and the two cysteines form a disulfide bridge with a distance of 2.2 Å.

The active site contains several amino acid residues, which are important for the structural and catalytic function of thioredoxin. A conserved Trp_{38}, which is present in the thioredoxin WCPPC sequence motif, is located at the surface of the active site and appears to interact with thioredoxins redox partners. In most thioredoxins, this Trp has the same location before the CXXC motif and it is also important for the thermodynamic stability of the protein[165]. Mutation of this conserved Trp by alanine has a dramatic effect, causing a formation of a domain-swapped dimer, which is kinetically stable for years and is devoid of any activities known for thioredoxin proteins[98]. Also, *Wb*Trx-1 is characterized by the presence of Pro_{40} and Pro_{41} between the two catalytic cysteins, both being in a cis conformation. Pro_{41} is known to be the key residue providing the reducing potential of thioredoxin. Replacing it by serine or thrionine has a substantial effect on the activity and stability of the protein[91].

The comparison between the active site of *Wb*Trx-1 with the active site of *human* thioredoxin (*Hs*Trx-1) oxidized and reduced are shown in Fig. 37. The superposition of *Wb*Trx-1 with *human* thioredoxin showed RMS value of 0.28 Å, while five atoms from *Wb*Trx-1 were aligned against five atoms from cytosolic *Hs*Trx-1.

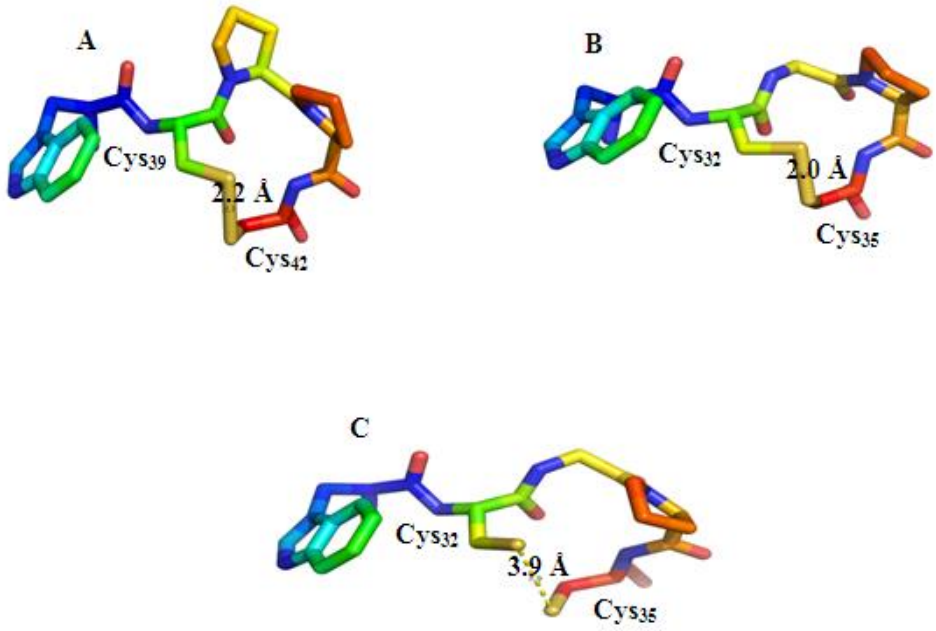

Figure 37: Stick representation: Comparison of the active site motif. (A) Oxidized *Wb*Trx-1 with a bond length of 2.2 Å, (B) oxidized human thioredoxin *Hs*Trx-1 (PDB ID: 1ERU) with a bond length of 2.0 Å and (C) reduced human thioredoxin (PDB ID: 1ERT) with a distance of 3.9 Å between the two cysteins.

5.4.8.1 Comparison of the active sites between related enzymes

The active site contains a conserved Trp, which is present in the characteristic thioredoxin WCPPC sequence motif. This residue is at the surface of the active site and appears to interact with thioredoxin redox partners. In most thioredoxin structures known so far, this Trp has a similar position as found in the original *E. coli* Trx, forming a flat surface close to the active site (see Fig.38)[165].

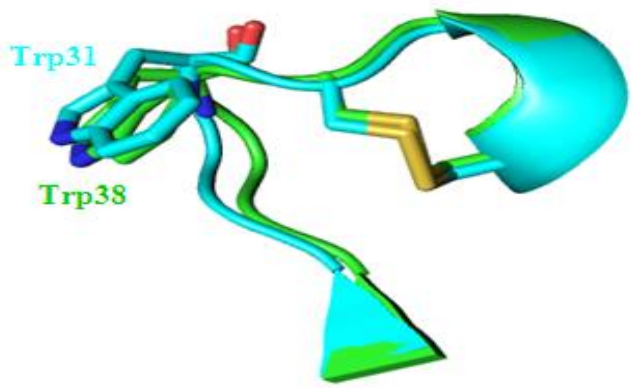

Figure 38: Cartoon plot showing the superposition of the *Wb*Trx-1 active site (green) with the *E.coli* thioredoxin active site (turquoise).

In contrast, the superposition of the *Wb*Trx-1 active site with the spinach thioredoxine (PDB ID: 1F9M) [166] shows that the Trp from spinach thioredoxin is at the surface of the protein, but has a slightly different position. It has become flipped out so that it interacts with neighbouring protein molecules in the crystals, as shown in Fig. 39.

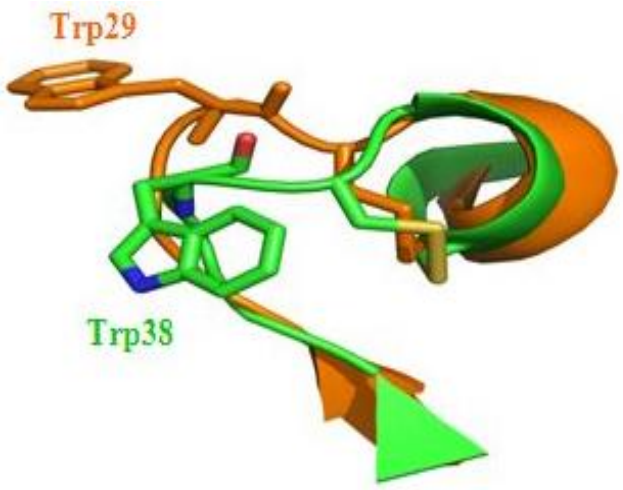

Figure 39: Cartoon plot of the superposition of the *Wb*Trx-1 active site (green) with the spinach thioredoxin active site (orange).

There is a highly conserved Asp_{26}, which was found in mammalians and *E.coli* thioredoxins, which is considered the key residue for activating the second Cys_{42} in the active site motif WCPPC as a nucleophile [102]. In *Wb*Trx-1, there is a tyrosin instead at the equivalent position, close to the cysteins active site, as shown in Fig. 40.

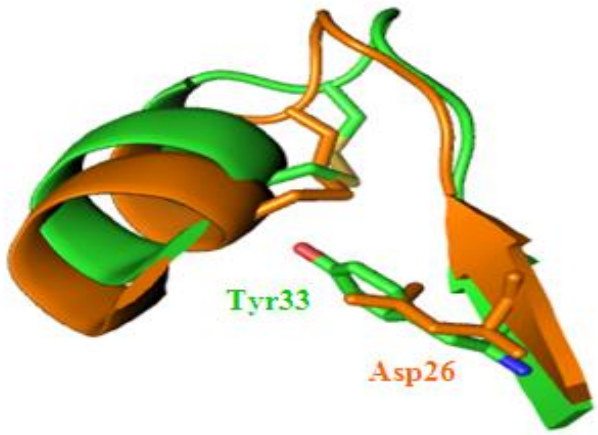

Figure 40: Cartoon plot of the superposition of *Wb*Trx-1 (green) with human thioredoxin (orange).

The superposition of *Wb*Trx-1 with thioredoxin from *Trypanosoma* brucei (PDB ID: 1R26) showed the presence of Try_{24} instead of a highly conserved Asp_{26} (see Fig. 41)[142].

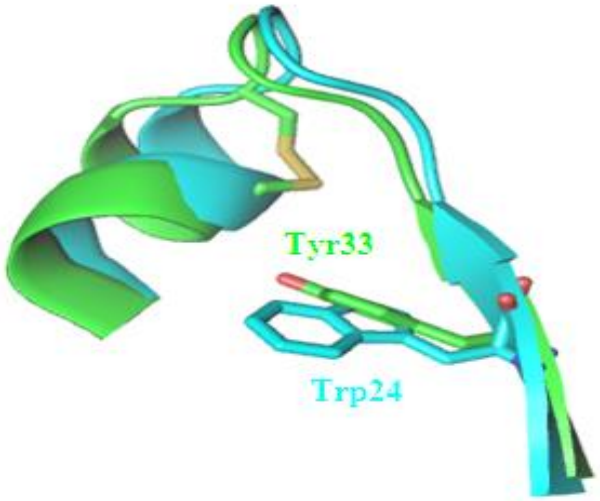

Figure 41: Cartoon plot showing the superposition of *Wb*Trx-1 (green) with *Trypanosoma brucei* (turquoise).

The function of this conserved Asp_{26} has been investigated.The mutation of this amino acid by alanin in *E.coli* thioredoxin decreases the K_m value in the reaction with thioredoxin reductase [105, 167]. Moreover, the mutation of Asp_{26} in *E.coli* had a dramatically lowered ability to serve as a hydrogen donor[95].

5.5 Inhibition of Thioredoxin (*Wb*Trx-1)

With the high expression of Trx observed in many cancers, it is not surprising that a number of different chemical inhibitors of Trx are being assessed for effectiveness as antitumor agents[168]. The most promising up to date is 1-methyl-propyl-2-imidazol disulfide, which is now known as PX-12 in the phase II trails for pancreatic cancer [169].

PX-12 is shown in Fig 42, it was originally discovered by screening numerous disulfide compounds for their ability to inhibit the growth of cancer cell lines *in vitro*[170]. At the highest dose PX-12 displayed 98% reduction against MCF-7 induced tumour formation, revealing its potential as a therapeutic agent[171]. PX-12 or 1-methyl-propyl-2-imidazol disulfide is a competitive, irreversible inhibitor of thioredoxin 1 (Trx1), which acts by binding to Cys_{73} of Trx1[172]. PX-12 causes inhibition of Trx-dependent cell growth[173] and has antitumor activity against human tumor xenografts in scid mice[174, 175]. Further investigation also revealed that cells and patients treated with PX-12 have decreased expression of VEGA[176], a necessary protein for angiogenesis and cancer metastasis. A phase

I clinical trial that administered PX-12 to patients with advanced solid tumors defined the dosage that could be tolerated by patients with minimal side effects[177]. A phase II clinical trial is now underway to test the efficacy of PX-12 treatment with advanced pancreatic cancer patients[169].

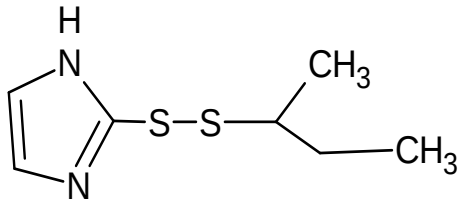

Figure 42: Chemical structure of PX-12 (1-methyl-propyl-2-imidazol disulfide).

The inhibition of *Wb*Trx-1 was performed using 1- Methylpropyl 2-Imidazolyl disulfide (PX-12) as an inhibitor, applying different concentrations ranging from 0.1 to 15 mM (see Fig. 43). First the inhibitor was incubated with *Wb*Trx-1 and the reaction was started with DTT. The turbidity of insulin was measured at 650 nm against the time. The IC_{50} values of inhibitor PX-12 reflected the affinity towards *Wb*Trx-1 with a value of approximately 9.0 mM.

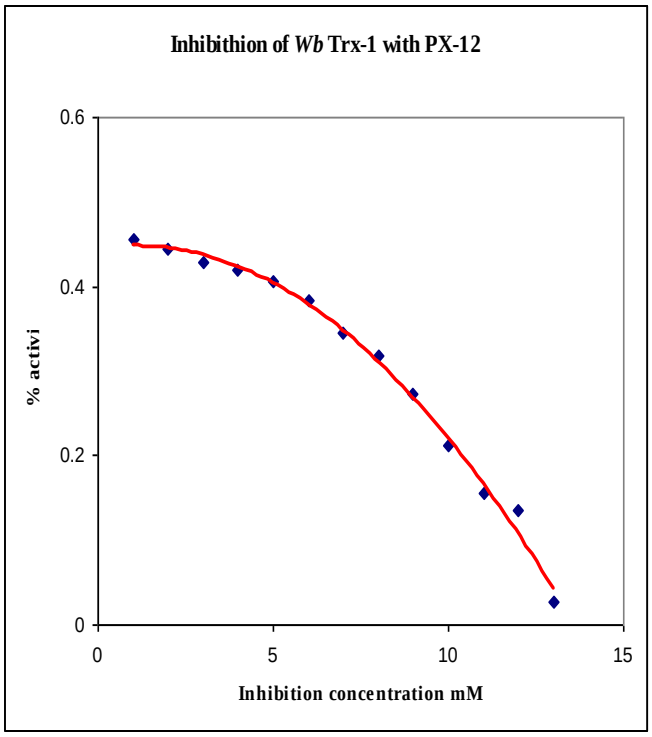

Figure 43: Inhibition of *Wb*Txr-1 by PX-12 inhibitor

5.6 Mutation

The conventional method for cloning a DNA fragment is to insert it into a vector and to ligate it. Although this method is commonly used, it is lab intensive because the ratio and concentrations of the DNA insert and the vector have to be optimized. Even then, the resulting library is often plagued with unwanted plasmids that have either no inserts or multiple inserts. These species have to be eradicated to avoid tedious screening, especially when producing random mutagenesis libraries.

MEGAWHOP is a novel cloning method of DNA fragments which was developed as substitute for the problematic ligation approach (2)[178]. In MEGAWHOP, the DNA fragment to be cloned is used as a megaprimer that replaces a homologous region in the template plasmid. After running whole plasmid PCR using the megaprimer, the resultant mixture is treated with the dam-methylated DNA specific restriction enzyme, DpnI. The treatment enables specific elimination of the template plasmid, because the template plasmid, which can be propagated in most *Escherichia coli* strains, is de-methylated. The DpnI-treated mixture is then introduced into *E. coli* to yield a library. Libraries produced by the MEGAWHOP method are virtually free from contamination by species without any inserts or with multiple inserts. A MEGAWHOP protocol that is especially ideal for creating random mutagenesis libraries is described below in Fig. 44.

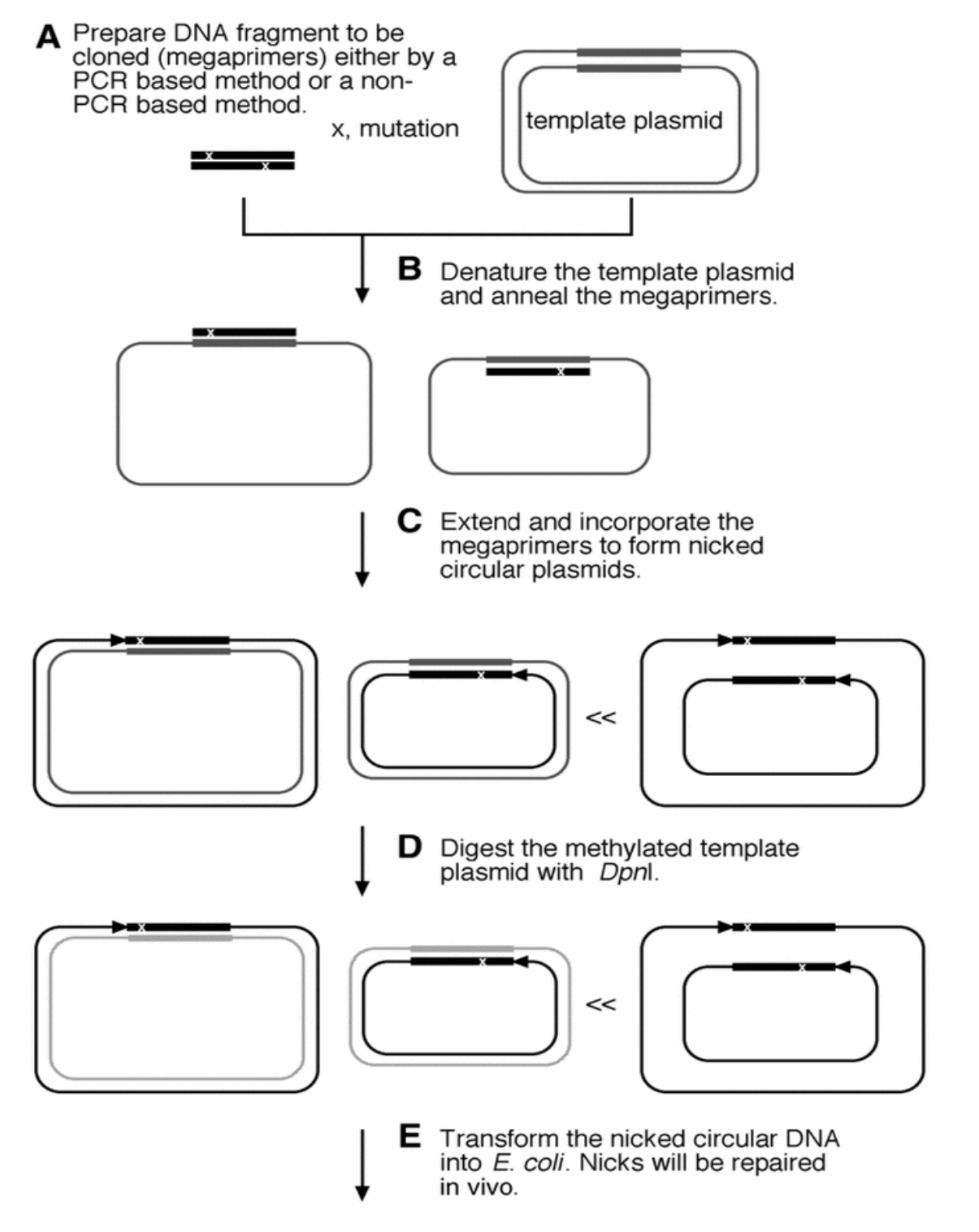

Figure 44: Random Mutagenesis Libraries by MEGAWHOP.

The mutations were stepwise introduced by the random mutagenesis libraries, therefore, two successive site-directed mutagenesis steps were performed to mutate the selected Cys residues into Ser residues. The expected size of the fragment was confirmed by agarose gel electrophoresis (see Fig. 45).

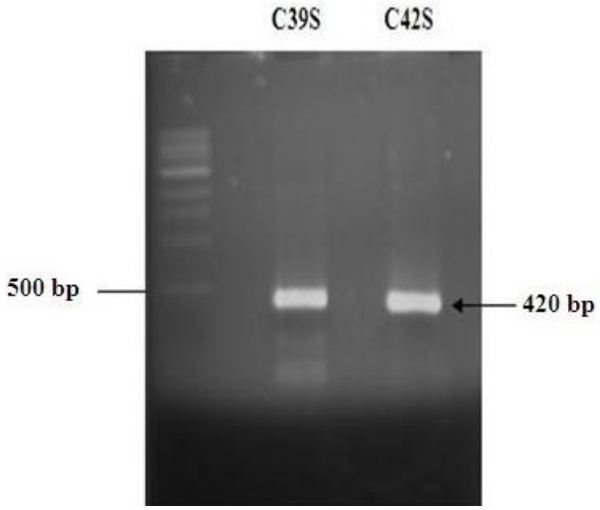

Figure 45: Gel electrophoretic analysis of the *Wb*Trx-1 gene, carrying the mutations C39S and C42S, using a 2% agarose gel.

5.7 Expression and purification of the *Wb*Trx-1 variant

The expression as well as the purification of the two mutants *Wb*Trx-1-C39S and *Wb*Trx-1-C42S was performed according to the established protocol of the *wild type Wb*Trx-1, with the observation of a dimer formation for the mutant *Wb*Trx-1-C42S, as shown in Fig. 46.

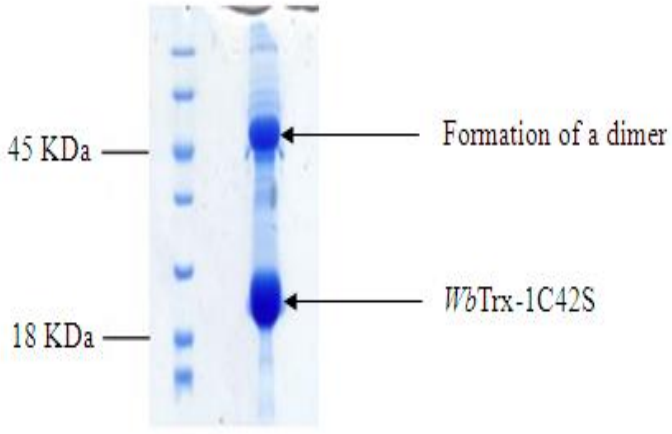

Figure 46: Expression of *Wb*Trx-1-C42S.

5.8 Crystallization of the *Wb*Trx-1 variant (*Wb*Trx-1-C39S)

The crystallization conditions were obtained after the PCT™ Pre-Crystallization Test, applying the hanging-drop vapour-diffusion method using the same protocol as used with the *wildtype*. *Wb*Trx-1-C39S crystals were obtained using the condition containing 25% PEG 3000, 200 mM NaCl, 200 mM $(NH_4)_2SO_4$ and 100 mM Tris/HCl pH 5.6. 2µl of the protein solution and 2µl of the reservoir solution were equilibrated against 1 ml of reservoir solution. Crystals of around 300×300×350 μm^3 were obtained after 3 weeks (see Fig. 47).

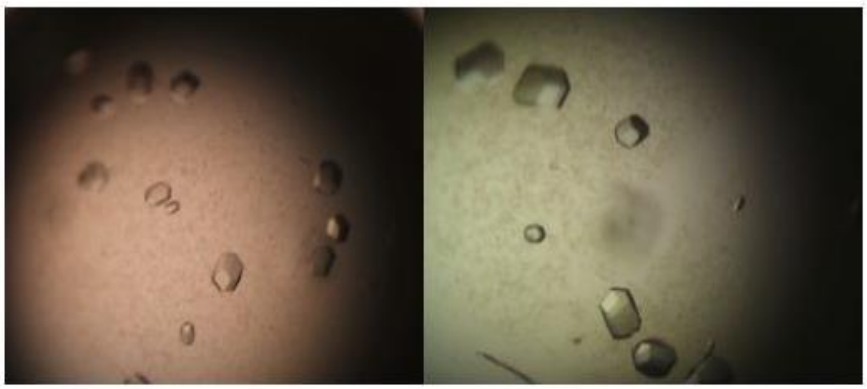

Figure 47: Crystals of the *Wb*Trx-1-C39S variant

5.8.1 Data collection

Diffraction data were collected at the same consortium beam line X13 at HASYLAB/DESY, Hamburg-Germany, as mentioned before and the ice production was prevented by soaking the crystals in the same mother liquor containing 20% glycerol before soaking. Sufficient data were collected with a maximum resolution of 2.45 Å. The data were processed using the HKL program package and the space group was identified to be Primitive Tetragonal $P4_22_12$ with the cell dimensions of a = b = 193.1 Å and c = 111.6 Å. The matthews coefficient[154] (V_M = 2.7 $Å^3$ / Da) suggested that twelve protein molecules were located in the asymmetric unit with a solvent content of 54.6%, as shown in Fig. 48.

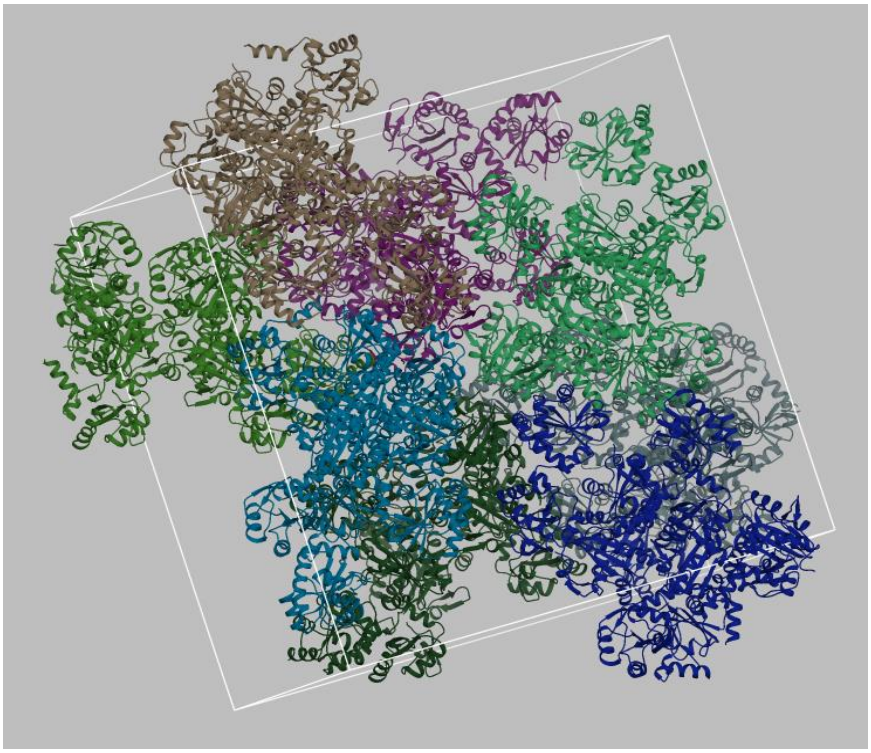

Figure 48: Posithion of the *Wb*Trx-1-C39S molecules in the unit cell.

5.8.2 Structure solution

The structure determination and the phase information were obtained by Molecular replacement (MR) using the coordinate form the *wild type* thioredoxin (PDB ID: 4FYU). The amino acids sequence between *Wb*Trx-1 and *Wb*Trx-1-C39S showed 99.3 % sequence identity (see Fig. 49).

```
4FYU    MADLLANIDLKKADGTVKKGSDALANKKVVALYFSAHWCPPCRQFTPILKEFYEEVDDDQ 60
C39S    MADLLANIDLKKADGTVKKGSDALANKKVVALYFSAHWSPPCRQFTPILKEFYEEVDDDQ 60
        ************************************.********************

4FYU    FEIVFVSLDHSEEDLNNYVKESHGDWYHVPFGSSEIEKLKNKYEVAGIPMLIVIKSDGNV 120
C39S    FEIVFVSLDHSEEDLNNYVKESHGDWYHVPFGSSEIEKLKNKYEVAGIPMLIVIKSDGNV 120
        ************************************************************

4FYU    ITKNGRADVSGKAPPQTLSSWLAAA 145
C39S    ITKNGRADVSGKAPPQTLSSWLAAA 145
        *************************
```

Figure 49: Sequence alignment between *Wb*Trx-1 (PDB ID: 4FYU) and *Wb*Trx-1-C39S. The figure was prepared using the ClustalW2. The active site residues are marked with a black box and the conserved residues with a star.

5.8.3 Model Building and Refinment

The model building and refinement of *Wb*Trx-1-C39S was performed using the programs Coot and Refmac5. The protein structure of approx. 16 KDa was crystallized and contains 144 of 145 amino acids with the absence of the first amino acid methionine. The model was refined up to 2.49 Å resolution with $R_{crystal}$ of 20.4% and R_{free} of 22.8%. The data collection and refinement parameters are shown in Table 9.

Table 9: Data collection and refinement statistics of *Wb*Trx-1-C39S.

Parameters	***Wb*Trx-1-C39S**
Space group	$P4_22_12$
a = b (Å)	193.1
c (Å)	111.6
V_M (Å^3/ Da)	2.7
Solvent content (%)	54.6
Completeness of data (%)	98.9 (83.4)
No. of total reflections	560817
No. of used reflections	73170
Average I/sigma intensity	20.8 (5.3)
Resolution (Å)	28.4-2.49
Redundancy	7.1 (7.0)
R_{merge} (%)	5.1 (34.8)
$R_{crystal}$ (%)	20.4 (23.9)
R_{free} (%)	22.8 (26.53)
Protein atoms	13536
Solvent atoms	750
Average B-factor (Å^2)	
Main-chain atoms	8.4
Side chain atoms and water	10.7
Root mean square deviation	
Bonds (Å)	0.014
Bond angles (^{o})	1.62
Residues in regions of the Ramachandran plot (%)	
Most favored	94.42 %
Allowed	5.58 %
Disallowed	0.0

Values in parentheses are for the highest resolution shell.
R_{merge}: $\sum_{hkl} \sum_{i|} I_i(hkl) - \rangle I(hkl) \langle | / \sum_{hkl} \sum_i I_i(hkl)$, where $\rangle I(hkl) \langle$ is the mean intensity of the observations $I_i(hkl)$ of reflection hkl.

5.8.4 Description of the molecule

The amino acid sequence of *Wb*Trx-1-C39S was applied to the ExPASy proteomics Server and some of the primary sequence statistics are shown in Table 10.

Chain ID	Chain A
Formula	**$C_{728}H_{1124}N_{186}O_{221}S_3$**
No. of amino acids	**145**
Molecular weight (Da)	**16114.2**
Theoretical pI	**5.16**
Total No. of atoms	**2262**
No. of negatively residues	**22**
No. of positively residues	**16**
No. of cysteines	**1**

Table 10: Statistical values of the primary amino acid sequence of *Wb*Trx-1-C39S.

The overall structure of *Wb*Trx-1-C39S is similar to other thioredoxins including the *wild type* of *Wb*Trx-1, which incorporates the classical thioredoxin fold with central β-sheets surrounded by α-helices. The central β sheet carries a motif of β_3-α_2-β_4-α_3-β_5-α_4-β_6 with alternating parallel ($\beta_3\beta_4\beta_5$) and anti-parallel ($\beta_5\beta_6$) beta strands. Moreover, the structure has two β hair pin bends, one at the N-terminal ($\beta_1\beta_2$) and the other at the C-terminal ($\beta_6\beta_7$). Helix 5 is broken into two halves, α_5A and α_5B, due to the presence of Pro_{132} and Pro_{133}. All residues are located in the electron density accept the first amino acid Methionine. The side chains of Lys_{18}, Lys_{19}, Asn_{26}, and Glu_{44} are all located at the surface of the protein and have incomplete electron density. The overall structure is shown in Fig. 50.

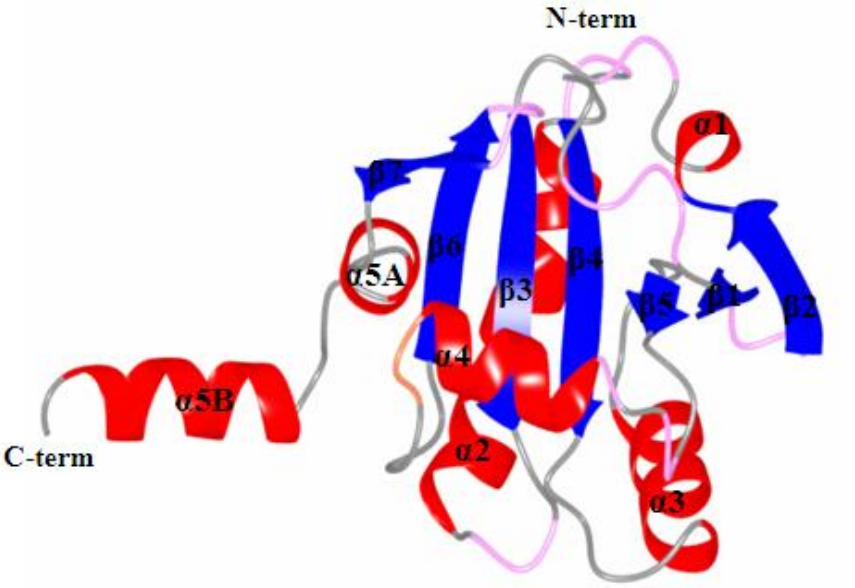

Figure 50: Overall structure of *Wb*Trx-1-C39S.

5.8.5 Comparison of *Wb*Trx-1-C39S structure with related enzymes

It is now necessary to compare *Wb*Trx-1-C39S with some other thioredoxins with respect to folding and conformation. Searching the protein data bank for related thioredoxins, which have the highest sequence homology with *Wb*Trx-1-C39S, revealed several examples. Next, the comparison of *Wb*Trx-1-C39S with tryparedoxin-1 from *Crithidia fasciculata* (PDB ID: 1QK8), *E.coli* thioredoxin (PDB ID: 2TRX) and human oxidized thioredoxin (PDB ID: 1ERU) will be shown respectively.

The amino acid alignment sequence between *Wb*Trx-1-C39S and tryparedoxin from *Crithidia fasciculate* (PDB ID: 1QK8) is shown in Fig. 51 with an identity of 38.1%.

```
C39S    ---MADLLANID-LKKADGTVKKGSDALANKKVVALYFSAHWSPPCRQFTPILKEFYEEV 56
1Qk8    MSGLDKYLPGIEKLRRGDGEVEVKS---LAGKLVFFYFSASWCPPCRGFTPQLIEFYDKF 57
           : . *..*: *::.** *:  *      *:* :**** *.**** *** * ***::.

C39S    DDDQ-FEIVFVSLDHSEEDLNNYVKESHGDWYHVPFGSSE-IEKLKNKYEVAGIPMLIVI 114
1Qk8    HESKNFEVVFCTWDEEEDGFAGYFAKMP--WLAVPFAQSEAVQKLSKHFNVESIPTLIGV 115
        .:.: **:** : *..*:.: .*. :    *  ***..** ::**.::::* .** ** :

C39S    KSD-GNVITKNGRADVSGKAPPQTLSSWLAAA 145
1Qk8    DADSGDVVTTRARATLV-KDPEGEQFPWKDAP 146
        .:* *:*:*...** :  * *     .*  *.
```

Figure 51: Sequence alignment between *Wb*Trx-1-C39S and tryparedoxin from *Crithidia fasciculata* (PDB ID: 1QK8). The figure was prepared using the ClustalW2. The active site residues are marked with a black box and the conserved residues with a star.

A comparison between *Wb*Trx-1-C39S in green with the tryparedoxin fom *Crithidia fasciculata* (PDB ID: 1QK8) in orange is shown in Fig. 52. 144 residues from *Wb*Trx-1-C39S are aligned against 143 residues from 1QK8. 94 Cα atoms have been aligned with a RMS deviation for all atoms of 1.04 Å. Some deletions and insertions have been observed.

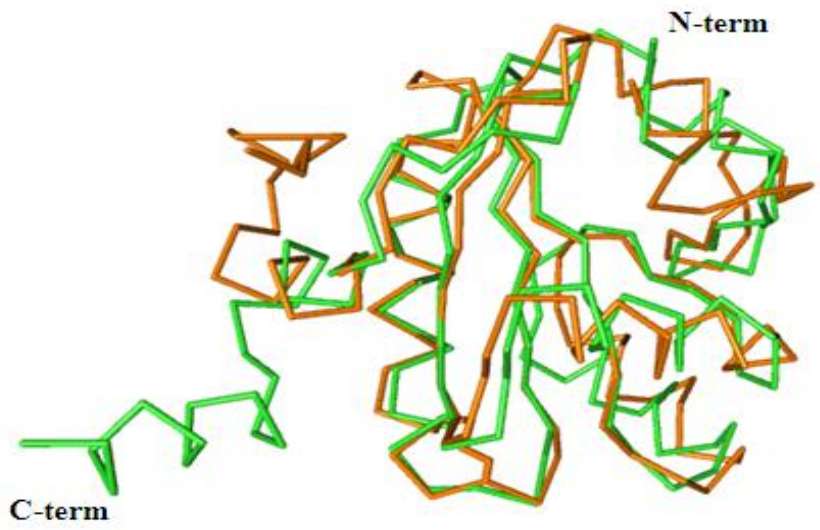

Figure 52: Stick represintation of the superposition of *Wb*Tr-x-1 (green) with the tryparedoxin fom *Crithidia fasciculata* (orange).

The sequence alignment between *Wb*Trx-1-C39S and *E.coli* thioredoxin is shown in Fig. 53, the identity is 21.3% between the two proteins.

```
C39S    MADLLANIDLKKADGTVKKGSDALANKKVVALYFSAHWSPPCRQFTPILKEFYEEVDDDQ 60
2TRX    -SDKIIHLTDDSFD------TDVLKADGAILVDFWAEWCGPCKMIAPILDEIADEYQG-K 52
         :* : ::  .. *      :*.*  . .: : * *.*. **: ::***.*: :* :. :

C39S    FEIVFVSLDHSEEDLNNYVKESHGDWYHVPFGSSEIEKLKNKYEVAGIPMLIVIKSDGNV 120
2TRX    LTVAKLNIDQNPGTAP------------------------KYGIRGIPTLLLFKNGEVA 87
        : :. :.:*:.                              ** : *** *:::*..  .

C39S    ITKNGRADVSGKAPPQTLSSWLAAA 145
2TRX    ATKVG--ALSKGQLKEFLDANLA—108
```

Figure 53: Sequence alignment between *Wb*Trx-1-C39S and thioredoxin from *E. coli* (PDB ID: 2TRX). The figure was prepared using the ClustalW2. The active site residues are marked with a black box and the conserved residues with a star.

*Wb*Trx-1-C39S is now compared with another thioredoxin from *E.coli* PDB ID: 2TRX). 144 residues from *Wb*Trx-1-C39S (green) were aligned against 108 residues from *E.Coli* thioredoxin (turquoise). 58 Cα atoms have been aligned with a RMS deviation of 1.50 Å. This higher RMS value is consistent with Fig. 54, which showed some deletions and insertions in loop and helical regions.

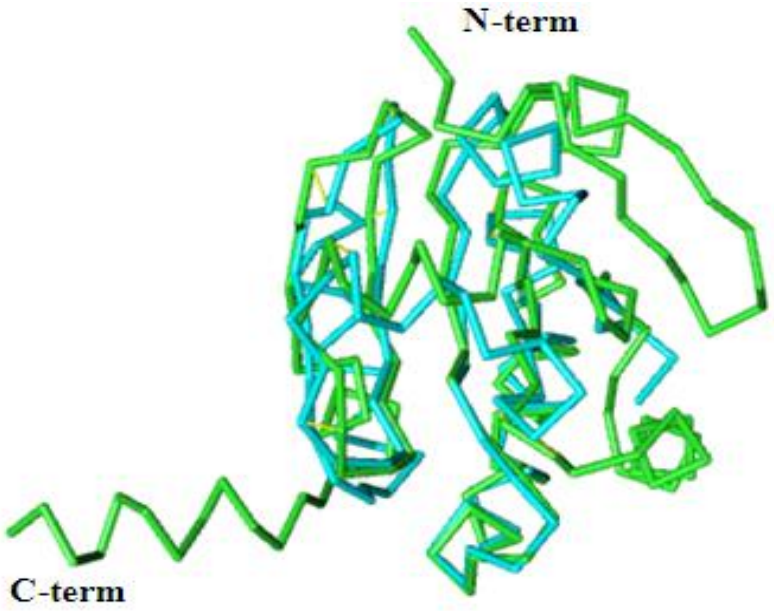

Figure 54: Stick represintation of the superposition of *Wb*Trx-1-C39S (green) with *E.Coli* thioredoxin (turquoise).

The sequence alignment between *Wb*Trx-1-C39S and *human* thioredoxin is shown in Fig. 55, the identity is 16.2 between the two proteins.

```
C39S    MADLLANIDLKKADGTVKKGSDALANKKVVALYFSAHWSPPCRQFTPILKEFYEEVDDDQ 60
1ERU    ---MVKQIESKTA---FQEALDAAG-DKLVVVDFSATWCGPCKMIKPFFHSLSEKYSN-- 51
           :: :*: *.*   .::. ** . .*:*.: *** *. **: :.*::::.: *: .:

C39S    FEIVFVSLDHSEEDLNNYVKESHGDWYHVPFGSSEIEKLKNKYEVAGIPMLIVIKSDGNV 120
1ERU    --VIFLEVDVDD----------------------CQDVASECEVKCMPTFQFFKKGQKV 86
          ::*:.:* .:                        :.: .: **  :* : .:*.. :*

C39S    ITKNGRADVSGKAPPQTLSSWLAAA 145
1ERU    GEFSGANKEKLEATINELV------ 105
           .*  . . :*. : *
```

Figure 55: Sequence alignment between *Wb*Trx-1-C39S and *human* thioredoxin (PDB ID: 1ERU). The figure was prepared using the ClustalW2. The active site residues are marked with a black box and the conserved residues with a star.

*Wb*Trx-1-C39S is finally compared with oxidized thioredoxin from human (PDB ID: 1ERU). 144 residues from *Wb*Trx-1-C39S (green) were aligned against 105 residues from human thioredoxin (rose). 53 Cα atoms have been aligned with a RMS deviation of 5.25 Å. This high RMS value is in consistent with Fig. 56, which showed more deletions and more insertions of loops and helices.

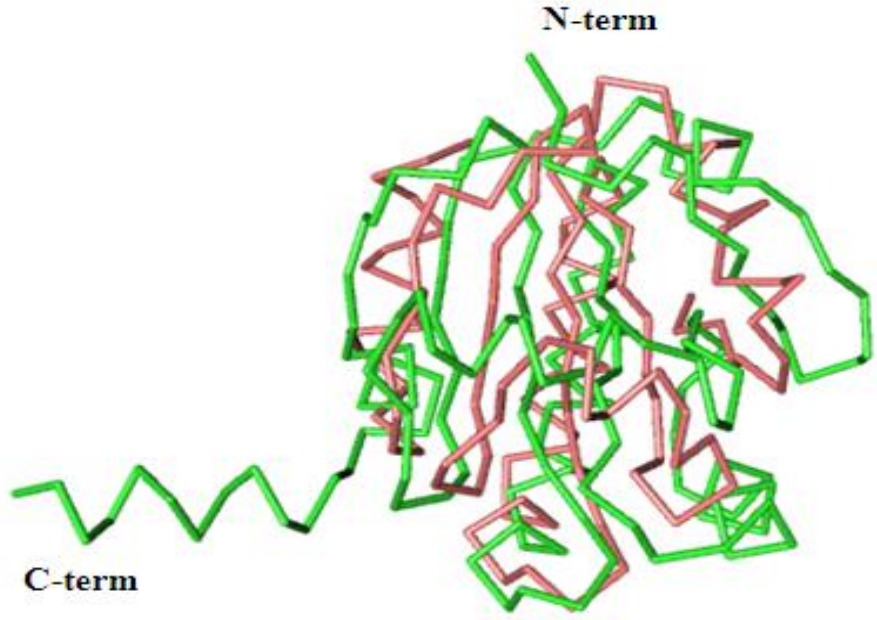

Figure 56: Stick represintation of the superposition of *Wb*Trx-1-C39S (green) with human thioredoxin (rose).

Pairwise least square superposition of the four structures showed that 36–65 % of the Cα-atoms are in common positions and gave a root mean square deviation of 1.05–5.25 Å. The paiwise superposition in the following order: *Wb*Trx-1–1QK8 > *Wb*Trx-1–2TRX > *Wb*Trx-1–1ERU are shown in Table 11.

	***Wb*-C39S – 1QK8**	***Wb*-C39S – 2TRX**	***Wb*-C39S – 1ERU**
Number of residues	**144 – 143**	**144 – 108**	**144 - 105**
Alignment residues	**94 (65 %)**	**58 (40 %)**	**53 (36 %)**
Root mean square deviation (Å)	**1.04**	**1.50**	**5.25**

Table 11. Pairwise superposition of Cα-atoms of *Wb*Trx-1-C39S, 1QK8, 2TRX, and 1ERU

5.8.6 Interactions between *Wb*Trx-1-C39S chains

*Wb*Trx-1-C39S was crystallized with twelve molecules in the asymmetric unit, from cahin A until chain L. The interfaces summary and the arrangement of *Wb*Trx-1-C39S twelve chains, is shown in Fig 57.

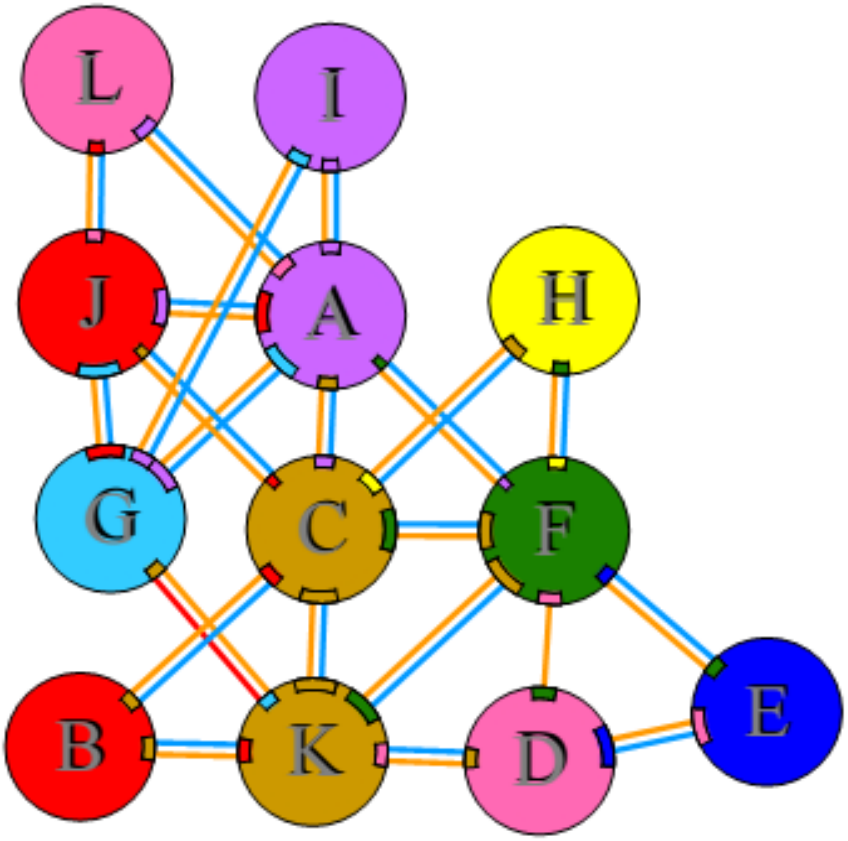

Figure 57: Schematic diagram of interactions between *Wb*Trx-1-C39S protein chains. Hydrogen bonds are indicated with blue lines, non-bond contacts are indicated with yellow lines and salt bridges are indicated with red lines.

The *Wb*Trx-1-C39S protein associated with some hydrogen bonds and non-covalent interactions across the interface of the twelve chains. The total number of hydrogen bonds and the non-covalent interactions are shown in Table 12.

Chains	No. of interface residues	No. of salt bridges	No. of hydrogen bonds	No. of non-covalent interactions
A←→C	6 : 6	-	4	40
A←→F	2 : 2	-	1	9
C←→J	3 : 2	-	1	12
A←→G	15 :13	-	4	69
C←→K	15:13	-	4	71
G←→J	15 :13	-	4	74
A←→I	5 :7	-	4	31
E←→F	5 :7	-	4	28
F←→H	5 :6	-	3	23
J←→L	6 : 7	-	3	21
A←→J	13 :14	-	3	58
C←→F	13 :16	-	3	64
D←→E	13 : 13	-	3	63
F←→K	13 :15	-	4	73
A←→L	10 : 10	-	2	34
B←→K	11 : 10	-	1	33
C←→H	11 : 11	-	2	37
D←→F	10 :11	-	-	26
G←→I	9 : 9	-	2	22
B←→C	8 : 5	-	4	39
D←→K	9 :5	-	4	50
G←→K	5 : 5	2	-	43

Table 12: Interactions across the interfaces of *Wb*Trx-1-C39S chains.

5.9 Active site

The active site motif of the variant *Wb*Trx-1-C39S contains the amino acid sequence WSPPC in the reduced form due to the single mutation of the first Cys into Ser. The active site contains also several residues, which are important for the structural function of the thioredoxin as mentioned before in the *wild type*. The active site is shown in Fig. 58, with a bond length of 3.5 Å between Ser_{39} and Cys_{42}.

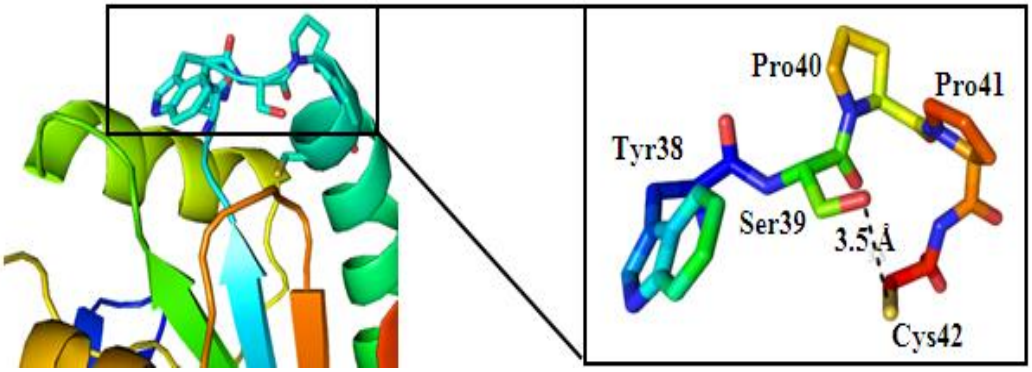

Figure 58: Zoom of the active site motif of *Wb*Trx-1-C39S with a bond length of 3.5 Å between Ser_{39} and Cys_{42}.

The comparison between the active site of *Wb*Trx-1-C39S with the active site of *human* thioredoxin (*Hs*Trx-1) oxidized and reduced are shown in Fig. 59. The superposition of *Wb*Trx-1-C39S with *human* thioredoxin showed RMS value of 0.11 Å, while five atoms from *Wb*Trx-1-C39S were aligned against five atoms from cytosolic *Hs*Trx-1.

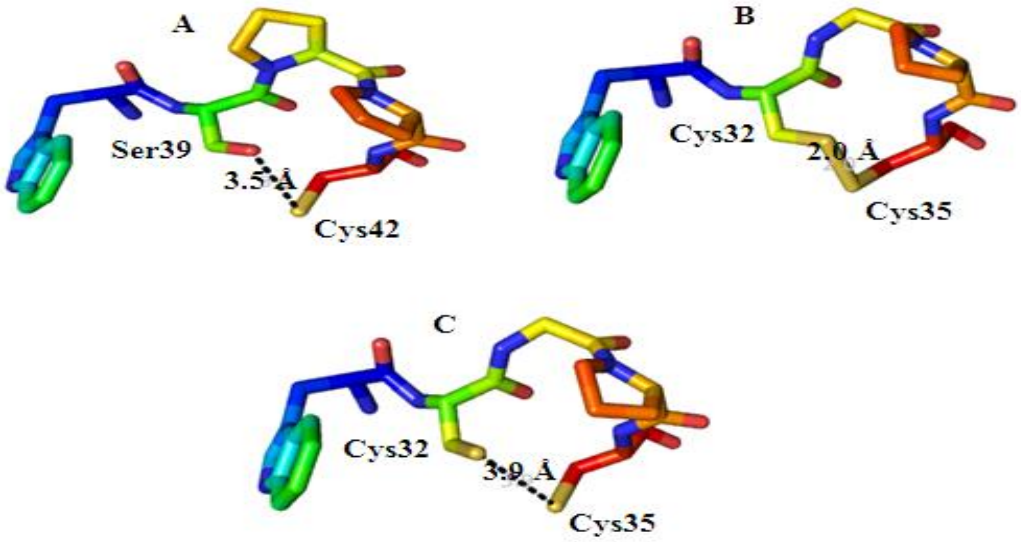

Figure 59: Stick representation: Comparison of the active site motif. (A) *Wb*Trx-1-C39S with a distance of 3.5 Å between Ser and Cys, (B) oxidized human thioredoxin *Hs*Trx-1 (PDB ID: 1ERU) with a bond length of 2.0 Å and (C) reduced human thioredoxin (PDB ID: 1ERT) with a distance of 3.9 Å between the two cysteins.

5.10 Comparison between *Wb*Trx-1 *wild type* and *Wb*Trx-1 variant

*Wb*Trx-1 was crystallized in an oxidized form with a disulfide bond between the two active site cysteines. The *Wb*Trx-1 crystal diffracted to 1.95 Å corresponding to the space group I Centered Tetregonal I422, with three molecules in the asymmetric unit. While the *Wb*Trx-1-C39S was crystallized in a reduced form and the crystal diffracted up to 2.49 Å corresponding to the space group Primitive Tetragonal $P4_22_12$ with twelve molecules in the asymmetric unit. The alignment of the amino acid sequence between the two proteins showed 99.3 % amino acid identity and the superposition of the two proteins showed structures identity with RMS deviation of 0.16 Å, as shown in Fig. 60.

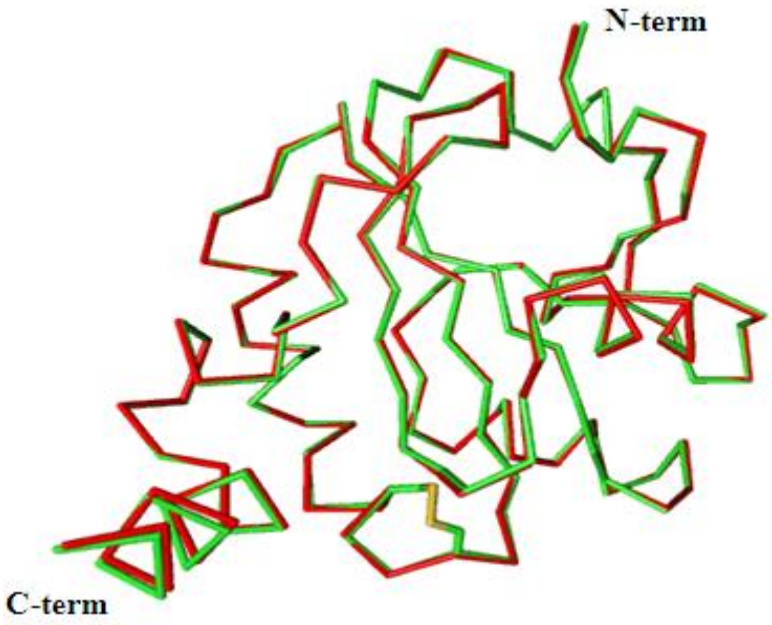

Figure 60: Stick represintation of the superposition of oxidized *Wb*Trx-1 (green) with reduced *Wb*Trx-1-C39S (red).

5.11 Docking of *Wb*Trx-1-C39S with small molecules

The used compounds for docking were known for their inhibitory activity towards thirodoxin. Since Hex 6.3 accepts only few file formats like PDB or MOL, the structures of the inhibitors were first drawn using the program chemSketch and saved in PDB format before docking. Then the receptor *Wb*Trx-1-C39S and the ligand were loaded and docking was carried out in the 'full rotation mode'. During the docking process, initially Fourier transformation takes place followed by steric scan, final search, refinement and finally total docking. From the total number of solutions, the ligand binding site with minimum energy (kJ mol^{-1}) value was taken as the best solution.

5.11.1 Docking of *Wb*Trx-1-C39S with histon deacetylases inhibitors SAHA and TSA

An alternative therapeutic approach is to inhibit Trx by the regulation of endogenous inhibitors. With this indirect targeting of Trx, Suberoylanilide gydroxamic acid (SAHA) functions can be obtained.

Histone deacetylase inhibitors (HDACis) are a relatively new class of anti cancer therapeutic agents that act by chromatin modification and thereby affect gene expression [179]. SAHA is shown in Fig. 61, it inhibits the growth of a broad spectrum of solid tumors, both *in vitro* and *in vivo*, but does not inhibit the growth of normal cells [180]. SAHA has been the subject of many clinical trials and is manufactured as the drug Zolinza by Merck. It was approved by the FDA in 2006 for the treatment of cutaneous T-cell lymphoma[181] and is currently being assessed in clinical trials for its effectiveness in treating other cancers[182]. The action of SAHA was shown to be mediated by its effects on the Trx system [183].

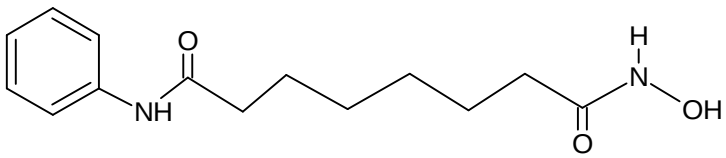

Figuer 61: Chemical structure of SAHA (Suberoylanilide gydroxamic acid).

The other homologous histone deacetylase is TSA (Trichostatin A), which serves as an antifungal antibiotic and selectively inhibits the class I and II mammalian histone deacetylases (HDAC)[184]. TSA is shown in Fig. 62, inhibits the eukaryotic cell cycle during

the beginning of the growth stage. TSA can be used to alter gene expression by interfering with the removal of acetyl groups from histones (histone deacetylases, HDAC) and therefore alters the ability of DNA transcription factors to access the DNA molecules inside the chromatin. It is a member of a larger class of histone deacetylase inhibitors (HDACIs) that have a broad spectrum of epigenetic activities. Thus, TSA has some potential as an anti-cancer drug[185]. One suggested mechanism is that TSA promotes the expression of apoptosis-related genes, leading to cancerous cells surviving at lower rates, thus slowing the progression of cancer[186]. Other mechanisms may include the activity of HDACIs to induce cell differentiation, thus acting to 'mature' some of the de-differentiated cells found in tumors. HDACIs have multiple effects on non-histone effector molecules. However the anti-cancer mechanisms are truly not understood at this time.

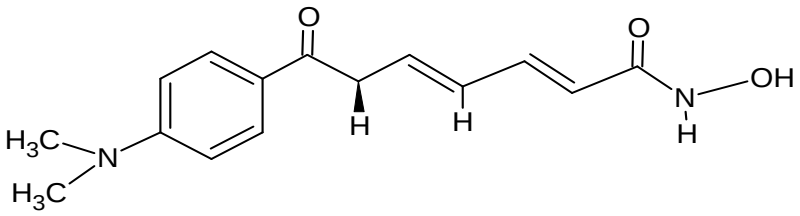

Figuer 62: Chemical structure of TSA (7-[4-(dimethylamino) phenyl]-N-hydroxy-4, 6-dimethyl-7-oxohepta-2, 4- dienamide).

The crystal structures of TSA and SAHA complexes with HDLP (Histon deacytylase like protein) homologues to HADC have been solved and provide a framework to understand the inhibition of the histon deacetylase family[187]. As TSA and SAHA frame the same family, the docking experiment was made with the *Wb*Trx-1-C39S as receptor and TSA as the ligand.

The result of the docking is shown in Fig. 63. The five carbon aliphatic chain of TSA fits between the loops L1 and L3 close to the N-terminal introducing a new pocket for inhibition and making several van der Waals contacts with all hydrophobic groups in the pocket between Asp_3, Leu_4, Leu_{24}, Lys_{27} from the N-terminal and Ser_{116} from the C-terminal with minimum energy of -214.8 kJ mol^{-1}.

.

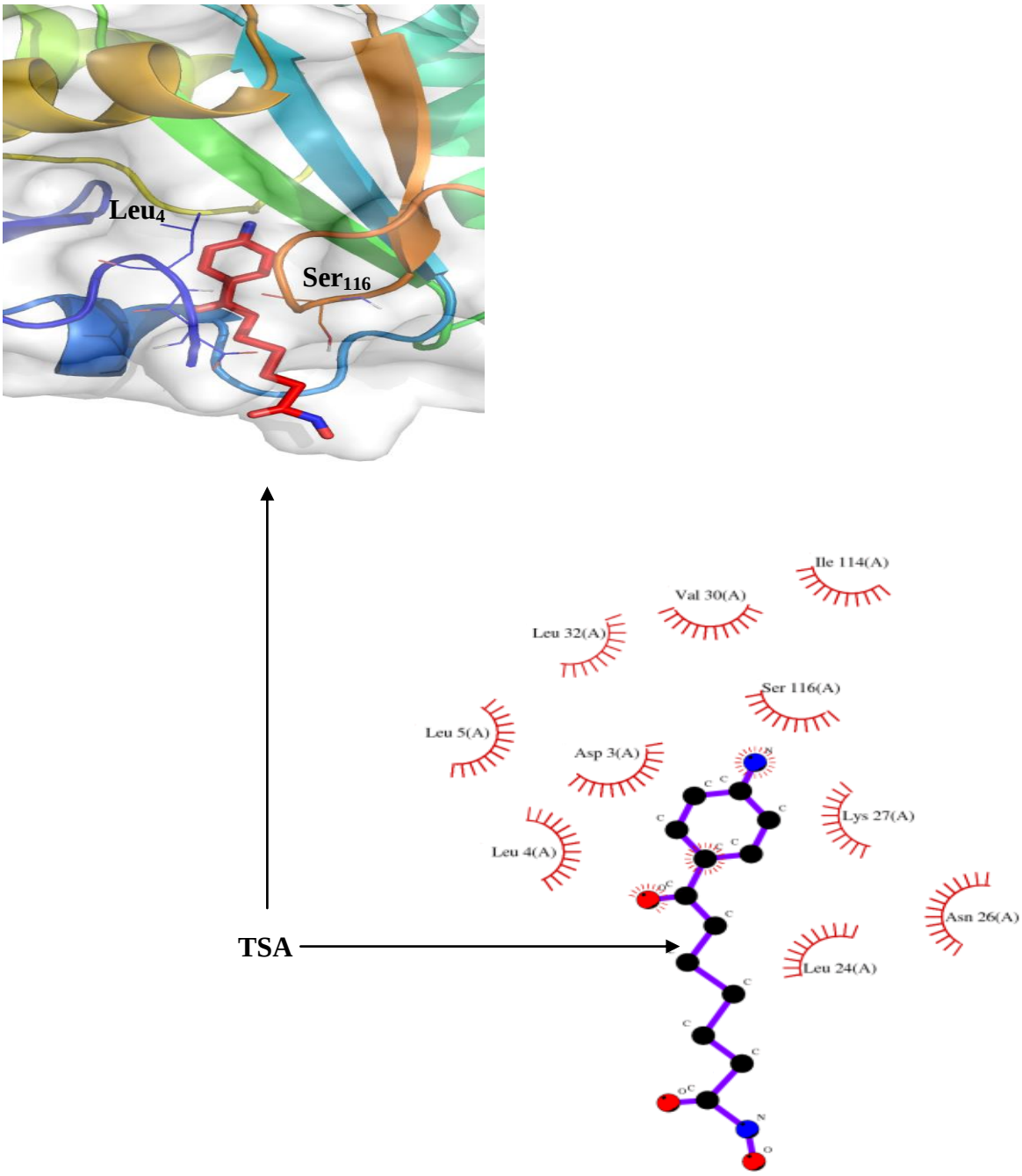

Figure 63: Cartoon representation of TSA docked with *Wb*Trx-1-C39S and the ligplot of interactions between the ligand and the protein amino acids. The structure is orientated to see the pocket introduced by the ligand.

5.11.2 Docking of *Wb*Trx-1-C39S with Triazol compound

Triazols are heterocyclic compounds containing two carbon atoms and three nitrogen atoms as part of the aromatic five member ring. Triazol attributes either one of a pair of isomeric chemical compounds, 1, 2, 3-Triazol or 1, 2, 4-Triazol.

1, 2, 4-Triazol has been used in a wide variety of therapeutically important agents. It has been used as antiviral (Ribavirin)[188], antimigraine (Rizatriptan)[189], antitumor (Vorozole)[190] and some examples of drugs containing 1, 2, 4-Triazol are used in current treatment as antifungal (Fluconazole and Itraconazole)[191]. Moreover N-substituted Triazol attached with different heterocyclic nuclei have been used as antioxidant[192].

3-mercapto-4-methyle-4H-1, 2, 4-Triazol (see Fig. 64) is an organosulphur compound that contains a sulphur-hydrogen bond, analogous to an OH group. The commonly use of this compound is as a reagent for the reduction of the protein disulfide of biological compounds in solution.

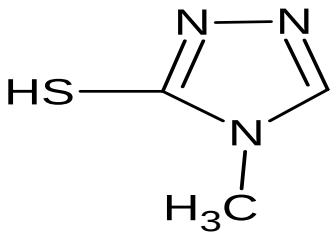

Figure 64. Chemical structure of 3-mercapto-4-methyle-4H-1, 2, 4-Triazol.

The result of docking using the *Wb*Trx-1-C39S molecule as a receptor with 3-mercapto-4-methyle-4H-1, 2, 4-Triazol as ligand shows also a binding site located close to the C-terminal of the structure between Pro_{109}, Leu_{111} and Arg_{126}, as shown in Fig.65, with hydrophobic intractions and minimum energy of -127.8 kJ mol^{-1}.

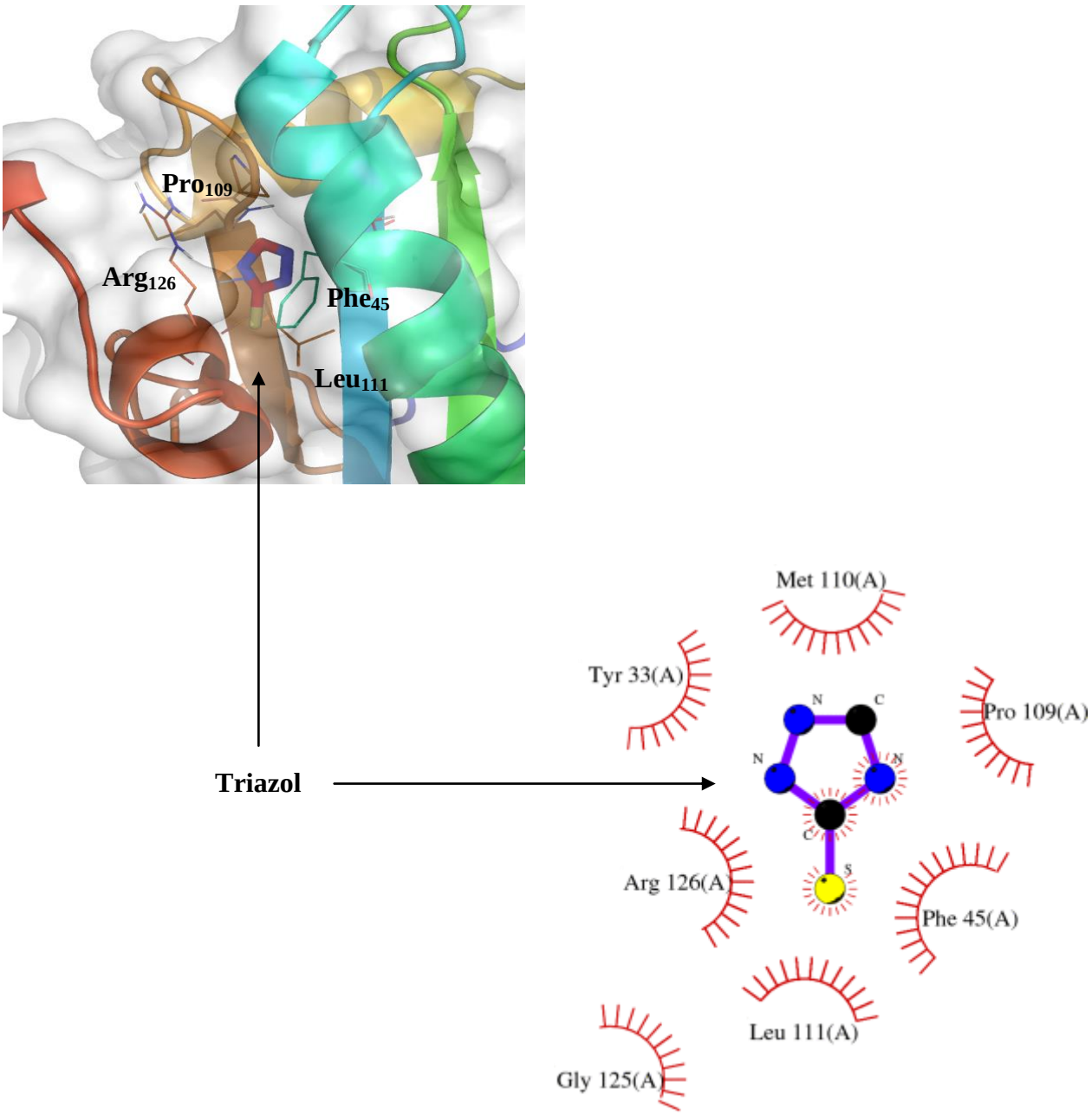

Figure 65: Cartoon representation of 3-mercapto-4-methyle-4H-1, 2, 4-Triazol docked with *Wb*Trx-1-C39S and the ligplot of interactions between the ligand and the protein amino acids. The structure is orientated to see the pocket introduced by the ligand.

5.11.3 Docking of *Wb*Trx-1-C39S with Cisplatin

The anticancer activity of cisplatin (4-2-diamminedichloroplatinum (II)) (see Fig. 66) has been discovered in 1960 and its later clinical success produced interest in the use of metal compounds in the treatment of cancer[193]. Many platinum compounds have been investigated and evaluated as potential chemotherapeutic agents but few of them have entered the clinical use[194, 195]. Cisplatin is responsible for the cure of 90 % of testicular cancer and plays a vital role in the treatment of several other cancers[196].

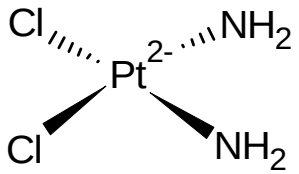

Figure 66: Chemical structure of 4-2-diamminedichloroplatinum.

The key observations that lead to the discovery of cisplatin are well documented[197]. It started with the growing of *E.coli* cells in ammonium chloride buffer containing platinum electrodes immersed in the buffer. After a period of time the *E.coli* cells appeared long like spaghetti, instead of their classical shape[198]. After more investigations, this phenomenon of *E.coli* growth promoted by the hydrolysis of the platinum products formed from the electrodes[199]. It was also reported that the cis form of the platinum complex is effective, whereas the trans form was found to be ineffective[200].

The platinum complexes were tested against Sarcoma 180 tumor in mice. The complexes demonstrate a potent activity against tumors and the mice survived without any signs of cancer after 6 months of treatment[201, 202].

Trx was considered as a validated cancer drug target, associated with aggressive tumor growth, resistance to standard therapy and decreased patient survival. The docking study was performed using *Wb*Trx-1 as a receptor and cisplatin as a ligand. The docking result shows a binding site close to the C-terminal between Pro_{109} and Met_{110}, as shown in Fig. 67, with hydrophobic interactions and minimum energy of -101.7 kJ mol^{-1}.

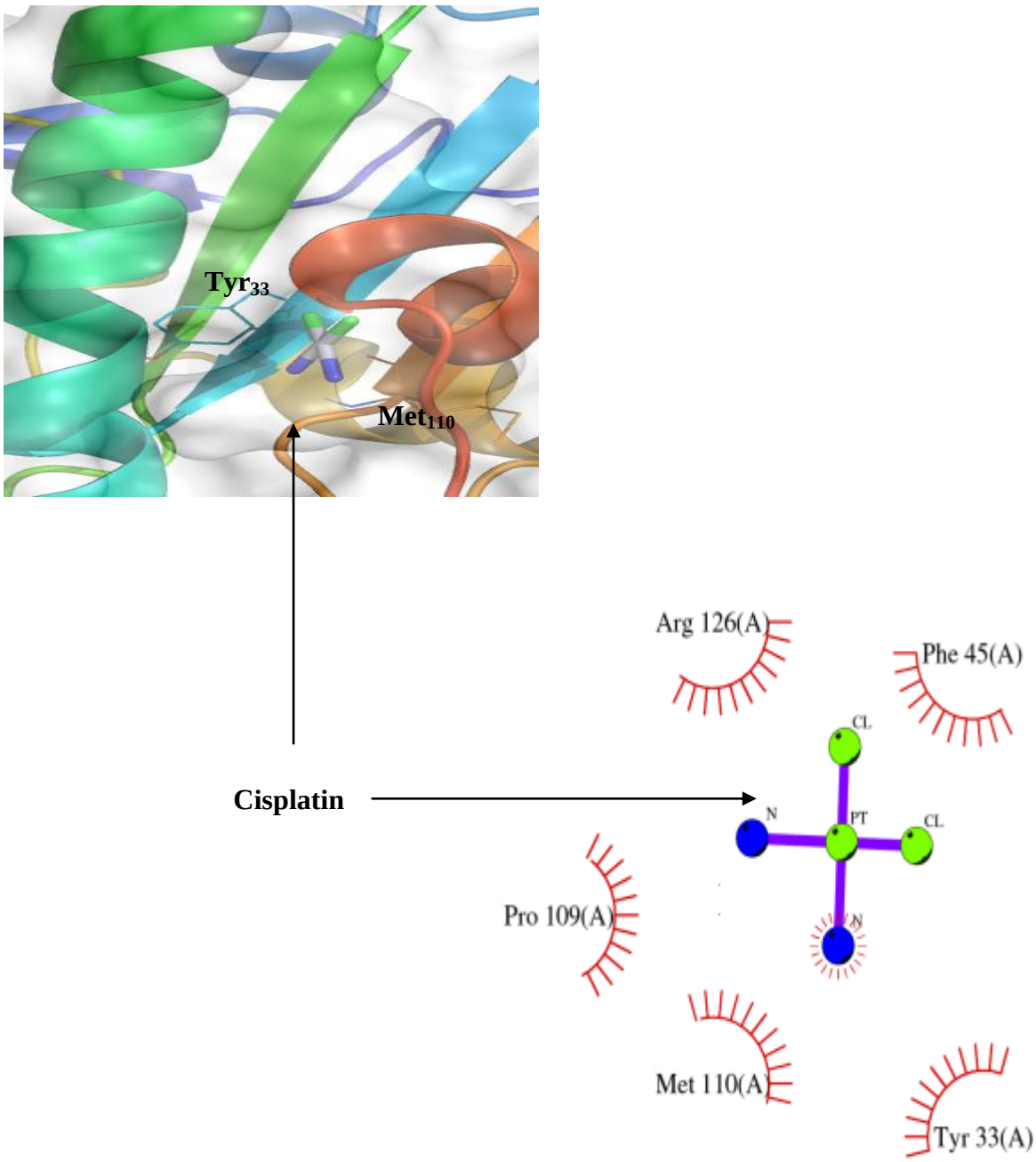

Figure 67: Cartoon representation of Cisplatin docked with *Wb*Trx-1-C39S and the ligplot of interactions between the ligand and the protein amino acids. The structure is orientated to see the pocket introduced by the ligand.

5.11.4 Docking of *Wb*Trx-1-C39S with arsenic trioxide (As_2O_3)

Arsenic trioxide (As_2O_3) (see Fig. 68) is an FDA approved therapeutic agent that has been highly successful in treating acute promyelocytic leukemia (APL)[203] and has shown interesting results in adult T-cell and some subtypes of leukaemia/lymphoma[204].

While, As_2O_3 has shown promising efficacy in preclinical models of solid tumors, this success has not been replicated in clinical trials due to its rapid renal clearance and dose limiting toxicity[205].

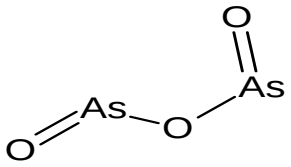

Figure 68: Chemical structure of diarsenic trioxide.

Recently, a nanoparticulate formulation of As_2O_3 was developed in order to improve the antitumor activity of As_2O_3 and to reduce the toxicity[206]. The new formulation of As_2O_3 has been shown to decrease the plasma clearance of arsenic, to improve the tumor delivery of arsenic, to inhibit triple negative breast cancer growth and to attenuate toxicity[207].

The docking study was performed using *Wb*Trx-1 as a receptor and As_2O_3 as a ligand. The docking result shows a binding site close to the N-terminal between Asp_9 and Ser_{93}, as shown in Fig. 69, with three hydrogen bonds and minimum energy of -99.2 kJ mol^{-1}.

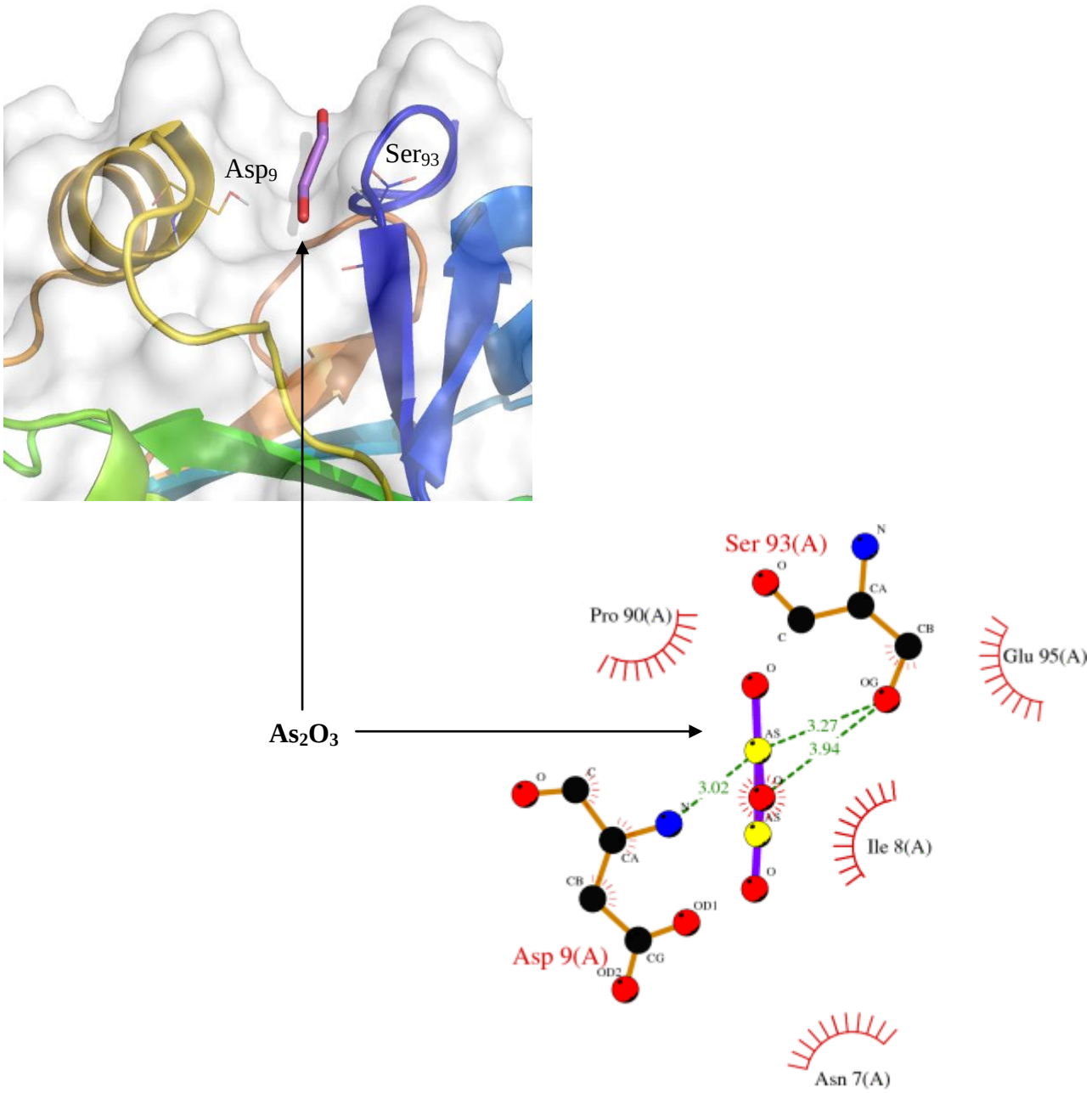

Figure 69: Cartoon representation of AS_2O_3 docked with *Wb*Trx-1-C39S and the ligplot of interactions between the ligand and the protein amino acids. The structure is orientated to see the pocket introduced by the ligand.

The results docking of *Wb*Trx-1-C39S molecule with different inhibitors using the program Hex 6.3 are given in Table 13.

Table 13: Hex 6.3 docking resuslts of *Wb*Trx-1-C39S variant with inhibitors.

No	Compound	Chemical structure	E. kJ mol^{-1}
1	TSA	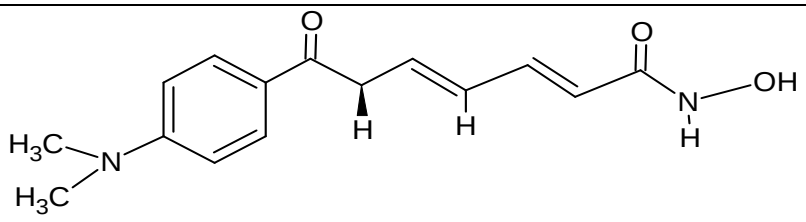	-214.8
2	Triazol	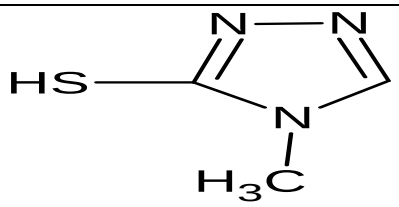	-127.8
3	Cisplatin	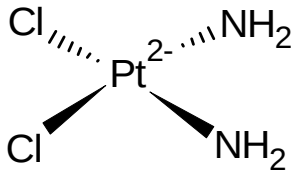	-101.7
4	Arsenic	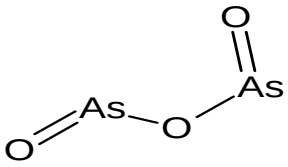	-99.2

Unfortunately, no crystals of the *Wb*Trx-1-C39S in complex with the inhibitor PX-12 could be obtained. This may be due to the difference in the pH of the reaction and the pH of crystal formation. The three dimenstional structure of *Wb*Trx-1 and the variant, used for the docking experiment with selective inhibitors have contributed to an understanding of the activity of the enzyme, the pocket site introduced by inhibitors support to understand how the inhibitor binds to the enzyme. Now there is an urgent need for screening small molecules that can inhibit the activity of the enzyme and lead to new drug discovery investigations.

6. References

1. G Dreyer, D Addiss, J Roberts *et al.*, *Progression of lymphatic vessel dilatation in the presence of living adult Wuchereria bancrofti.* Trans R Soc Trop Med Hyg, 2002. **96**(2): p. 157-61.
2. WHO, *Global programme to eliminate lymphatic filariasis (GPELF).* Progress report 2000-2009 and strategic plan 2010-2020, 2010: p. 1-79.
3. CL King, & Freedman, D.O, *Filariasis. In G.T.Stickland, Hunter's Tropical Medicine and Emerging Infectious Disease,*. W.B. Sanders Company. , 2000. **(8th ed)**: p. 740 - 752.
4. EA Ottesen, *Lymphatic filariasis: Treatment, control and elimination.* Adv Parasitol, 2006. **61**: p. 395-441.
5. S Manguin, MJ Bangs, J Pothikasikorn *et al.*, *Review on global co-transmission of human Plasmodium species and Wuchereria bancrofti by Anopheles mosquitoes.* Infect Genet Evol. **10**(2): p. 159-77.
6. M Bonofiglio, J Hay, C McPherson, *Lymphatic filariasis: inflammatory response to Wolbachia bacteria in filarial worms.* Lymphology, 2007. **40**(4): p. 191-2.
7. WHO, *Global programme to eliminate lymphatic filariasis (GPELF)* Progress report 2000-2009 and strategic plan 2010-202, 2010: p. 1-79.
8. S Babu, CP Blauvelt, V Kumaraswami *et al.*, *Regulatory networks induced by live parasites impair both Th1 and Th2 pathways in patent lymphatic filariasis: implications for parasite persistence.* J Immunol, 2006. **176**(5): p. 3248-56.
9. JS McCarthy, M Zhong, R Gopinath *et al.*, *Evaluation of a polymerase chain reaction-based assay for diagnosis of Wuchereria bancrofti infection.* J Infect Dis, 1996. **173**(6): p. 1510-4.
10. M Zhong, J McCarthy, L Bierwert *et al.*, *A polymerase chain reaction assay for detection of the parasite Wuchereria bancrofti in human blood samples.* Am J Trop Med Hyg, 1996. **54**(4): p. 357-63.
11. JW Mak, *Recent advances in the laboratory diagnosis of filariasis.* Malays J Pathol, 1989. **11**: p. 1-5.
12. SA Williams, SM DeSimone, LA McReynolds, *Species-specific oligonucleotide probes for the identification of human filarial parasites.* Mol Biochem Parasitol, 1988. **28**(2): p. 163-9.

13. S Dissanayake, X Min, WF Piessens, *Detection of amplified Wuchereria bancrofti DNA in mosquitoes with a nonradioactive probe.* Mol Biochem Parasitol, 1991. **45**(1): p. 49-56.
14. KB Mullis, *Target amplification for DNA analysis by the polymerase chain reaction.* Ann Biol Clin (Paris), 1990. **48**(8): p. 579-82.
15. RM Ramzy, HA Farid, IH Kamal *et al.*, *A polymerase chain reaction-based assay for detection of Wuchereria bancrofti in human blood and Culex pipiens.* Trans R Soc Trop Med Hyg, 1997. **91**(2): p. 156-60.
16. DA Boakye, HA Baidoo, E Glah *et al.*, *Monitoring lymphatic filariasis interventions: Adult mosquito sampling, and improved PCR - based pool screening method for Wuchereria bancrofti infection in Anopheles mosquitoes.* Filaria J, 2007. **6**: p. 13.
17. GJ Weil, PJ Lammie, N Weiss, *The ICT Filariasis Test: A rapid-format antigen test for diagnosis of bancroftian filariasis.* Parasitol Today, 1997. **13**(10): p. 401-4.
18. A Rocha, C Braga, M Belem *et al.*, *Comparison of tests for the detection of circulating filarial antigen (Og4C3-ELISA and AD12-ICT) and ultrasound in diagnosis of lymphatic filariasis in individuals with microfilariae.* Mem Inst Oswaldo Cruz, 2009. **104**(4): p. 621-5.
19. S Janardhan, P Pandiaraja, V Pandey *et al.*, *Development and characterization of monoclonal antibodies against WbSXP-1 for the detection of circulating filarial antigens.* J Helminthol. **85**(1): p. 1-6.
20. RM Maizels, E Sartono, A Kurniawan *et al.*, *T-cell activation and the balance of antibody isotypes in human lymphatic filariasis.* Parasitol Today, 1995. **11**(2): p. 50-6.
21. TB Nutman, V Kumaraswami, *Regulation of the immune response in lymphatic filariasis: perspectives on acute and chronic infection with Wuchereria bancrofti in South India.* Parasite Immunol, 2001. **23**(7): p. 389-99.
22. G Dreyer, Z Medeiros, MJ Netto *et al.*, *Acute attacks in the extremities of persons living in an area endemic for bancroftian filariasis: differentiation of two syndromes.* Trans R Soc Trop Med Hyg, 1999. **93**(4): p. 413-7.
23. SM Asio, PE Simonsen, AW Onapa, *Mansonella perstans filariasis in Uganda: patterns of microfilaraemia and clinical manifestations in two endemic communities.* Trans R Soc Trop Med Hyg, 2009. **103**(3): p. 266-73.
24. A Hoerauf, K Pfarr, S Mand *et al.*, *Filariasis in Africa--treatment challenges and prospects.* Clin Microbiol Infect. **17**(7): p. 977-85.

25. KM Pfarr, AY Debrah, S Specht *et al.*, *Filariasis and lymphoedema.* Parasite Immunol, 2009. **31**(11): p. 664-72.
26. P Jungmann, J Figueredo-Silva, G Dreyer, *Bancroftian lymphadenopathy: a histopathologic study of fifty-eight cases from northeastern Brazil.* Am J Trop Med Hyg, 1991. **45**(3): p. 325-31.
27. MJ Taylor, A Hoerauf, M Bockarie, *Lymphatic filariasis and onchocerciasis.* Lancet. **376**(9747): p. 1175-85.
28. RK Shenoy, *Clinical and pathological aspects of filarial lymphedema and its management.* Korean J Parasitol, 2008. **46**(3): p. 119-25.
29. AY Debrah, S Mand, S Specht *et al.*, *Doxycycline reduces plasma VEGF-C/sVEGFR-3 and improves pathology in lymphatic filariasis.* PLoS Pathog, 2006. **2**(9): p. e92.
30. AY Debrah, L Batsa, A Albers *et al.*, *Transforming growth factor-beta1 variant Leu10Pro is associated with both lack of microfilariae and differential microfilarial loads in the blood of persons infected with lymphatic filariasis.* Hum Immunol. **72**(11): p. 1143-8.
31. AY Debrah, S Mand, MR Toliat *et al.*, *Plasma vascular endothelial growth Factor-A (VEGF-A) and VEGF-A gene polymorphism are associated with hydrocele development in lymphatic filariasis.* Am J Trop Med Hyg, 2007. **77**(4): p. 601-8.
32. RK Ong, RL Doyle, *Tropical pulmonary eosinophilia.* Chest, 1998. **113**(6): p. 1673-9.
33. A Solanki, J Ahluwalia, *Asymptomatic filariasis.* Blood. **117**(14): p. 3707.
34. EA Ottesen, *Immunopathology of Lymphatic Filariasis in Man.* Springer Semininars Immunopathology, 1980. **2**: p. 2373-385.
35. E Lobos, R Zahn, N Weiss *et al.*, *A major allergen of lymphatic filarial nematodes is a parasite homolog of the gamma-glutamyl transpeptidase.* Mol Med, 1996. **2**(6): p. 712-24.
36. E Palumbo, *Filariasis: diagnosis, treatment and prevention.* Acta Biomed, 2008. **79**(2): p. 106-9.
37. PE Simonsen, SK Dunyo, *Comparative evaluation of three new tools for diagnosis of bancroftian filariasis based on detection of specific circulating antigens.* Trans R Soc Trop Med Hyg, 1999. **93**(3): p. 278-82.
38. P Turner, B Copeman, D Gerisi *et al.*, *A comparison of the Og4C3 antigen capture ELISA, the Knott test, an IgG4 assay and clinical signs, in the diagnosis of Bancroftian filariasis.* Trop Med Parasitol, 1993. **44**(1): p. 45-8.

39. G Dreyer, F Amaral, J Noroes *et al., Ultrasonographic evidence for stability of adult worm location in bancroftian filariasis.* Trans R Soc Trop Med Hyg, 1994. **88**(5): p. 558.
40. S Mand, Y Marfo-Debrekyei, M Dittrich *et al., Animated documentation of the filaria dance sign (FDS) in bancroftian filariasis.* Filaria J, 2003. **2**(1): p. 3.
41. RK Shenoy, A John, S Hameed *et al., Apparent failure of ultrasonography to detect adult worms of Brugia malayi.* Ann Trop Med Parasitol, 2000. **94**(1): p. 77-82.
42. S Mand, T Supali, J Djuardi *et al., Detection of adult Brugia malayi filariae by ultrasonography in humans in India and Indonesia.* Trop Med Int Health, 2006. **11**(9): p. 1375-81.
43. A Kurniawan, M Yazdanbakhsh, R van Ree *et al., Differential expression of IgE and IgG4 specific antibody responses in asymptomatic and chronic human filariasis.* J Immunol, 1993. **150**(9): p. 3941-50.
44. M Haarbrink, AJ Terhell, K Abadi *et al., Anti-filarial IgG4 in men and women living in Brugia malayi-endemic areas.* Trop Med Int Health, 1999. **4**(2): p. 93-7.
45. Y Moreno, JF Nabhan, J Solomon *et al., Ivermectin disrupts the function of the excretory-secretory apparatus in microfilariae of Brugia malayi.* Proc Natl Acad Sci U S A. **107**(46): p. 20120-5.
46. SD Fernando, C Rodrigo, S Rajapakse, *Current evidence on the use of antifilarial agents in the management of bancroftian filariasis.* J Trop Med. **2011**: p. 175941.
47. S Omura, A Crump, *The life and times of ivermectin - a success story.* Nat Rev Microbiol, 2004. **2**(12): p. 984-9.
48. EA Ottesen, WC Campbell, *Ivermectin in human medicine.* J Antimicrob Chemother, 1994. **34**(2): p. 195-203.
49. J Horton, *Albendazole: a broad spectrum anthelminthic for treatment of individuals and populations.* Curr Opin Infect Dis, 2002. **15**(6): p. 599-608.
50. KY Dadzie, AC Bird, K Awadzi *et al., Ocular findings in a double-blind study of ivermectin versus diethylcarbamazine versus placebo in the treatment of onchocerciasis.* Br J Ophthalmol, 1987. **71**(2): p. 78-85.
51. A Hoerauf, *Filariasis: new drugs and new opportunities for lymphatic filariasis and onchocerciasis.* Curr Opin Infect Dis, 2008. **21**(6): p. 673-81.
52. MY Osei-Atweneboana, K Awadzi, SK Attah *et al., Phenotypic evidence of emerging ivermectin resistance in Onchocerca volvulus.* PLoS Negl Trop Dis. **5**(3): p. e998.

53. HF Cross, M Haarbrink, G Egerton *et al., Severe reactions to filarial chemotherapy and release of Wolbachia endosymbionts into blood.* Lancet, 2001. **358**(9296): p. 1873-5.
54. NW Brattig, *Pathogenesis and host responses in human onchocerciasis: impact of Onchocerca filariae and Wolbachia endobacteria.* Microbes Infect, 2004. **6**(1): p. 113-28.
55. A Hoerauf, L Volkmann, C Hamelmann *et al., Endosymbiotic bacteria in worms as targets for a novel chemotherapy in filariasis.* Lancet, 2000. **355**(9211): p. 1242-3.
56. A Hoerauf, S Mand, K Fischer *et al., Doxycycline as a novel strategy against bancroftian filariasis-depletion of Wolbachia endosymbionts from Wuchereria bancrofti and stop of microfilaria production.* Med Microbiol Immunol, 2003. **192**(4): p. 211-6.
57. MJ Bockarie, RM Deb, *Elimination of lymphatic filariasis: do we have the drugs to complete the job?* Curr Opin Infect Dis. **23**(6): p. 617-20.
58. J Nordberg, ES Arner, *Reactive oxygen species, antioxidants, and the mammalian thioredoxin system.* Free Radic Biol Med, 2001. **31**(11): p. 1287-312.
59. A Holmgren, *Thioredoxin.* Annu Rev Biochem, 1985. **54**: p. 237-71.
60. A Holmgren, *Thioredoxin and glutaredoxin systems.* J Biol Chem, 1989. **264**(24): p. 13963-6.
61. TC Laurent, EC Moore, P Reichard, *Enzymatic Synthesis of Deoxyribonucleotides. Iv. Isolation and Characterization of Thioredoxin, the Hydrogen Donor from Escherichia Coli B.* J Biol Chem, 1964. **239**: p. 3436-44.
62. A Holmgren, M Bjornstedt, *Thioredoxin and thioredoxin reductase.* Methods Enzymol, 1995. **252**: p. 199-208.
63. LM Landino, TE Skreslet, JA Alston, *Cysteine oxidation of tau and microtubule-associated protein-2 by peroxynitrite: modulation of microtubule assembly kinetics by the thioredoxin reductase system.* J Biol Chem, 2004. **279**(33): p. 35101-5.
64. J Messens, S Silver, *Arsenate reduction: thiol cascade chemistry with convergent evolution.* J Mol Biol, 2006. **362**(1): p. 1-17.
65. M Benhar, MT Forrester, DT Hess *et al., Regulated protein denitrosylation by cytosolic and mitochondrial thioredoxins.* Science, 2008. **320**(5879): p. 1050-4.
66. D Ravi, H Muniyappa, KC Das, *Endogenous thioredoxin is required for redox cycling of anthracyclines and p53-dependent apoptosis in cancer cells.* J Biol Chem, 2005. **280**(48): p. 40084-96.

67. G Powis, D Mustacich, A Coon, *The role of the redox protein thioredoxin in cell growth and cancer.* Free Radic Biol Med, 2000. **29**(3-4): p. 312-22.
68. T Nakamura, H Nakamura, T Hoshino *et al.*, *Redox regulation of lung inflammation by thioredoxin.* Antioxid Redox Signal, 2005. **7**(1-2): p. 60-71.
69. R Kern, A Malki, A Holmgren *et al.*, *Chaperone properties of Escherichia coli thioredoxin and thioredoxin reductase.* Biochem J, 2003. **371**(Pt 3): p. 965-72.
70. CH Lillig, A Holmgren, *Thioredoxin and related molecules--from biology to health and disease.* Antioxid Redox Signal, 2007. **9**(1): p. 25-47.
71. HE Huber, S Tabor, CC Richardson, *Escherichia coli thioredoxin stabilizes complexes of bacteriophage T7 DNA polymerase and primed templates.* J Biol Chem, 1987. **262**(33): p. 16224-32.
72. M Russel, P Model, *The role of thioredoxin in filamentous phage assembly. Construction, isolation, and characterization of mutant thioredoxins.* J Biol Chem, 1986. **261**(32): p. 14997-5005.
73. M Saitoh, H Nishitoh, M Fujii *et al.*, *Mammalian thioredoxin is a direct inhibitor of apoptosis signal-regulating kinase (ASK) 1.* EMBO J, 1998. **17**(9): p. 2596-606.
74. S Dai, C Schwendtmayer, P Schurmann *et al.*, *Redox signaling in chloroplasts: cleavage of disulfides by an iron-sulfur cluster.* Science, 2000. **287**(5453): p. 655-8.
75. HF Gilbert, *Molecular and cellular aspects of thiol-disulfide exchange.* Adv Enzymol Relat Areas Mol Biol, 1990. **63**: p. 69-172.
76. ES Arner, A Holmgren, *Physiological functions of thioredoxin and thioredoxin reductase.* Eur J Biochem, 2000. **267**(20): p. 6102-9.
77. A Holmgren, BO Soderberg, H Eklund *et al.*, *Three-dimensional structure of Escherichia coli thioredoxin-S2 to 2.8 A resolution.* Proc Natl Acad Sci U S A, 1975. **72**(6): p. 2305-9.
78. G Roos, A Garcia-Pino, K Van Belle *et al.*, *The conserved active site proline determines the reducing power of Staphylococcus aureus thioredoxin.* J Mol Biol, 2007. **368**(3): p. 800-11.
79. JL Martin, *Thioredoxin--a fold for all reasons.* Structure, 1995. **3**(3): p. 245-50.
80. B Xia, A Vlamis-Gardikas, A Holmgren *et al.*, *Solution structure of Escherichia coli glutaredoxin-2 shows similarity to mammalian glutathione-S-transferases.* J Mol Biol, 2001. **310**(4): p. 907-18.

81. B Heras, MA Edeling, HJ Schirra *et al., Crystal structures of the DsbG disulfide isomerase reveal an unstable disulfide.* Proc Natl Acad Sci U S A, 2004. **101**(24): p. 8876-81.
82. JL Martin, JC Bardwell, J Kuriyan, *Crystal structure of the DsbA protein required for disulphide bond formation in vivo.* Nature, 1993. **365**(6445): p. 464-8.
83. P Reinemer, HW Dirr, R Ladenstein *et al., The three-dimensional structure of class pi glutathione S-transferase in complex with glutathione sulfonate at 2.3 A resolution.* EMBO J, 1991. **10**(8): p. 1997-2005.
84. B Ren, W Huang, B Akesson *et al., The crystal structure of seleno-glutathione peroxidase from human plasma at 2.9 A resolution.* J Mol Biol, 1997. **268**(5): p. 869-85.
85. SJ Harrop, MZ DeMaere, WD Fairlie *et al., Crystal structure of a soluble form of the intracellular chloride ion channel CLIC1 (NCC27) at 1.4-A resolution.* J Biol Chem, 2001. **276**(48): p. 44993-5000.
86. M Depuydt, SE Leonard, D Vertommen *et al., A periplasmic reducing system protects single cysteine residues from oxidation.* Science, 2009. **326**(5956): p. 1109-11.
87. H Eklund, FK Gleason, A Holmgren, *Structural and functional relations among thioredoxins of different species.* Proteins, 1991. **11**(1): p. 13-28.
88. JL Pan, JC Bardwell, *The origami of thioredoxin-like folds.* Protein Sci, 2006. **15**(10): p. 2217-27.
89. TH Xia, JH Bushweller, P Sodano *et al., NMR structure of oxidized Escherichia coli glutaredoxin: comparison with reduced E. coli glutaredoxin and functionally related proteins.* Protein Sci, 1992. **1**(3): p. 310-21.
90. A Bairoch, R Apweiler, *The SWISS-PROT protein sequence data bank and its supplement TrEMBL in 1999.* Nucleic Acids Res, 1999. **27**(1): p. 49-54.
91. G Krause, J Lundstrom, JL Barea *et al., Mimicking the active site of protein disulfide-isomerase by substitution of proline 34 in Escherichia coli thioredoxin.* J Biol Chem, 1991. **266**(15): p. 9494-500.
92. A Lewin, A Crow, CT Hodson *et al., Effects of substitutions in the CXXC active-site motif of the extracytoplasmic thioredoxin ResA.* Biochem J, 2008. **414**(1): p. 81-91.
93. A Chakrabarti, S Srivastava, CP Swaminathan *et al., Thermodynamics of replacing an alpha-helical Pro residue in the P40S mutant of Escherichia coli thioredoxin.* Protein Sci, 1999. **8**(11): p. 2455-9.

94. F de Lamotte-Guery, C Pruvost, P Minard *et al., Structural and functional roles of a conserved proline residue in the alpha2 helix of Escherichia coli thioredoxin.* Protein Eng, 1997. **10**(12): p. 1425-32.
95. FK Gleason, *Mutation of conserved residues in Escherichia coli thioredoxin: effects on stability and function.* Protein Sci, 1992. **1**(5): p. 609-16.
96. ID Kuntz, *Protein folding.* J Am Chem Soc, 1972. **94**(11): p. 4009-12.
97. GD Rose, *Prediction of chain turns in globular proteins on a hydrophobic basis.* Nature, 1978. **272**(5654): p. 586-90.
98. A Garcia-Pino, S Martinez-Rodriguez, K Wahni *et al., Coupling of domain swapping to kinetic stability in a thioredoxin mutant.* J Mol Biol, 2009. **385**(5): p. 1590-9.
99. A Merlino, C Ercole, D Picone *et al., The buried diversity of bovine seminal ribonuclease: shape and cytotoxicity of the swapped non-covalent form of the enzyme.* J Mol Biol, 2008. **376**(2): p. 427-37.
100. D Xu, CJ Tsai, R Nussinov, *Mechanism and evolution of protein dimerization.* Protein Sci, 1998. **7**(3): p. 533-44.
101. H Eklund, C Cambillau, BM Sjoberg *et al., Conformational and functional similarities between glutaredoxin and thioredoxins.* EMBO J, 1984. **3**(7): p. 1443-9.
102. V Menchise, C Corbier, C Didierjean *et al., Crystal structure of the wild-type and D30A mutant thioredoxin h of Chlamydomonas reinhardtii and implications for the catalytic mechanism.* Biochem J, 2001. **359**(Pt 1): p. 65-75.
103. G Roos, N Foloppe, K Van Laer *et al., How thioredoxin dissociates its mixed disulfide.* PLoS Comput Biol, 2009. **5**(8): p. e1000461.
104. MA Wouters, RA George, NL Haworth, *"Forbidden" disulfides: their role as redox switches.* Curr Protein Pept Sci, 2007. **8**(5): p. 484-95.
105. V Dillet, HJ Dyson, D Bashford, *Calculations of electrostatic interactions and pKas in the active site of Escherichia coli thioredoxin.* Biochemistry, 1998. **37**(28): p. 10298-306.
106. N Foloppe, J Sagemark, K Nordstrand *et al., Structure, dynamics and electrostatics of the active site of glutaredoxin 3 from Escherichia coli: comparison with functionally related proteins.* J Mol Biol, 2001. **310**(2): p. 449-70.
107. G Bulaj, T Kortemme, DP Goldenberg, *Ionization-reactivity relationships for cysteine thiols in polypeptides.* Biochemistry, 1998. **37**(25): p. 8965-72.
108. G Roos, P Geerlings, J Messens, *Enzymatic catalysis: the emerging role of conceptual density functional theory.* J Phys Chem B, 2009. **113**(41): p. 13465-75.

109. BW Lennon, CH Williams, Jr., ML Ludwig, *Twists in catalysis: alternating conformations of Escherichia coli thioredoxin reductase.* Science, 2000. **289**(5482): p. 1190-4.

110. Z Shaked, RP Szajewski, GM Whitesides, *Rates of thiol-disulfide interchange reactions involving proteins and kinetic measurements of thiol pKa values.* Biochemistry, 1980. **19**(18): p. 4156-66.

111. RE Hansen, H Ostergaard, JR Winther, *Increasing the reactivity of an artificial dithiol-disulfide pair through modification of the electrostatic milieu.* Biochemistry, 2005. **44**(15): p. 5899-906.

112. PA Fernandes, MJ Ramos, *Theoretical insights into the mechanism for thiol/disulfide exchange.* Chemistry, 2004. **10**(1): p. 257-66.

113. H Ostergaard, A Henriksen, FG Hansen *et al.*, *Shedding light on disulfide bond formation: engineering a redox switch in green fluorescent protein.* EMBO J, 2001. **20**(21): p. 5853-62.

114. G Bulaj, DP Goldenberg, *Mutational analysis of hydrogen bonding residues in the BPTI folding pathway.* J Mol Biol, 2001. **313**(3): p. 639-56.

115. AT Setterdahl, PT Chivers, M Hirasawa *et al.*, *Effect of pH on the oxidation-reduction properties of thioredoxins.* Biochemistry, 2003. **42**(50): p. 14877-84.

116. Y Balmer, WH Vensel, CK Tanaka *et al.*, *Thioredoxin links redox to the regulation of fundamental processes of plant mitochondria.* Proc Natl Acad Sci U S A, 2004. **101**(8): p. 2642-7.

117. SD Lemaire, B Guillon, P Le Marechal *et al.*, *New thioredoxin targets in the unicellular photosynthetic eukaryote Chlamydomonas reinhardtii.* Proc Natl Acad Sci U S A, 2004. **101**(19): p. 7475-80.

118. F Montrichard, F Alkhalfioui, H Yano *et al.*, *Thioredoxin targets in plants: the first 30 years.* J Proteomics, 2009. **72**(3): p. 452-74.

119. K Motohashi, PG Romano, T Hisabori, *Identification of thioredoxin targeted proteins using thioredoxin single cysteine mutant-immobilized resin.* Methods Mol Biol, 2009. **479**: p. 117-31.

120. K Maeda, C Finnie, B Svensson, *Identification of thioredoxin h-reducible disulphides in proteomes by differential labelling of cysteines: insight into recognition and regulation of proteins in barley seeds by thioredoxin h.* Proteomics, 2005. **5**(6): p. 1634-44.

121. N Le Moan, G Clement, S Le Maout *et al.*, *The Saccharomyces cerevisiae proteome of oxidized protein thiols: contrasted functions for the thioredoxin and glutathione pathways.* J Biol Chem, 2006. **281**(15): p. 10420-30.

122. D Vertommen, M Depuydt, J Pan *et al.*, *The disulphide isomerase DsbC cooperates with the oxidase DsbA in a DsbD-independent manner.* Mol Microbiol, 2008. **67**(2): p. 336-49.

123. C Fu, C Wu, T Liu *et al.*, *Elucidation of thioredoxin target protein networks in mouse.* Mol Cell Proteomics, 2009. **8**(7): p. 1674-87.

124. P Hagglund, J Bunkenborg, K Maeda *et al.*, *Identification of thioredoxin disulfide targets using a quantitative proteomics approach based on isotope-coded affinity tags.* J Proteome Res, 2008. **7**(12): p. 5270-6.

125. JK Kumar, S Tabor, CC Richardson, *Proteomic analysis of thioredoxin-targeted proteins in Escherichia coli.* Proc Natl Acad Sci U S A, 2004. **101**(11): p. 3759-64.

126. M Russel, *Filamentous phage assembly.* Mol Microbiol, 1991. **5**(7): p. 1607-13.

127. S Ghosh, SM Hamdan, TE Cook *et al.*, *Interactions of Escherichia coli thioredoxin, the processivity factor, with bacteriophage T7 DNA polymerase and helicase.* J Biol Chem, 2008. **283**(46): p. 32077-84.

128. M Chamberlin, *Isolation and characterization of prototrophic mutants of Escherichia coli unable to support the intracellular growth of T7.* J Virol, 1974. **14**(3): p. 509-16.

129. A Miranda-Vizuete, AE Damdimopoulos, J Gustafsson *et al.*, *Cloning, expression, and characterization of a novel Escherichia coli thioredoxin.* J Biol Chem, 1997. **272**(49): p. 30841-7.

130. D Ritz, H Patel, B Doan *et al.*, *Thioredoxin 2 is involved in the oxidative stress response in Escherichia coli.* J Biol Chem, 2000. **275**(4): p. 2505-12.

131. JF Collet, JC D'Souza, U Jakob *et al.*, *Thioredoxin 2, an oxidative stress-induced protein, contains a high affinity zinc binding site.* J Biol Chem, 2003. **278**(46): p. 45325-32.

132. E Herrero, J Ros, G Belli *et al.*, *Redox control and oxidative stress in yeast cells.* Biochim Biophys Acta, 2008. **1780**(11): p. 1217-35.

133. EG Muller, *Thioredoxin deficiency in yeast prolongs S phase and shortens the G1 interval of the cell cycle.* J Biol Chem, 1991. **266**(14): p. 9194-202.

134. JR Pedrajas, E Kosmidou, A Miranda-Vizuete *et al.*, *Identification and functional characterization of a novel mitochondrial thioredoxin system in Saccharomyces cerevisiae.* J Biol Chem, 1999. **274**(10): p. 6366-73.

135. K Hirota, M Matsui, S Iwata *et al., AP-1 transcriptional activity is regulated by a direct association between thioredoxin and Ref-1.* Proc Natl Acad Sci U S A, 1997. **94**(8): p. 3633-8.

136. J Qin, GM Clore, AM Gronenborn, *The high-resolution three-dimensional solution structures of the oxidized and reduced states of human thioredoxin.* Structure, 1994. **2**(6): p. 503-22.

137. GM Kuster, DA Siwik, DR Pimentel *et al., Role of reversible, thioredoxin-sensitive oxidative protein modifications in cardiac myocytes.* Antioxid Redox Signal, 2006. **8**(11-12): p. 2153-9.

138. WH Watson, J Pohl, WR Montfort *et al., Redox potential of human thioredoxin 1 and identification of a second dithiol/disulfide motif.* J Biol Chem, 2003. **278**(35): p. 33408-15.

139. E Gelhaye, N Rouhier, N Navrot *et al., The plant thioredoxin system.* Cell Mol Life Sci, 2005. **62**(1): p. 24-35.

140. E Gelhaye, N Rouhier, JP Jacquot, *The thioredoxin h system of higher plants.* Plant Physiol Biochem, 2004. **42**(4): p. 265-71.

141. IW Boucher, PJ McMillan, M Gabrielsen *et al., Structural and biochemical characterization of a mitochondrial peroxiredoxin from Plasmodium falciparum.* Mol Microbiol, 2006. **61**(4): p. 948-59.

142. R Friemann, H Schmidt, S Ramaswamy *et al., Structure of thioredoxin from Trypanosoma brucei brucei.* FEBS Lett, 2003. **554**(3): p. 301-5.

143. G Boumis, F Angelucci, A Bellelli *et al., Structural and functional characterization of Schistosoma mansoni Thioredoxin.* Protein Sci. **20**(6): p. 1069-76.

144. UK Laemmli, *Cleavage of structural proteins during the assembly of the head of bacteriophage T4.* Nature, 1970. **227**(5259): p. 680-5.

145. A Holmgren, *Thioredoxin catalyzes the reduction of insulin disulfides by dithiothreitol and dihydrolipoamide.* J Biol Chem, 1979. **254**(19): p. 9627-32.

146. D Ollis, S White, *Protein crystallization.* Methods Enzymol, 1990. **182**: p. 646-59.

147. A McPherson, AJ Malkin, YG Kuznetsov, *The science of macromolecular crystallization.* Structure, 1995. **3**(8): p. 759-68.

148. A Weichsel, JR Gasdaska, G Powis *et al., Crystal structures of reduced, oxidized, and mutated human thioredoxins: evidence for a regulatory homodimer.* Structure, 1996. **4**(6): p. 735-51.

149. SW Provenche, *A constrained regularization method for inverting data represented by linear algebraic or integral equations.* Comput. Phys. Commun, 1982. **27**: p. 213-229.

150. TS Walter, EJ Mancini, J Kadlec *et al.*, *Semi-automated microseeding of nanolitre crystallization experiments.* Acta Crystallogr Sect F Struct Biol Cryst Commun, 2008. **64**(Pt 1): p. 14-8.

151. OZaM W., *Processing of X-ray Diffraction Data Collected in Os.* Methods Enzymol 1997. **276**: p. 307-326.

152. A Vagin, A Teplyakov, *Molecular replacement with MOLREP.* Acta Crystallogr D Biol Crystallogr. **66**(Pt 1): p. 22-5.

153. MD Winn, CC Ballard, KD Cowtan *et al.*, *Overview of the CCP4 suite and current developments.* Acta Crystallogr D Biol Crystallogr. **67**(Pt 4): p. 235-42.

154. BW Matthews, *Solvent content of protein crystals.* J Mol Biol, 1968. **33**(2): p. 491-7.

155. P Emsley, K Cowtan, *Coot: model-building tools for molecular graphics.* Acta Crystallogr D Biol Crystallogr, 2004. **60**(Pt 12 Pt 1): p. 2126-32.

156. AA Vagin, RA Steiner, AA Lebedev *et al.*, *REFMAC5 dictionary: organization of prior chemical knowledge and guidelines for its use.* Acta Crystallogr D Biol Crystallogr, 2004. **60**(Pt 12 Pt 1): p. 2184-95.

157. AT Brunger, *Free R value: a novel statistical quantity for assessing the accuracy of crystal structures.* Nature, 1992. **355**(6359): p. 472-5.

158. DW Ritchie, GJ Kemp, *Protein docking using spherical polar Fourier correlations.* Proteins, 2000. **39**(2): p. 178-94.

159. F Sanger, *Fractionation of oxidized insulin.* Biochem J, 1949. **44**(1): p. 126-8.

160. OZaM W., *Processing of X-ray Diffraction Data Collected in Oscillation Mode.* Methods in Enzymology, 1997. **276**: p. 307-326.

161. GJ Kleywegt, TA Jones, *Phi/psi-chology: Ramachandran revisited.* Structure, 1996. **4**(12): p. 1395-400.

162. SF Altschul, TL Madden, AA Schaffer *et al.*, *Gapped BLAST and PSI-BLAST: a new generation of protein database search programs.* Nucleic Acids Res, 1997. **25**(17): p. 3389-402.

163. A Fiorillo, G Colotti, A Boffi *et al.*, *The crystal structures of the tryparedoxin-tryparedoxin peroxidase couple unveil the structural determinants of Leishmania detoxification pathway.* PLoS Negl Trop Dis. **6**(8): p. e1781.

164. Y Qi, NV Grishin, *Structural classification of thioredoxin-like fold proteins.* Proteins, 2005. **58**(2): p. 376-88.

165. SK Katti, DM LeMaster, H Eklund, *Crystal structure of thioredoxin from Escherichia coli at 1.68 A resolution.* J Mol Biol, 1990. **212**(1): p. 167-84.

166. G Capitani, Z Markovic-Housley, G DelVal *et al.*, *Crystal structures of two functionally different thioredoxins in spinach chloroplasts.* J Mol Biol, 2000. **302**(1): p. 135-54.

167. HJ Dyson, MF Jeng, LL Tennant *et al.*, *Effects of buried charged groups on cysteine thiol ionization and reactivity in Escherichia coli thioredoxin: structural and functional characterization of mutants of Asp 26 and Lys 57.* Biochemistry, 1997. **36**(9): p. 2622-36.

168. DL Kirkpatrick, S Watson, M Kunkel *et al.*, *Parallel syntheses of disulfide inhibitors of the thioredoxin redox system as potential antitumor agents.* Anticancer Drug Des, 1999. **14**(5): p. 421-32.

169. G Powis, DL Kirkpatrick, *Thioredoxin signaling as a target for cancer therapy.* Curr Opin Pharmacol, 2007. **7**(4): p. 392-7.

170. MW Kunkel, DL Kirkpatrick, JI Johnson *et al.*, *Cell line-directed screening assay for inhibitors of thioredoxin reductase signaling as potential anti-cancer drugs.* Anticancer Drug Des, 1997. **12**(8): p. 659-70.

171. DL Kirkpatrick, G Ehrmantraut, S Stettner *et al.*, *Redox active disulfides: the thioredoxin system as a drug target.* Oncol Res, 1997. **9**(6-7): p. 351-6.

172. JE Oblong, EL Chantler, A Gallegos *et al.*, *Reversible inhibition of human thioredoxin reductase activity by cytotoxic alkyl 2-imidazolyl disulfide analogues.* Cancer Chemother Pharmacol, 1994. **34**(5): p. 434-8.

173. P Wipf, TD Hopkins, JK Jung *et al.*, *New inhibitors of the thioredoxin-thioredoxin reductase system based on a naphthoquinone spiroketal natural product lead.* Bioorg Med Chem Lett, 2001. **11**(19): p. 2637-41.

174. DL Kirkpatrick, M Kuperus, M Dowdeswell *et al.*, *Mechanisms of inhibition of the thioredoxin growth factor system by antitumor 2-imidazolyl disulfides.* Biochem Pharmacol, 1998. **55**(7): p. 987-94.

175. BF Jordan, M Runquist, N Raghunand *et al.*, *The thioredoxin-1 inhibitor 1-methylpropyl 2-imidazolyl disulfide (PX-12) decreases vascular permeability in tumor xenografts monitored by dynamic contrast enhanced magnetic resonance imaging.* Clin Cancer Res, 2005. **11**(2 Pt 1): p. 529-36.

176. AF Baker, T Dragovich, WR Tate *et al.*, *The antitumor thioredoxin-1 inhibitor PX-12 (1-methylpropyl 2-imidazolyl disulfide) decreases thioredoxin-1 and VEGF levels in cancer patient plasma.* J Lab Clin Med, 2006. **147**(2): p. 83-90.
177. RK Ramanathan, DL Kirkpatrick, CP Belani *et al.*, *A Phase I pharmacokinetic and pharmacodynamic study of PX-12, a novel inhibitor of thioredoxin-1, in patients with advanced solid tumors.* Clin Cancer Res, 2007. **13**(7): p. 2109-14.
178. AV Bryksin, I Matsumura, *Overlap extension PCR cloning: a simple and reliable way to create recombinant plasmids.* Biotechniques. **48**(6): p. 463-5.
179. BC Smith, JM Denu, *Chemical mechanisms of histone lysine and arginine modifications.* Biochim Biophys Acta, 2009. **1789**(1): p. 45-57.
180. C Zhang, V Richon, X Ni *et al.*, *Selective induction of apoptosis by histone deacetylase inhibitor SAHA in cutaneous T-cell lymphoma cells: relevance to mechanism of therapeutic action.* J Invest Dermatol, 2005. **125**(5): p. 1045-52.
181. BS Mann, JR Johnson, MH Cohen *et al.*, *FDA approval summary: vorinostat for treatment of advanced primary cutaneous T-cell lymphoma.* Oncologist, 2007. **12**(10): p. 1247-52.
182. KB Glaser, *HDAC inhibitors: clinical update and mechanism-based potential.* Biochem Pharmacol, 2007. **74**(5): p. 659-71.
183. LM Butler, X Zhou, WS Xu *et al.*, *The histone deacetylase inhibitor SAHA arrests cancer cell growth, up-regulates thioredoxin-binding protein-2, and down-regulates thioredoxin.* Proc Natl Acad Sci U S A, 2002. **99**(18): p. 11700-5.
184. T Vanhaecke, P Papeleu, G Elaut *et al.*, *Trichostatin A-like hydroxamate histone deacetylase inhibitors as therapeutic agents: toxicological point of view.* Curr Med Chem, 2004. **11**(12): p. 1629-43.
185. DC Drummond, CO Noble, DB Kirpotin *et al.*, *Clinical development of histone deacetylase inhibitors as anticancer agents.* Annu Rev Pharmacol Toxicol, 2005. **45**: p. 495-528.
186. S Shankar, RK Srivastava, *Histone deacetylase inhibitors: mechanisms and clinical significance in cancer: HDAC inhibitor-induced apoptosis.* Adv Exp Med Biol, 2008. **615**: p. 261-98.
187. MS Finnin, JR Donigian, A Cohen *et al.*, *Structures of a histone deacetylase homologue bound to the TSA and SAHA inhibitors.* Nature, 1999. **401**(6749): p. 188-93.

188. S Crotty, D Maag, JJ Arnold *et al.*, *The broad-spectrum antiviral ribonucleoside ribavirin is an RNA virus mutagen.* Nat Med, 2000. **6**(12): p. 1375-9.

189. DJ Williamson, RG Hill, SL Shepheard *et al.*, *The anti-migraine 5-HT(1B/1D) agonist rizatriptan inhibits neurogenic dural vasodilation in anaesthetized guinea-pigs.* Br J Pharmacol, 2001. **133**(7): p. 1029-34.

190. RC Coombes, C Harper-Wynne, M Dowsett, *Aromatase inhibitors and their use in the sequential setting.* Endocr Relat Cancer, 1999. **6**(2): p. 259-63.

191. HA Torres, RY Hachem, RF Chemaly *et al.*, *Posaconazole: a broad-spectrum triazole antifungal.* Lancet Infect Dis, 2005. **5**(12): p. 775-85.

192. KIaP Valentina, *Synthesis and biological activities of novel 1,2,4-triazolo-[3,4-b]-1,3,4-thiadiazoles* Der Pharma Chemica, 2010. **2**(2): p. 16-22

193. B Rosenberg, *Some Biological Effects of Platinum Compounds.* Plat. Met. Rev, 1971. **15**: p. 42–51.

194. TW Hambley, *The influence of structure on the activity and toxicity of Pt anti-cancer drugs.* Coord. Chem. Rev., 1997(21): p. 181–223.

195. E Wong, CM Giandomenico, *Current status of platinum-based antitumor drugs.* Chem Rev, 1999. **99**(9): p. 2451-66.

196. RB Weiss, MC Christian, *New cisplatin analogues in development. A review.* Drugs, 1993. **46**(3): p. 360-77.

197. B Rosenberg, *In Cisplatin: Chemistry and Biochemistry of a Leading Anticancer Drug;*. Lippert, B., Ed.; Verlag Helvetica Chimica Acta: Zurich; Wiley-VCH: Weinheim, Germany, , 1999: p. 3-27.

198. B Rosenberg, L Vancamp, T Krigas, *Inhibition of Cell Division in Escherichia Coli by Electrolysis Products from a Platinum Electrode.* Nature, 1965. **205**: p. 698-9.

199. B Rosenberg, L Van Camp, EB Grimley *et al.*, *The inhibition of growth or cell division in Escherichia coli by different ionic species of platinum(IV) complexes.* J Biol Chem, 1967. **242**(6): p. 1347-52.

200. B Rosenberg, E Renshaw, L Vancamp *et al.*, *Platinum-induced filamentous growth in Escherichia coli.* J Bacteriol, 1967. **93**(2): p. 716-21.

201. B Rosenberg, L VanCamp, JE Trosko *et al.*, *Platinum compounds: a new class of potent antitumour agents.* Nature, 1969. **222**(5191): p. 385-6.

202. B Rosenberg, L VanCamp, *The successful regression of large solid sarcoma 180 tumors by platinum compounds.* Cancer Res, 1970. **30**(6): p. 1799-802.

203. MS Tallman, JK Altman, *How I treat acute promyelocytic leukemia.* Blood, 2009. **114**(25): p. 5126-35.

204. G Kchour, M Tarhini, MM Kooshyar *et al.*, *Phase 2 study of the efficacy and safety of the combination of arsenic trioxide, interferon alpha, and zidovudine in newly diagnosed chronic adult T-cell leukemia/lymphoma (ATL).* Blood, 2009. **113**(26): p. 6528-32.

205. TE Bael, BL Peterson, JA Gollob, *Phase II trial of arsenic trioxide and ascorbic acid with temozolomide in patients with metastatic melanoma with or without central nervous system metastases.* Melanoma Res, 2008. **18**(2): p. 147-51.

206. H Chen, R Ahn, J Van den Bossche *et al., Folate-mediated intracellular drug delivery increases the anticancer efficacy of nanoparticulate formulation of arsenic trioxide.* Mol Cancer Ther, 2009. **8**(7): p. 1955-63.

207. RW Ahn, F Chen, H Chen *et al., A novel nanoparticulate formulation of arsenic trioxide with enhanced therapeutic efficacy in a murine model of breast cancer.* Clin Cancer Res. **16**(14): p. 3607-17.

7. Risk and safety Statements

7.1 Chemicals used (GHS classification)

Compound	CAS-No.	Supplier	GHS Hazard	Hazard Statements	Precautionary Statements
Acetic acid	64-19-7	Chem.-solute	**GHS02 GHS05**	H226, H314	P280, P305+351+338 P310
Acrylamide 30%	79-06-1	Carl Roth	**GHS06 GHS08**	H301,H312,H316, H317,H319,H332, H340,H350 H361f,H372	P201,P280, P301+310, P305+351+338 P308+313
Agarose	34369-07-8	Serva`	-	-	-
$(NH_4)_2SO_4$	7283-202	Carl Roth	-	-	-
Ampicillin	69-52-3	Carl Roth	**GHS08**	H334,H317	P280,P261, P302+P352 P342+P311
AMP-PCP	7414-564	Sigma	**GHS06**	H301,H311,H315 H319,H331,335	P261,P280, P301+P310, P305+351+P38
APS	7727-54-0	Carl Roth	**GHS03 GHS07 GHS08**	H272,H302,H315, H317 H319,H334,H335	P280 P305+351+338 P302+352, P304+341, P342+311
Bromopheol blue	115-39-9	Appli-chem	-	-	-
$CaCl_2$	10043-52-4	Merck	**GHS07**	H319	P305+351+338

Compound	CAS-No.	Supplier	GHS Hazard	Hazard Statements	Precautionary Statements
Coomassie Brilliant Blue R250	6104-59-2	Serva	-	-	-
DDT	578517	Appli-chem	**GHS07**	H302,H315,H319, H335	P302+352, P305+351+338
EDTA	60-004	Sigma	**GHS07**	H319	P305+351+338
Ethanol	64-17-5	Carl Roth	**GHS02**	H225	P210
Ethidium bromide	1239-45-8	Sigma	**GHS06 GHS08**	H302,H330,H341	P260,P281, P284,P310
Glycerol	56-81-5	Sigma	**-**	-	-
Guanidinhy-drochloric	50-01-1	Appli-Chem.	**GHS07**	H302,H315,H319	P305+351+P38 8,P302+P352
Hydrochlor-ic acid>25%	7647-01-0	Merck	**GHS05 GHS07**	H314,H335	P261,P280,P30, P305+351+338
Imidazol	288-32-4	Carl Roth	**GHS05 GHS06 GHS08**	H301,H314,H361	P260,P281, P303+361+353 P301+330+331 P305+361+383 P308+P313
Isopropanol	67-63-0	Carl Roth	**GHS02 GHS07**	H225,H319,H336	P210,P233, P305+315+338

Compound	**CAS-No.**	**Supplier**	**GHS Hazard**	**Hazard Statements**	**Precautionary Statements**
Li_2SO_4	10102-25-7	Merck	**GHS07**	H302	-
Methanol	67-56-1	Carl Roth	**GHS02 GHS06 GHS08**	H225,H301,H311, H331,H370	P210,P280,P233 P302+P352, P309,P310
2-Mercapto-ethanol	60-24-2	Fisher Scientifc	**GHS06 GHS09**	H302,H411,H315 H335,H311,H319	P280,P312,P302+P350,P261, P273, P301+P312,P305+P351+P338
NaCl	7647-14-5	Carl Roth	-	-	-
NaH_2PO_4	10049-21-5	Appli-Chem.	-	-	-
NaOH	1310-73-2	Merck	**GHS05**	H314	P261,P310, P305+351+338
Ni(II)SO_4	10101-97-0	Appli-Chem.	**GHS07 GHS08 GHS09**	H332,H315,H334, H317,H341, H350i, H360D,H372.H410	P280,P273, P201 P342+P311, P308+P313, P302+P352
PEG 3000	25322-68-3	Sigma	-	-	-

Compound	CAS-No.	Supplier	GHS Hazard	Hazard Statements	Precautionary Statements
PEG 3350	25322-68-3	Sigma	-	-	-
SDS	151-21-3	Sigma	**GHS02 GHS06**	H228,H302,H311, H319,H335	P210,P261, P280,P312, P305+351+338
TEMD	110-18-9	Merck	**GHS02 GHS05 GHS07**	H225,H302, H314,H332	P261,P280, P305+351+338
Tris	1185-53-1	Fluka	**GHS07**	H315,H319,H335	P261, P305+351+335
Yest Extract	8013-01-2	Serva	-	-	-

7.2 Commercial Protein Screens and Kits

Name	Supplier	Risk label	Risk phrases	Safety pshrases
PCT	Hampton	-	-	-
Floppy Choppy	Jena Bio Science	**C, Xn, xi**	R35, R41, R42 R36, 37, 38	S22, S26, S45, S24, S25 S36, 37, 39
Macrosol	Molecular Dimensions	**T, N**	R10, R45, R46, R60, R61, R25, R36, 37, 38, R48, 20, 22, R51, 53	S20, S26, S45, S53,S61, S36, 37, 39

Name	Supplier	Risk label	Risk phrases	Safety phrases
Morpheus	Molecular Dimensions	**T, N**	R10, R45, R46 R60, R61, R63, R23,25,R36,37,38, R48,20,22, R51,53	S20, S26, S45, S53,S61, S36, 37, 39
PACT premier	Molecular Dimensions	**T**	R23,25 R52,53	S20, S36, S45, S61
Stura/Footprint	Molecular Dimensions	**T, N**	R10, R45, R46, R60, R61, R25, R36, 37, 38, R48, 20, 22, R51, 53	S20, S26, S45, S53,S61, S36, 37, 39
AmSO$_4$ Suit	Qiagen	**T+ , N**	R10, R25,26, R45,46, R60,61 R48,23,25, R51,53	S45, S53, S61 S36, 37
Classic Suite	Qiagen	**T , N**	R10, R45, R46, R60, R61, R23, R25,R36,37,38, R48,20,22, R51,53	S20, S26, S45, S53, S36,37,39
ComPAS Suite	Qiagen	**T**	R10, R45, R23,24,25, R36,38 R39,23,24,25, R51, 53	S13, S26, S45 S53,S61, S36, 37, 39
Cryos Suite	Qiagen	**T, N**	R10, R45, R46 R60, R61, R23,25,R36,37,38, R48,20,22, R51,53	S20, S26, S45, S53,S61, S36, 37, 39
JCSG + Suite	Qiagen	**T, N**	R10, R21, R41, R45, R23,25, R37,38, R51,53	S13,S20, S26, S45, S53 S36,37,39

Name	Supplier	Risk label	Risk phrases	Safety phrases
Pure Link PCR Purification Kit	Invitrogen	**Xn**	R22,R36,38	S28, S24,25
peqGOLD Plasmid Mini Kit	Peqlab	-	-	-

7.3 GHS and risk symbols and information about hazard, risk, safety and precaution statements

 • Oxidizers	 • Flammables • Self reactives • Pyrophorics • Self-Heating • Emits flammable gas • Organic peroxides	 • Explosives (Divisions 1.1 to 1.4 only) • Self reactives • Organic peroxides
 • Acute toxicity (severe)	 • Corrosive to metals • Skin corrosion • Serious eye damage/eye irritation	 • Gases under pressure
 • Carcinogen • Respiratory sensitizer • Reproductive toxicity • Target Organ toxicity • Mutagenicity • Aspiration toxicity	 • Aquatic Toxicity (acute) • Aquatic Toxicity (chronic)	 • Irritant • Dermal sensitizer • Acute toxicity (harmful)

Figure 64: GHS pictograms Adapted from http://en.wikipedia.org/wiki/Hazard_symbol

GHS Hazard Statements	
H 225	Highly flammable liquid and vapour
H 226	Flammable liquid and vapour
H 228	Flammable solid
H 272	May intensify fire; oxidizer
H 301	Toxic if swallowed
H 302	Harmful if swallowed
H 311	Toxic in contact with skin
H 312	Harmful in contact with skin
H 314	Causes severe skin burs and eye damage
H 315	Causes skin irritation
H 316	Causes mild skin irritation
H 317	May causes an allergic skin reaction
H 318	Causes serious eye damage
H 319	Causes serious eye irritation
H 330	Fatal if inhaled
H 331	Toxic if inhaled
H 332	Harmful if inhaled

GHS Hazard Statements	
H 334	May causes allergy or asthma symptoms or breathing difficulties if inhaled
H 335	May cause respiratory irritation
H 336	My cause drowsiness or dizziness
H 340	May cause genetic defects
H 341	Suspected of causing genetic defects
H 350	May cause cancer
H 350i	May cause cancer by inhalation
H 360	May damage fertility or unborn child
H 369D	May damage the unborn child
H 361	Suspected of damaging fertility or unborn child
H 361f	Suspected of damaging fertility
H 370	Causes damage to organs
H 372	Causes damage to organs through prolonged or repeated exposure
H 410	Very toxic to aquatic life with long lasting effects
H 411	Toxic to aquatic life with long effects

GHS Precautionary Statements	
P 201	Obtain special instruction before use
P 210	Keep away From heat-sparks-open flames-hot surface-no smoking
P 233	Keep container tightly closed
P 260	Do not breath dust-fume-gas-mist-vapors-spray
P 261	Avoid breath dust-fume-gas-mist-vapors-spray
P 264	Wash …. thoroughly after handling
P 273	Avoid release to the environment
P 280	Use personal protective gloves-protective clothing-eye-protection-face protection
P 281	Use personal protective equipment as required
P 284	Ware respiratory protection
P 309	If exposed you feel unwell
P 310	Immediately call a POISON CENTER or doctor
P 311	Call a POISON CENTER or doctor
P 312	Call a POISON CENTER or doctor if you feel unwell
P 321	Specific treatment

GHS Precautionary Statements	
P 362	Take off contaminated clothing and wash before use
P 501	Dispose of contents
P 301 + P 310	If SWALLOWED: Immediately call a POISON CENTER or doctor
P 301 + P 312	If SWALLOWED: call a POISON CENTER or doctor
P 301 + P 330 + P 331	If SWALLOWED: Rinse mouth. Do NOT induce vomiting
P 302 + P 352	If ON SKIN: wash with soap and water
P 303 + P 361 + P 353	If ON SKIN (or hair): Remove-take off immediately all contaminated clothing. Rinse skin with water-shower
P 304 + P 341	If INHALED: If breathing is difficult, remove victim to fresh air and keep at rest in a position for breathing
P 305 + P 351 + P 338	If IN EYES: Rinse cautiously with water for several minutes. Remove contact lenses if present
P 308 + P 313	If exposed or concerned: Get medical advise-attention
P 332 + P 313	If skin irritation occurs: Get medical advise-attention
P 342 + P 311	Call a POISON CENTER or doctor
P 403 + P 233	Store in a well-ventilated place and keep tightly closed

Risk statements	
R 8	Contact with combustible materials
R 10	May cause fire
R 20	Flammable
R 21	Harmful by inhalation
R 22	Harmful in contact with skin
R 25	Harmful if swallowed
R 35	Toxic if swallowed
R 36	Causes severe burns
R 38	Irritation to eyes irritating to skin
R 41	Risk to serious damage to eyes
R 42	May causes sensitization by inhalation
R 43	May causes sensitization by skin contact
R 45	May cause cancer
R 46	May cause heritable genetic damage
R 60	May impair fertility
R 61	May cause harm to the unborn child
R 39/R 23/24/25	Toxic: danger of very serious irreversible effects through inhalation, in contact with skin and if swallowed

Risk statements	
R 36/37/38	Irritation to eyes, respiratory system and skin
R 23/24/25	Toxic by inhalation, in contact with skin and swallowed
R 20/21/22	Harmful by inhalation, in contact with skin and swallowed
R48/20/22	Harmful: danger of serious damage to health by prolonged exposure through inhalation and if swallowed
R 23/25	Toxic by inhalation and if swallowed
R 36/38	Irritating to eyes and skin
R 51/53	Toxic to aquatic organism, may cause long term adverse effects in the aquatic environment
R 37/38	Irritating to respiratory system and skin

Safety Statements	
S 20	When using do not eat or drink. Do not breath dust
S 22	In case of contact with eyes, rinse immediately with plenty of water and seek medical advise
S 26	In case of accident or if you feel unwell seek medical advise immediately
S 28	After contact with skin, wash immediately with plenty of…(specified by the manufacture)
S 45	If swallowed, seek medical advise immediately and show the container or label
S 46	Avoid exposure – obtain special instructions before use

Safety Statements	
S 53	Avoid release to the environment
S 61	Refer to special instruction – safety data sheet
S 24/25	Avoid contact with skin and eyes
S 36/37	Wear suitable protective clothing and gloves
S 36/37/39	Wear suitable protective clothing, gloves and eye/face protection

8. Acknowledgement

- First of all I kneel to Allah truly thankful for supporting me to continue my research and complete my thesis.
- I send all my respect and gratitude to the Egyptian Ministry of High Education for financially supporting my Ph.D. program.
- I'd like to dedicate this work to my family specially my wife (Wafaa and my children (Sohila, Sama and Sahar)
- I would like to express my deepest appreciation to Prof. Christian Betzel. It would have been very difficult to continue my life in Germany without his help and support. More importantly, his kindness and scientific guidance were major factors that helped me to continue in this thesis. I thank him for introducing me into the field of "crystallography",
- Deeply thank to Dr. rer. nat. Markus Perbandt for helping me and supporting during my thesis. I wish him a great success in his career.
- I'd like to thank all of the people in the Laboratory for Structural Biology of Infection and Inflammation at DESY, and also in the Laboratory of Biochemistry and Molecular Biology.
- Thanks to everyone else who's been in the lab at any stage in the past four years for providing me with help and support.

Nasser Yousef

9. Curriculum Vitae

Personal Data

Family Name: Yousef

First Name: Nasser

Address: Sedanstrasse 23, 20146 - Hamburg

Date of Birth: 23 October 1970

Birthplace: El-Qalyoubia, Egypt

Nationality: Egyptian

Graduation

1989: High Secondary School, Qalyoubia, Egypt.

1989-1993: B. Sc. In Biochemistry, Faculty of Agricultural, Ain Shames University, Egypt.

1995-2001: M. Sc. in Biochemistry, Faculty of Agricultural Banha University, Egypt.

2001 2008: Working at National Organization for Drug and Research (NODCAR), Egypt

Since 2008: Ph.D. student at the University of Hamburg, Germany.

Work experience

1995-2001, during this period I pursued my Master degree.

Topic: Biochemical studies on agricultural wastes.

2001 2009: Quality control at National Organization for Drug and Research (NODCAR), Egypt.

Since 2009: Scholarship to obtain a Ph.D. degree at the University of Hamburg, funded by Ministry of Higher Education.

Publications

1. A Krem, **N Yousef**, A Begum et al., *Preliminary Crystallographic Analysis of a Cruciferin Protin from seeds of Moringa oleifera*. Protein J.2014 Jun; **33**(3): p. 253-7

Manuscript in preparation

2. **N Yousef**, M Perbandt, Prince R, A Akrem et al., *Crystal structure of thioredoxin from Wuchereria bancrofti at 1.95 Å resolution.*

Selbständigkeitserklärung

Hiermit versichere ich an Eides statt, dass ich die vorliegende Arbeit selbständig und ohne unerlaubte fremde Hilfe angefertigt habe. Ich habe keine anderen als die im Literaturverzeichnis angeführten Quellen benutzt und sämtliche Textstellen, die wörtlich oder sinngemäß aus veröffentlichten oder unveröffentlichten Schriften entnommen wurden und alle Angaben, die auf mündlichen Auskünften beruhen, als solche kenntlich gemacht. Zusammenarbeiten sind im Text genannt. Die Arbeit wurde zuvor keiner Prüfungsbehörde in gleicher oder ähnlicher Form vorgelegt.

Nasser Yousef